2007

Measurement of metal migration in sediment caps with x-ray fluorescene

Ming Yin
Louisiana State University and Agricultural and Mechanical College

MEASUREMENT OF METAL MIGRATION IN SEDIMENT CAPS WITH X-RAY FLUORESCENCE

A Dissertation
Submitted to the Graduate Faculty of the
Louisiana State University and
Agricultural and Mechanical College
in partial fulfillment of the
requirements for the degree of
Doctor of Philosophy

in

The Department of Chemical Engineering

by
Ming Yin
B.S., Beijing University, China, 1992
M.S., Xiamen University, China, 2000
August, 2007

Acknowledgements

I would like to thank Drs. Reible, Willson and Valsaraj for their guidance during my research. Especially I sincerely appreciate Dr.Willson for his consistent guidance throughout the whole research and dissertation writing processes. Also I would like to thank Dr. Judy Wornat and Dr. Julius Langlinais for serving on my committee.

I am also grateful to Dr. Raghunathan Ravikrishna and all other colleagues in our group as they provide various ways of assistance to my research. I specially wish to appreciate the assistance of CAMD staff, especially Dr.Roland Tittsworth, Christopher Bianchetti, Dr. Kyungmin Ham and Russell Louis.

Finally I need to acknowledge the funding from EPA Hazardous Substance Research Center South and Southwest, Louisiana Water Resources Research Institute and CICEET.

Table of Contents

List of Tables

List of Figures

Abstract

Sand is often used as a passive barrier to slow release of metals from contaminated sediment and to separate benthic organisms from the sediment. Materials that effectively adsorb metals have the potential to provide significantly greater effectiveness by further retarding metal release. In this thesis, the effectiveness of apatite and *Phosphil*®, which contain phosphate in a form that can absorb many metals, is evaluated with a series of sorption and migration column experiments using Cr, Cu, Zn and Pb.

Langmuir shape isotherms were observed suggesting that the effectiveness of these materials decreases at high concentration. The sorption isotherm experiments also revealed that the phosphate cap materials were much more sorbing than sand and therefore would more effectively retard contaminant migration.

Column experiments designed to study metal transport from field contaminated sediment had difficulty achieving measurable migration depths (due to intermixing between sediment and cap materials) within a reasonable time scale. An analytical model of contaminant migration was developed for this situation. Metal migration in the same capping materials was studied utilizing experimental columns in which high concentrations of metals were ponded over a solid layer of capping materials. Migration profiles were measured in two ways: a "traditional" sectioning method followed by ICP-MS analysis of the section; and non-destructive scanning using synchrotron X-ray Fluorescence. This method allowed determination of metal profiles with sub-mm resolution. In migration experiment Zn migrated fastest among all four metals and sand exhibited the least retardation of any metals. These are consistent with the equilibrium sorption data. Although the experiments with a high concentration metal solution allowed

the observation of metal migration in reasonable periods of time, the experimental setup resulted in buoyancy effects which artificially enhanced metal migration.

A finite difference model incorporating Langmuir isotherm and non-equilibrium effects and using the initial observed profile as an initial condition was developed to simulate metal migration in these systems and therefore quantify the effectiveness of the various cap materials. Model inferred retardation factors indicated metal sorption in the order of *Phosphil* > Florida Phosphate > sand (e.g. Cu in tetra-element system were 100, 43 and 0.46 ‘respectively).

Chapter 1

Introduction

Contaminated sediments are a major environmental concern. Common contaminants in sediments include nutrients, halogenated hydrocarbons or persistent organic, polycyclic aromatic hydrocarbons (PAH) and metals (EPA, 2006). Heavy metals are one of the most prevalent contaminants. The Coastal Sediment Database (COSED) reported that 12 – 16% of all sediments surveyed from around the U.S. contained heavy metal concentrations above background levels (U.S.ACE, 2001). Heavy metals are persistent environmental contaminants compared with organic matters which can decay with time. The toxicity of metal species has been well recognized. For example, exposure to copper can lead to its accumulation in liver, brain, kidney, and cornea, leading to the classic impairment and stigmata of Wilson disease and Indian childhood cirrhosis. No organ system is immune to the effects of lead poisoning and the organ of most concern is the brain (Moore et al., 1984).

Metal contaminants in sediments in ponds, lakes and rivers present special problems. Dredging is often discouraged as a heavy metals-contaminated sediment cleanup option due to the metal contaminants can be widely dispersed to the overlying flowing waters when the sediment is disturbed. One non-removal technology showing special promise is in-situ capping, which seals off contaminated sediments under a layer (or layers) of capping materials such as sand, soil, rock or reactive barriers, etc. Sand has been effective material to isolate metals in sediment. Additional containment may be needed to achieve remediation objective under some conditions. Apatite is one of the reactive capping materials that can retard many metal contaminants more effectively than conventional

capping materials (e.g. sand). Thus, the knowledge about the fate and transport of metals in these capping materials and sediment will provide a powerful tool for the design and evaluation of the capping systems.

To study the transport of metals from contaminated sediments in water-saturated capping materials, and to evaluate the effectiveness of phosphate materials, a set of column migration experiments were conducted in 2001-2003 using contaminated field sediment from Newton Creek and Anacostia River sediment, Sand, Florida Phosphate, and North Carolina Phosphate were evaluated as capping layers. This pilot-scale research was designed to prepare the technology for field deployment of reactive barriers in Anacostia River, which began in 2003 as part of an EPA sponsored project located in Washington, D.C. The Anacostia River capping project is a federally funded project led by The Hazardous Substance Research Centers/South & Southwest to demonstrate innovative sediment capping technology on the Anacostia River. The Anacostia flows from Maryland to the District of Columbia and is one of the nation's 10 most endangered rivers. In the Anacostia demonstration contaminated sediment is covered by layers of alternative materials that can degrade or control sediment-bound contaminants more efficiently than sand.

High spatial resolution (less them 0.5 mm) Synchrotron X-ray Fluorescence (XRF) was used to measure the metal migration profiles in those transport columns. A diffusion based model assuming constant retardation factor was developed to model these profiles. No measurable migration depths were detected even the migration was allowed to occur for over 400 days. First, this indicates that the cap materials used are effective barriers for field contaminated sediment. Second, most of the detected migration depths were within 3 mm which is within the intermixing zone of cap and sediment and it was difficult to

differentiate the migration characteristics of different metals and materials (Yin et al., 2004).

It is well known that the metal migration is heavily impacted by sorption isotherm. To further understand the metal migration the Cr, Cu, Zn and Pb sorption isotherms for several materials were measured. The sediment and capping materials used in Anacostia River capping project are of great interests in our research. Phosphil (one apatite from North Carolina) is one of capping material used in that capping site. Florida Phosphate is another apatite material that has the potential to be commercially applied in real capping systems. Sand is a conventional capping material. In chapter 3 the metal isotherms of all these capping materials and Anacostia river sediment are measured. The selected metals are Cr, Cu, Zn and Pb which are the most significant metal contaminants in Anacostia river sediment (Table 3.2, chapter 3).

The sorption isotherm is determined by the interaction of metal species between the water and solid (e.g., sediments or capping materials) phases. This interaction is controlled by the metal species aqueous chemistry and the physical-chemical character of the solid materials. A number of models have been developed which can be categorized into two categories: empirical equations (sorption isotherm, e.g. Langmuir isotherm, Freundlich isotherm) and mechanistic models (e.g. ion exchange, surface complexation) (Merkel et al., 2002). Various sorption isotherms of metal species and different solid materials have been reported. For example, Lee at al. (1996) and Malakul et al. (1998) conducted equilibrium batch experiments for the partitioning of metal species on soils and clays. Results indicated that the Langmuir isotherm was an appropriate model to describe the adsorption data for their soils and clays. On the other hand, Zehetner and

Wenzel (2000) found that the partitioning of Ni and Cu onto acidic forest soils could be best represented by the Freundlich isotherm.

The sorption of metal involves a number of processes, including surface adsorption, dissolution and subsequent precipitation, ion exchange, etc. The contribution of these mechanisms to the observed sorption is often not well understood so that the applicability of the isotherm data for specific system is limited and usually can not be extended to other similar systems.

The sorption isotherm experiments in chapter 3 indicate that most of the isotherms can be fitted by a Langmuir isotherm. A characteristic of the Langmuir isotherm is that at low concentration ranges the partition coefficient or the retardation factors are higher than in high concentration range. In chapter 4 and chapter 5, experimental results are described using specially-designed migration columns where relatively high concentration metal solutions overlie solid layer. This simulates the situation of a high concentration metal pollution accident.

The technique focused on in this dissertation to measure the metal migration profiles is Synchrotron X-ray Fluorescence (XRF). This Synchrotron x-ray technique provides high spatial and time measurement resolution and is non-destructive to the sample. Tokunaga et al. (1998) investigated Selenium diffusion and reduction at the water-sediment boundary using synchrotron micro-XANES spectroscopy. Using the same technique (Tokunaga et al., 2001) also investigated the Chromium diffusion and reduction in soil aggregate. In chapter 5, measurements of the migration profiles of Cr, Cu and Zn in Florida Phosphate and Anacostia river sediment by XRF at LSU's Center for Advanced Microstructures and Devices (CAMD) are described. This synchrotron technique also has constraints. First, due to matrix competitive effects, the metal species

cannot be detected as sensitively as by traditional destructive analytical techniques such as ICP-MS. Second, because beam time is limited the ability to do experiments is also limited. This is why in chapter 4 another technique (ICP-MS) was used to measure the metal migration profiles. That technique requires the slicing of the migration cores followed by destructive ICP-MS analysis. These experiments in chapter 4 provide a preliminary idea how far the metals will migrate under certain circumstances.

Once the isotherm and migration data are obtained, a mathematical model is useful to investigate the relationship between them. The isotherm can be incorporated into the transport equation as a function of concentration in pore water. To simulate the conditions of the experiments, the Langmuir isotherm was incorporated into the diffusion equation to predict migration. Serrano (2001) obtained series solution to approximate the analytical solution of this non-linear equation but its validity is limited by initial conditions and Langmuir parameters. A finite difference method was adopted to numerically solve this nonlinear partial differential equation. At low concentration ranges, the Langmuir isotherm can be approximated as a linear isotherm and an analytical solution was obtained.

The overall objective of the work in this dissertation is to evaluate the sorption-related retardation of metal contaminants in various capping materials and sediment by investigation of the metal migration profiles The metal species of focus are Cr(III), Cu(II), Zn(II) and Pb(II).

The specific objectives include:

- Measure the metal migration profiles from field sediment (Newton Creek sediment and Anacostia River sediment) into capping materials (sand, Florida

Phosphate, North Carolina Phosphate, etc) by XRF. Develop a diffusion based model assuming constant retardation factor to fit the experimental migration profiles resulting in a retardation factor for each combination of metal and material.

- Examine the metal sorption isotherms of apatite materials (Florida Phosphate, Phosphil, etc) and sediment (Anacostia River sediment) and provide a basis for the subsequent diffusion modeling.

- Investigate the metal migration from a ponded metal solution into capping materials by measuring the migration profile by different analysis techniques (ICP-MS and XRF).

- Develop a diffusive model connecting the results from batch experiments (isotherm) and dynamic (migration) experiments. This model is based on the following hypotheses:

  1) The adsorption and desorption of metals in solid particles are reversible.

  2) The interaction of metals and the plastic materials (polypropylene and polyethene) used in the transport column experiments can be neglected. Then according to the symmetric geometry of the columns used in those experiments, one dimensional diffusion can be assumed.

  3) Metal migration between solid particles occurs through the water phase. There is no 'direct' migration from particle to particle.

1.1 References

Choy, B. and D.D. Reible, *Diffusion Models of Environmental Transport*, CRC/Lewis Publishers (2000).

EPA (US Environmental Protection agency), “Contaminated sediment in water”, 2006, http://www.epa.gov/OST/cs/aboutcs/sources.html.

Lee, S. Z., Allen, H. E., Hunag, C. P., Sparkes D. L., Sanders, P. F. and Peijnenburg, W. J. G. M., (1996). “Predicting soil-water partition coefficients for cadmium.” Environmental Science and Technology, 30 (12), 3418-3424.

Malakul, P., Srinivasan, K. R. and Wang, H. Y. (1998). “Metal adsorption and desorption characteristics of surfactant-modified clay complexes.” Ind. Eng. Chem. Res., 37 (12), 4269-4301.

Merkel, B.J., Planer-Friedrich, B., *Groundwater Geochemistry* (Springer Berlin Heidelberg New York, 2002)

Moore, J.W and Ramamoorthy. S, *Heavy Metals in Natural Waters* (Springer-Verlag, 1984).

Serrano, S.E., Solute Transport under Non-Linear Sorption and Decay, *Wat. Res.* Vol. 35, No. 6, pp. 1525–1533, 2001

Tokunaga, T. K., Wan, J., Firestone, M. K.; Hazen, T. C.; Schwartz, E., Sutton, S. R., Newville, M., 2001, Chromium diffusion and reduction in soil aggregates, *Environ. Sci. Technol, 35*, 3169-3174.

Tokunaga, T. K.; Wan, J.; Pena, J.; Sutton, S. R.; Newville, M., 2004, Hexavalent Uranium Diffusion into Soils from Concentrated Acidic and Alkaline Solutions, *Environ. Sci. Technol., 38*, 3056-3062.

U.S. ACE (2001) *The U.S. Waterway System – Transportation facts*, Navigation Data Center, U. S. Army Corps of Engineers, Alexandria, VA.

Yin, M., C.S. Willson, and D.D. Reible, 2004, Investigation of Heavy Metal Migration from Contaminated Sediment to Capping material using XRF, presented at the 2004 AICHE Annual Meeting, November 7-12, 2004, Austin, TX.

Zehetner, F. and Wenzel, W. W. (2000) “Nickel and copper sorption in acid forest soils.” Soil Science, 165 (6), 463-472.

Chapter 2
UNH Experiment: Metal Migration Detected by X-ray Fluorescence

2.1 Introduction

To evaluate the effectiveness of phosphate-based reactive capping materials to inhibit heavy metal migration from field contaminated sediment, a set of pilot scale metal migration tank experiments were conducted. Field contaminated sediments (from Newton Creek, N.Y. and Anacostia River, Washington DC) were capped by capping materials of sand, Florida Phosphate and North Carolina Phosphate in a laboratory. This pilot-scale research was designed to prepare the technology for field deployment of reactive barrier in Anacostia River, which began in 2003 as part of an EPA sponsored project located in Washington, D.C.

Experiments were established in the Jackson Estuarine Research Laboratory (JEL) at the University of New Hampshire (UNH). Experiments were set up in 30 liter tanks with continuous estuarine water flow over the capped materials (Crannell et al., 2004). A number of 1 inch columns were removed at specified times frozen and shipped to LSU. At LSU the metal concentration depth profiles of these columns were measured using synchrotron X-ray Fluorescence (XRF) with high resolution (space and time) at the CAMD facility. This practice will also give us an idea of the advantages and disadvantages of the analytical method using synchrotron X-ray when applied in the materials of cap system (sediment, Phosphate, etc). The metal profiles obtained from these measurements were analyzed by a two layer diffusion model.

2.2 Background of Analysis Technique: Synchrotron XRF

2.2.1 Synchrotron Radiation Source

Synchrotron radiation is emitted when a fast electron interacts with a magnetic field. In a high-energy electron storage ring photons are emitted with energies ranging from infrared to short wavelength X-rays. Synchrotron radiation has a number of unique properties:

- High intensity in the X-ray range compared with conventional laboratory generated X-rays, making it possible to conduct X-ray spectroscopy and X-ray scattering experiments on environmental samples whose concentrations are normally relatively low.
- High degree of collimation (i.e. small divergence of beam) allows for the focusing of hard X-ray beams to sub-μm diameters and soft x-rays to 50 μm diameters (SSRL, 2003). This property leads to spatial resolution on the order of microns, which is very useful for environmental samples that are often heterogeneous on spatial scales of a few μm or less.
- Wide and continuous energy spectrum allows for "tuning" of the energy with a monochromator.
- High time resolution, high beam intensity leads to short acquisition time compared with conventional X-ray sources

Synchrotron radiation has become an indispensable tool in a wide range of research fields, e.g., determining the structure of materials and molecules, the electronic (chemical) structure of surfaces and interfaces; analyzing tiny trace element concentrations in micron-sized regions; measuring local molecular structures in

disordered systems (e.g., solutions and catalysts); and obtaining 3-D computed tomography (CT) scan images with micron resolution.

There are about 70 synchrotron radiation sources worldwide. In the U.S. there are seven, including the Center for Advanced Microstructures and Devices (CAMD) at LSU. Figure 2-1 is the spectral brilliance of CAMD ring. We can notice that when energy approaches Copper Kα line the beam intensity drops dramatically.

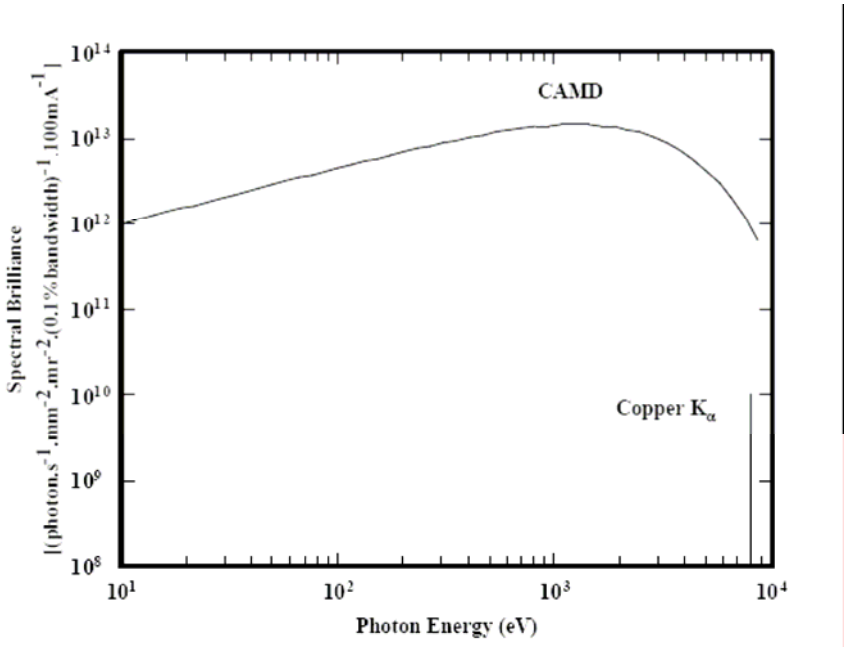

Figure 2-1. Spectral brilliance curve of CAMD ring

2.2.2 X-Ray Fluorescence Spectroscopy (XRF)

From the demonstration of the first principles in the 1940's to the development of the first commercial instruments in the 1970's (Jenkins,1988), XRF has become a well-established and mature multi-element technique. XRF is capable of non-destructively yielding accurate quantitative information on the elemental composition of a variety of materials in a short period of time. Solids can be analyzed directly with little or no sample preparation. All elements with atomic numbers greater than 11 can be detected (Bertin, 1975).

When an X-ray excitation source strikes a sample, the X-ray is absorbed by the atom by transferring all of its energy to an inner electron. If the X-ray has sufficient energy, the electrons are ejected from inner shells, creating vacancies that present an unstable condition within the atom. When the atom returns to its stable condition the electrons from outer shells are transferred to inner shells, giving off a characteristic X-ray whose energy is the difference of the two binding energies of the corresponding shells. Figure 2-2 (AMP TEK) illustrates 'K-line' emission process. Kα line emission is produced when an electron in L shell transfers to K shell and Kβ line is produced when electron transfers from M to K shell, and so on for Kγ, etc. The 'L-line' emission process is similar.

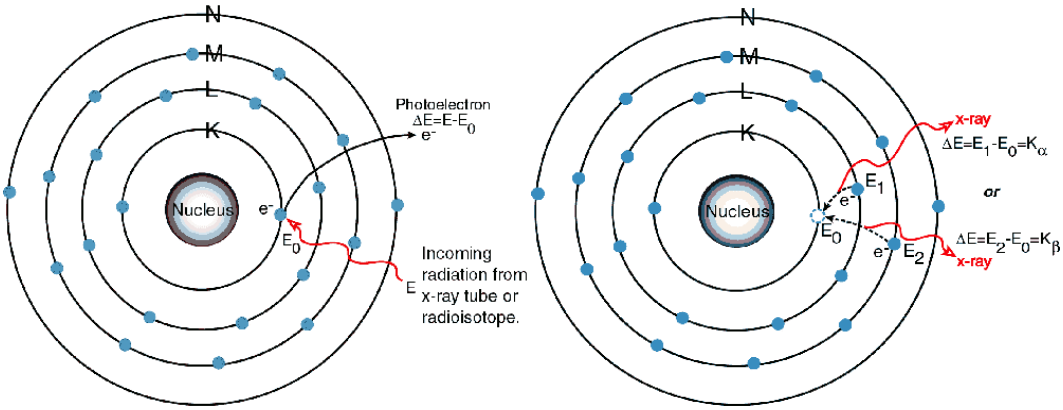

Figure 2-2. Illustration of 'K-line' emission

For a particular energy (wavelength) of fluorescent light emitted by an element, the number of photons per unit time (generally referred to as peak intensity or count rate) is related to the amount of that element in the sample. The counting rates for all detectable elements within a sample are usually calculated by counting, for a set amount of time, the number of photons that are detected for the various elements' characteristic X-ray energy lines. Therefore, by determining the energy of the X-ray peaks in a sample's spectrum, and by calculating the count rate of the various elemental peaks, it is possible to qualitatively establish the elemental composition of the samples and to quantitatively

measure the concentration of these elements. Table 2-1 lists the K edge emission energies of several elements that will be investigated in this chapter. K edge refers to a sudden increase in the attenuation coefficient of photons occurring at photon energy just above the binding energy of the K shell electron of the atoms interacting with the photons.

Table 2-1 Emission energies of some metals (Thompson, et al., 2001)

Atomic number	Element	Kα (keV)	Kβ (keV)
20	Ca	3.69	4.01
24	Cr	5.41	5.95
26	Fe	6.40	7.06
29	Cu	8.05	8.90
30	Zn	8.64	9.57

X-ray fluorescence can be measured and quantified in two ways: wave length dispersive and energy dispersive XRF. Wavelength dispersive XRF uses a crystal to separate the various wavelengths. For every angle of incident radiation, the only wavelength reflected to the detector is the one that conforms to Bragg's formula. In the more commonly utilized energy dispersive XRF all wavelengths enter the detector at once. The detector registers an electric current proportional to the photon energy. These pulses are separated electronically using a pulse analyzer. The resolution and detection limit are better for wavelength dispersive XRF while energy dispersive XRF has the advantages of simplicity of instrumentation and less acquisition time.

Choosing optimal acquisition conditions for XRF analysis is a complex problem. There must be a significant source peak (excitation peak) above the absorption edge energy of the element of interest. This edge may be either the K or L edge depending on which one is within the measurable range of the detector instrument. The closer the source energy is to the absorption edge, the higher the intensity and sensitivity will be for the element of interest. The other fundamental principle is that the background x-rays within the element of interest region should be reduced as much as practical. The

difficulty is that these two principles work in opposition to each other; i.e. the best sensitivity is often achieved when the background is highest, and the background is lowest when the sensitivity is worst. Optimal analytical performance is achieved by finding the best compromise between these two principles.

A typical XRF spectrum from an irradiated sample will display multiple peaks of different intensities, each peak corresponding to a particular element. The area under each element's characteristic peaks reflects the element's concentration.

Conventional XRF detection limits can be down to microgram-per-gram (ppm) level and for synchrotron XRF it can be femtogram-per-microgram (ppb) level (Falkenberg, 2002). This is based primary on instrument detection limits and strength of incident x-ray. For method detection limits that includes the sample preparation process and analysis time, typically achieved detection limits vary between 10 and 100 ppm.

Matrix effect is a major issue when using the XRF technique. If one considers a thick specimen free from all sources of positional and chemical error in an X-ray spectrometer free from all sources of instrumental and operational error, the intensity of a spectral line in matrix M (I_A, M) is a function of the weight fraction of analyte A W_{AM}, the analyte-line intensity from pure A I_{AA} and the matrix M (Falkenberg, 2002), i.e.,

$$I_{AA} = f(W_{AM}, I_{AA}, M)$$

There are many approaches to the absorption-enhancement problem. Most of these methods involve the use of calibration standards. Intensity data are converted to analytical concentration by use of calibration curves or mathematical relationships derived from measurements on standards (e.g., Bertin, 1975).

2.3 Materials and Method

2.3.1 Sediment and Capping Materials

Three sediment samples were gathered from locations along the U.S. East Coast. These included sediments from Newtown Creek, N.Y., Anacostia River, D.C., and Great Bay, N.H. The Clean Great Bay Sediment was used as uncontaminated reference sediment.

Reactive capping materials (i.e. Florida and North Carolina phosphate) were collected from the IMC Agrico mine in Mulberry, Florida and the PCS-Phosphate Mine in Aurora, North Carolina. They are fine sandy materials concentrated through the "single floatation" process to remove clay particles. Single floatation is a standard beneficiation washing and separation process to increase the concentration of calcium phosphate minerals above the raw mined product. The non reactive capping material used in this study is Ottawa sand which is high purity, commercially sold, silica sands (SiO_2).

2.3.2 Migration Tank Experiment Configuration

Design and construction of the tanks is shown in Figure 2-4. Tanks were constructed from high density polyethylene, divided vertically into two sections and supported with side bracings. One half of the tank was filled with 1, 2 and 4 inch diameter columns. Water continually flowed over the tanks.

The experiments were conducted in twenty tanks using a three-level factorial design with two external and three internal replications (Figure 2-5), testing for the effects of barrier material (clean sediment, Ottawa sand, Florida phosphate, and North Carolina phosphate) over two contaminated sediments (Newtown Creek and Anacostia River). No tracer was added to all these materials.

2.3.3 Sample Preparation

At specified times (30, 120, 400 days) a certain number of 1 inch columns in the UNH migration tanks were removed. To avoid disturbing the metal profile of the cores the sample columns were frozen and shipped to LSU (Figure 2-5). The samples are packed in polypropylene graduate tubes.

The polypropylene tubes are too thick for the XRF scanning directly (i.e. the thick tubes will attenuate the X-ray too much, especially for relatively low energy beam line). To achieve optimum XRF spectra, the samples were processed by the following steps:

- Cut the frozen tube in half; the recommended cutting direction is from capping layer to contaminated sediment.
- Put the cut columns back into freezer for 10 minutes.
- Clean the cut surface of the half columns by plastic knife; the direction of clean action should be vertical to the axis of the sample tube.
- Wrap the half column by thin plastic film and vacuum sealed by vacuum package machine.
- Allow the vacuum sealed samples warm up to room temperature.

Figure 2-3. Frozen columns from UNH

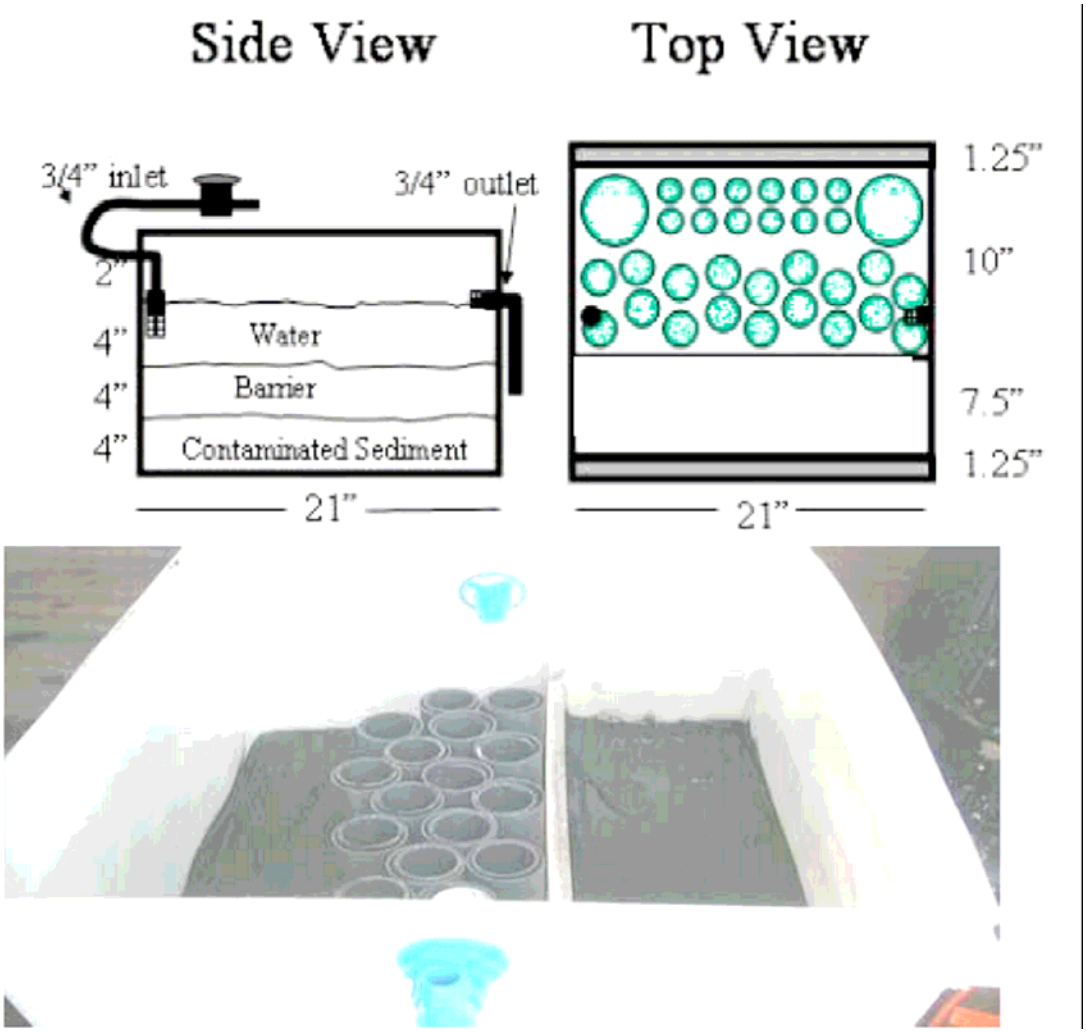

Figure 2-4. Construction of UNH migration tanks (Crannell et al., 2004)

Figure 2-5. Configuration of UNH migration tanks (Crannell et al., 2004)

2.3.4 XRF Experiment Set Up

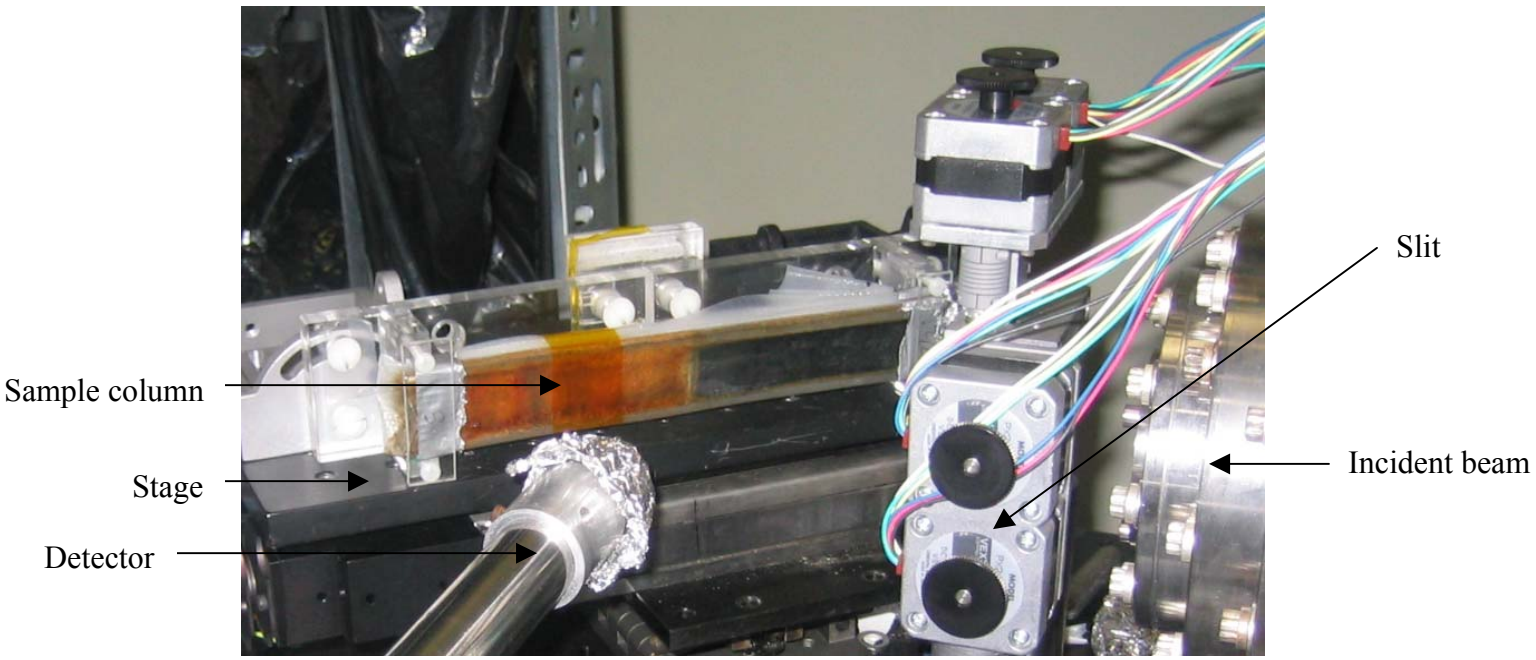

Figure 2-6. XRF experiment set up

The XRF analysis in CAMD was carried out in white light mode which means the multi-energy beam does not go through monochromator so that all the original energy spectrum of incident beam comes out and strike the sample. The experiment set up is shown in Figure 2-6. The white light X-ray beam goes through two slits and shapes the beam to a 0.5 mm x 10 mm vertical rectangle. This slim beam hit the sample which is placed 45^0 to the incident beam and horizontally sits on a computer controlled motor stage whose moving precision is 1 μM. When the sample is hit by X-ray, fluorescence X-ray is produced and gives off. The fluorescence X-ray is detected by the Ge detector that is placed vertical to the incident beam.

This set up is based on the energy spatial distribution property of CAMD beamline. Along vertical direction, the high energy part of X-ray in CAMD tends to concentrate to the horizontal central plane. The higher the energy level, the more it will concentrate to

the center. And this center will often shift with time. Along horizontal direction this phenomena is not obvious. Therefore, if the slit is very small in the vertical direction (i.e. the outcoming beam will be like a horizontal line), the high energy part of the beam will often be blocked because of the shift of the energy center. So we open the slit vertically and narrow it horizontally to a 'vertical line'. Thus no matter how the vertical energy center of the beam shifts, all the high energy parts of the beam will go through the slit.

2.3.5 XRF Data Processing

The data collected by the computer connected with the detector is raw spectra; i.e., a plot of energy versus counts. To extract the element composition information from the spectra the following data processing procedure is done:

i) Normalize the spectra by ring current

ii) Create and then subtract baseline using Origin®

iii) Deconvolute overlapped peaks (e.g. Cu Kβ and Zn Kα) and integrate all characteristic peaks by Peakfit®

The integrals of the characteristic peaks represent the relative concentrations along sample column. If the absolute concentration of one point is known (e.g. measured by ICP-MS) the absolute concentrations of all other points can be calculated.

2.4 Results and Discussion

Figure 2-7 is a typical XRF spectrum of Newton Creek sediment. Fe Kα (6.4 keV) and Kβ (7.0 keV) are the most significant peaks in this spectrum.

After data processing (described in 2.3.5) the spectra of each point scanned can be transformed to metal concentrations. Thus the metal concentration profiles are obtained.

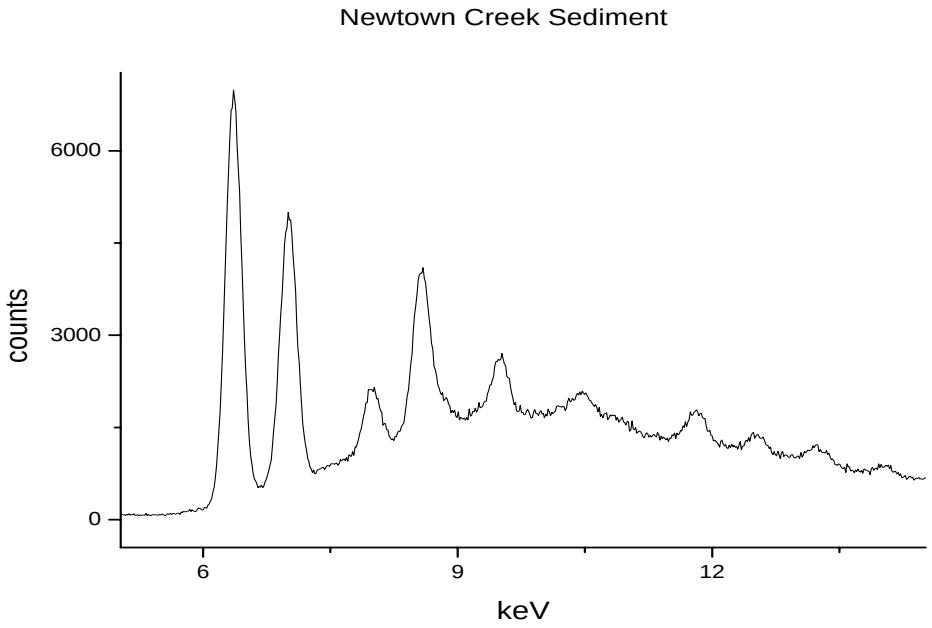

Figure 2-7. XRF spectra of Newton Creek Sediment

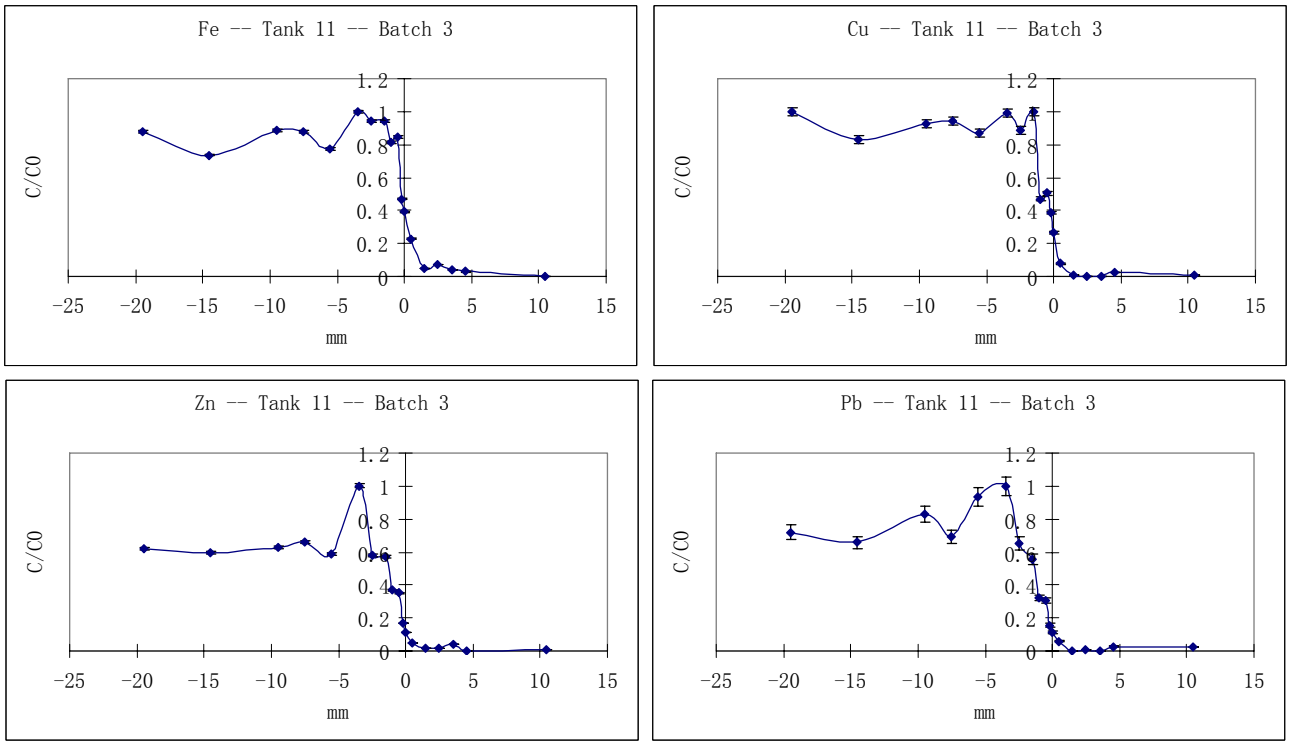

Figure 2-8. Metal migration profiles from Newton Creek Sediment to Florida Phosphate (migration time: 400 days)

Figure 2-8 is a set of typical metal migration profile. The error bars represent standard deviations (in the population, mean or just range of data?) come from the three scans (at different currents) on the same location on one sample in XRF experiment. Generally the error bars are small, indicating the excellent reproducibility of XRF measurement.

From these migration profiles we can see that for all the metals the migration spread ΔZ (i.e. the length of the transition zone from the background concentration (Cs) in contaminated sediment layer to the background concentration (Cc) in cap layer, the starting point of the transition zone is defined as the point where concentration C = Cc +0.99*(Cs-Cc) and the end point is the point where the concentration C = Cc+0.01*(Cs-Cc)) are within 4 mm and that there is no significant difference between different metals. Table 2-2 summarizes the ΔZ from 30 days' and 400 days' samples. The samples with migration time of 30 days actually represent the initial condition of migration so the ΔZ of them are most likely induced by intermixing. Two observations can be made by investigating the ΔZ data in Table 2-2. One is after 400 days' migration the growth of ΔZ is at the same magnitude of the length of intermixing zone (i.e. ΔZ of 30 days' profiles). Another is for different metals there is no significant difference of ΔZ observed.

Table 2-2 Migration spread (ΔZ) (mm)

Capping material	Migration time	Newton Creek sediment				Anacostia River sediment			
		Fe	Cu	Zn	Pb	Fe	Cu	Zn	Pb
Florida Phosphate	30 days	2	2	2	2	3	1	2.5	2.5
	400 days	2	3	3	4	6	3.5	4	7
Ottawa Sand	30 days	1	2	1	3	1.5	1	2	5.5
	400 days	2	3	3	4	2	2	2	2
GreatBay Sediment	30 days	4	3	3	3				
	400 days	5	3.5	3	4.5				
North Carolina Phosphate	30 days	7	4	4	4				
	400 days	5.5	4.5	3.5	3.5				

2.5 Two Layer Diffusion Model

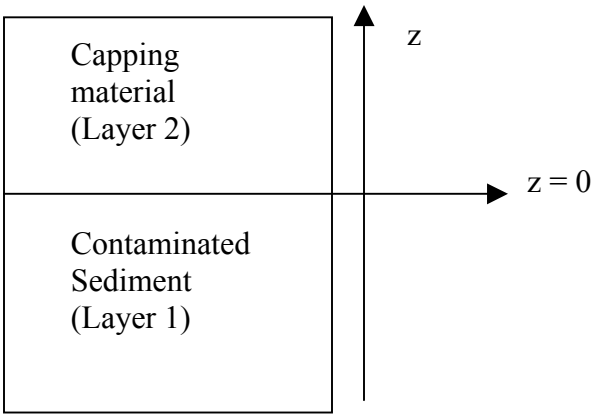

Figure 2-9. Two-layer Model Concept

To describe the data obtained from XRF measurement a diffusion based model were developed assuming constant retardation factor and porosity. As shown in Figure 2-9, the samples studied in this chapter are modeled as two layers (layer 1 is contaminated sediment, layer 2 is capping material, interface is at z = 0). The assumption is that the solid mediums are fully saturated with water and therefore, there are only two phases in each layer: water (mobile) and solid.

The effective diffusivity of the mobile metal species through the porous media may be estimated by the relationship derived by Millington and Quirk (1961):

$$D_{A(eff)} = D_A \varepsilon^{4/3} \tag{1}$$

D_A is the diffusivity of species A in water, for our case.

In this two phase' system, the retardation factor is defined as:

$$R_f = \frac{c_{A,total}}{c_{A,mobile\ phase}} \tag{2}$$

Over a differential volume, the mass balance equation is:

$$\frac{\partial c_{A,total}}{\partial t} = -\nabla j_A \pm reactions \tag{3}$$

where j_A is the flux of species A.

Now assume a simple one-dimensional pure diffusion model. The diffusion only occurs in the z direction (along the column). There are no sources or sinks for the metals (other than reversible sorption). Then the mass balance equation becomes:

$$\frac{\partial c_{A,total}}{\partial t} = D_{A(eff)} \frac{\partial^2 c_{A,mobile\ \ phase}}{\partial z^2} \tag{4}$$

From equation (2), gives, $c_{A,mobile\ phase} = c_{A,total} / R_f$

Substituting it into equation (4), gives

$$\frac{\partial c_{A,total}}{\partial t} = \frac{D_{A(eff)}}{R_f} \frac{\partial^2 c_{A,total}}{\partial z^2} \tag{5}$$

Thus the differential equations in the two layers are:

$$\frac{\partial c_{A,1}}{\partial t} = \left(\frac{D_{A(eff),1}}{R_{f,1}} \right) \frac{\partial^2 c_{A,1}}{\partial z^2} \qquad z \le 0 \tag{6}$$

$$\frac{\partial c_{A,2}}{\partial t} = \left(\frac{D_{A(eff),2}}{R_{f,2}} \right) \frac{\partial^2 c_{A,2}}{\partial z^2} \qquad z > 0 \tag{7}$$

Here $c_{A,1}$ The total concentration of metal A in layer 1 (Sediment)

$c_{A,2}$ The total concentration of metal A in layer 2 (Capping material)

$R_{f,1}$ Retardation factor of layer 1 for metal A (Sediment)

$R_{f,2}$ Retardation factor of layer 2 for metal A (Capping material)

$D_{A(eff),1}$ Effective diffusivity of metal A in layer 1(Sediment)

$D_{A(eff),2}$ Effective diffusivity of metal A in layer 2 (Capping material)

The Initial conditions are:

$$c_{A,1}(z,t)\big|_{t=0} = c_{A0,1} \qquad z \le 0 \tag{8}$$

$$c_{A,2}(z,t)\big|_{t=0} = c_{A0,2} \qquad z > 0 \tag{9}$$

Assuming that there is perfect contact between the layers, the boundary conditions become

$$\frac{c_{A,1}(z,t)}{R_{f,1}} = \frac{c_{A,2(z,t)}}{R_{f,2}} \qquad z = 0, t \ge 0 \tag{10}$$

$$\frac{D_{A(eff),1}}{R_{f,1}}\frac{\partial c_{A,1}}{\partial z} = \frac{D_{A(eff),2}}{R_{f,2}}\frac{\partial c_{A,2}}{\partial z} \qquad z = 0, t \ge 0 \tag{11}$$

$$c_{A,1}\big|_{z=-\infty} = c_{A0,1} \qquad z = -\infty, t \ge 0 \tag{12}$$

$$c_{A,2}\big|_{z=+\infty} = c_{A0,2} \qquad z = +\infty, t \ge 0 \tag{13}$$

The porosity of two layers and the molecular diffusivity D_A in water at 25 ^{0}C are known. The effect of temperature can be described with, $D_A = \frac{1.173 \cdot 10^{-16} T\sqrt{\phi \cdot M}}{\mu \cdot V_m^{0.6}}$ (Wilke and Chang, 1955), T is temperature, μ is viscosity of the solvent (which is related with T), ϕ and V_m is parameter related with solvent. Therefore, D_A at other temperatures can be calculated from D_A at 25 ^{0}C.

Solving the PDE ((6), (7)) with its I.C. ((8), (9)) and B.C. ((10)-(13)) by Laplace transform gives

$$c_{A,1} = \left(\frac{R_{f,1}\cdot c_{A0,2} - R_{f,2}\cdot c_{A0,1}}{R_{f,2} + \sqrt{\frac{D_{A(eff),1}\cdot R_{f,1}\cdot R_{f,2}}{D_{A(eff),2}}}}\right)\cdot erfc\left(-\sqrt{\frac{R_{f,1}}{4\cdot D_{A(eff),1}\cdot t}}\cdot z\right) + c_{A0,1} \qquad z \le 0 \qquad (14)$$

$$c_{A,2} = \left(\frac{R_{f,2}\cdot c_{A0,1} - R_{f,1}\cdot c_{A0,2}}{R_{f,1} + \sqrt{\frac{D_{A(eff),2}\cdot R_{f,1}\cdot R_{f,2}}{D_{A(eff),1}}}}\right)\cdot erfc\left(-\sqrt{\frac{R_{f,2}}{4\cdot D_{A(eff),2}\cdot t}}\cdot z\right) + c_{A0,2} \qquad z > 0 \qquad (15)$$

Using MathCAD, $R_{f,1}$ and $R_{f,2}$ can be fitted from the diffusion profile data. Figures 10-12 show three typical fitting examples. When $R_{f,1} \neq R_{f,2}$, there is a 'gap' between two layers. That is because the continuum assumption is in liquid phase, not in solid phase. COD is coefficient of determination which reflects the fitting extent.

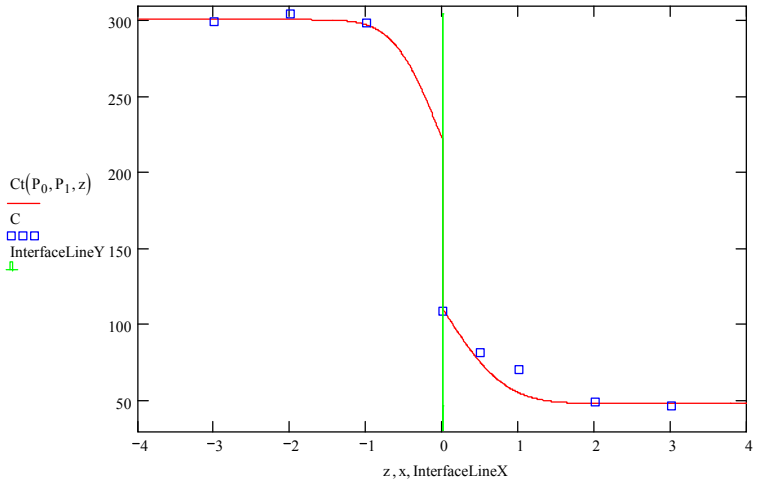

$R_{f,1}$=70090 $R_{f,2}$=35030 COD=0.996 ($R_{f,1} > R_{f,2}$)

Figure 2-10: Pb diffusion fitting of Newtown Creek Sediment/Florida Phosphate

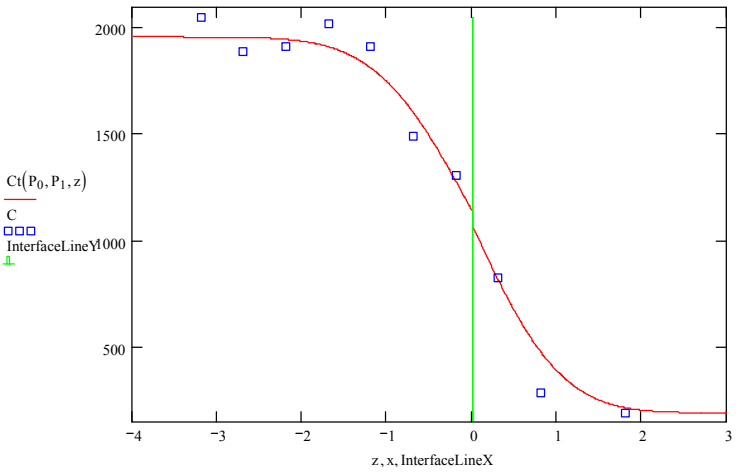

$R_{f,1}$=14100 $R_{f,2}$=13260 COD=0.967 ($R_{f,1} \approx R_{f,2}$)

Figure 2-11: Fe diffusion fitting of Anacostia River Sediment/Florida Phosphate

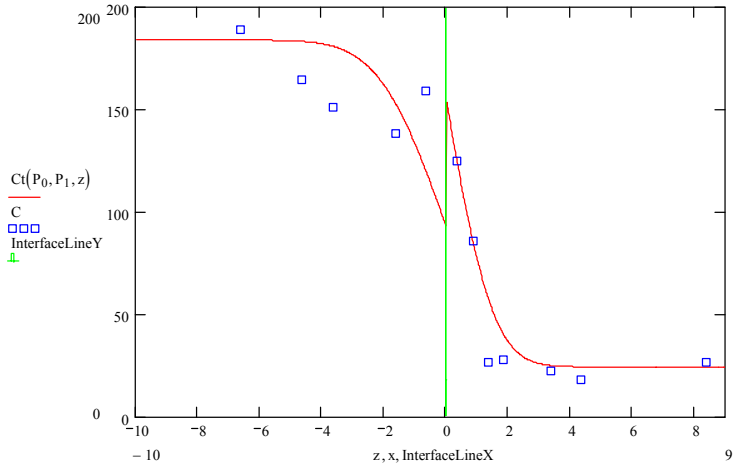

$R_{f,1}$=8124 $R_{f,2}$=13540 COD=0.901 ($R_{f,1} < R_{f,2}$)

Figure 2-12: Br diffusion fitting of Newtown Creek Sediment/N.C. Phosphate

Table 2-3 is a summary of the retardation factor (R_f) regressed from 400 days' migration profiles. Noted that most of the values of R_f are at the order of 10^3 - 10^4 indicating that in these capping system the metal migration are effectively retarded by cap layer.

Table 2-3 Retardation factor (R_f) of capping materials (COD: coefficient of determination, reflecting the fitness)

		Fe	Cu	Zn	Pb
Florida Phosphate	R_f	25000	6079	60820	35030
	COD	0.96	0.94	0.96	0.99
North Carolina Phosphate	R_f	2305	18420	16190	4042
	COD	0.91	0.89	0.97	0.98
Ottawa Sand	R_f	6657	148500	37520	13930
	COD	0.94	0.93	0.91	0.97
GreatBay Sediment	R_f		11750	27860	7144
	COD		0.92	0.93	0.81

The intermixing at the beginning is neglected when doing the fitting to obtain the retardation factors in Table 2-3. From Table 2-2 it can be seen that for some of the materials ΔZ in 400 days are larger than those in 30 days. Although the cores detected in 30 days and 400 days were different cores (that means initial intermixing will be different), the retardation factors (when considering intermixing) can still be estimated by evaluating the differences of ΔZ. For this calculation, the intermixing is simulated by x days of diffusion, then the two profiles of 30 days and 400 days can be seen as the diffusion profiles after (x+30) days and (x+400) days. The two profiles are fit by varying the two variables: x and retardation factor. Table 2-4 shows the retardation factors coming from this fitting procedure. For those cases in which ΔZ of 30 days' are larger than 400 days' this method is not applicable. It can be predicted that when considering intermixing the estimated retardation factors should be larger than those in Table 2-3. The result in Table 2-4 is consistent with this prediction generally. This table also shows that Pb in Florida Phosphate has largest retardation factor which means Florida Phosphate is the best barrier for Pb among these three cap materials.

Table 2-4 Retardation factor (R_f) of capping materials (considering intermixing)

Metal / Cap materials	Cu	Zn	Pb
Florida Phosphate	8.25e4	7.5e4	9.0e4
Ottawa Sand	8.25e4	1.05e5	6.0e4
Great Bay Sediment	4.5e4		5.25e4

2.6 Summary

The metal migration profiles of the columns from UNH migration tanks were measured by synchrotron X-ray Fluorescence (XRF). It was demonstrated that XRF can detect metal migration profiles on the order of mm. Comparison of 30 days' and 400 days' migration profiles reveals that metal migrations are still within or close to the intermixing zone even after 400 days' migration. In other words there is no significant metal migration occur in these capping systems in 400 days. This indicates that under natural condition (using field sediment as migration source) in which the pore water concentration of metals studied is low (e.g. for Pb in Anacostia River sediment that is in ppb level) the cap materials used in this research are good barriers for the metals studied. At the same time this experiment can not provide information to differentiate the effectiveness of different capping materials and migration behavior of different metals due to insufficient migration depths.

2.7 References

Bertin, E.P., *Principles and Practice of X-ray Spectrometric Analysis*, 2nd edn, Plenum Press, New York (1975).

Choy, B. and D.D. Reible, *Diffusion Models of Environmental Transport*, CRC/Lewis Publishers (2000) 184 pp.

Crannell, B.S., Eighmy, T., Willson, C., Reible, D., Yin, M., "Pilot-Scale Reactive Barrier Technologies for Containment of Metal-Contaminated Sediments and Dredge Materials," A Final Report Submitted to the NOAA/UNH Cooperative Institute for Coastal and Estuarine Environmental Technology (CICEET), 2004.

Falkenberg, G, 2002, X-ray Fluorescence (XRF), *Applications of Synchrotron Radiation in Environmental Science, CAMD Summer School* 2002.

Jenkins, R., X-Ray Fluorescence Spectrometry; John Wiley and Sons: New York, 1988, p 51-53, 78-83, 87.

Millington, R.J., Quirk, J.M. (1961) Gas Diffusion, *Trans. Faraday Society*, 57, 1200

Thompson, A.C., Vaughan, D., X-Ray Data Booklet, Lawrence Berkeley National Laboratory, University of California, January 2001.

SSRL, 2003 Report of EnvironSync, Molecular Environmental Science: An Assessment of Research Accomplishments, Available Synchrotron Radiation Facilities, and Needs

Chapter 3

Sorption Isotherm of Metal Species in Sediment and Capping Materials

3.1 Introduction

The interaction of dissolved and sorbed metal species is controlled by metal species aqueous chemistry and the physical-chemical characteristics of the solid materials. A number of models have been developed which can be separated into two categories: empirical equations (sorption isotherm, e.g. Langmuir isotherm, Freundlich isotherm) and mechanistic models (e.g. ion exchange, surface complexation) (Merkel et al., 2002).

Sorption isotherms of metal species describe the equilibrium partitioning of metals between pore water and solid phases. The risk of metal contamination to the environment mostly depends on how much contaminant exists in mobile phase (in most cases, the water phase). Knowledge of the metal sorption isotherm gives us a tool to calculate the metal water phase concentration when the total concentration is known, which is typically much easier to obtain. Sorption isotherms are also the basis for metal fate-and-transport models in porous media. When local instantaneous equilibrium and reversible sorption isotherm can be assumed, the diffusion behavior of metal species in water saturated porous media can be derived from respective sorption isotherm mathematically.

Various sorption isotherms of metal species and different solid materials have been reported (Celis et al., 2000; Reddad et al., 2002; Ko et al., 2003; Prasad et al., 2004; Xiao et al., 2004). Among them the Langmuir and Freundlich isotherms are most frequently applied. Within this context, ‘sorption’ is just a generalized term involving a number of process, including surface adsorption, dissolution and subsequent precipitation (complexation), ion exchange, etc. There is a number of underlying geochemistry

processes that are not well understood and limit the broad applicability of these semi-empirical models. Therefore the usefulness of most of the reported isotherms is limited to specific systems and materials. To study the metal partitioning and transport in our specific sediment and capping systems, it is necessary to first determine the corresponding metal species isotherms. In this chapter, the isotherms of four metal species (Cr(+3), Cu(+2), Zn(+2), Pb(+2)) with 3 capping materials (Florida Phosphate, Phosphil, sand) and Anacostia River sediment under acidic conditions experiment are obtained.

3.2 Background and Literature Review

3.2.1 Metals Speciation, Discharge and Toxicity in Natural Water

The metals being studied in this dissertation are Cr, Cu, Zn and Pb, which are the four major contaminated metals (concentrations greater than 100 ppm) in Anacostia River sediment (Yin, et al., 2004).

3.2.1.1 Chromium

Chromium is not found as a free metal in nature. The most common oxidation numbers of Cr are 6 and 3. Cr (+6) exists only as oxidized species such as CrO_3, CrO_4^{2-} and $Cr_2O_7^{2-}$ and is strongly oxidizing. The most common oxidation state of Cr is +3 which forms large numbers of stable complexes such as Cr_2O_3, $CrCl_3$ etc (Moore et al., 1984).

The principal chromium emissions into surface waters were historically from metal finishing processes such as electroplating, pickling and bright dipping. Soil contamination by chromium includes land disposal of slags as by-products of ferrochrome and chromium steel production or deliberate use of mineral fertilizers. Certain phosphate fertilizers also contain high levels of chromium (Jaworski, 1980).

Cr(+6) is easily reduced by Fe(+2), dissolved sulfides and certain organic compounds with sulfydryl groups. By contrast Cr(+3) is oxidized rapidly by a large excess of MnO_2 and slowly by oxygen at conditions approximating natural waters (Moore, et al., 1984). Cr(+6) is found to be more toxic than Cr(+3) compounds and the solubility of Cr(+6) in water (especially under neutral to basic pH condition) is high and cause high mobility. Acute exposure to Cr(+6) causes nausea, diarrhea, liver and kidney damage, dermatitis, internal hemorrhaging, and respiratory problems (Mohan, et al., 2005).

3.2.1.2 Copper

Copper is widely distributed in nature in the free state and in sulfides, arsenics, chlorides and carbonates. The oxidation states of (+1), (+2), (+3) are typical and Cu (+2) is most common. In aquatic environments, Cu can exist in three broad categories: particulate, colloidal and soluble. The dissolved phase could contain both the free ions as well as complex to organic and inorganic ligands (Moore et al., 1984).

Discharge of mine tailings and fly ash is the major source of solid copper waste. Other sources include fertilizer production and municipal and industrial sewage. Approximately 17,000 metric tons of solid copper wastes are deposited into the oceans annually (Nriagu, 1979).

In estuarine and coastal waters 40-60% of total copper is associated with colloidal matter of organic and inorganic forms (Batley and Gardner, 1978). Copper is sorbed rapidly to sediments. The sorption rate varies with the type of clay/sediment, pH, competing cations and the presence of ligands and the Fe/Mn oxides.

Copper is more toxic in freshwaters and much less toxic in the marine environment due to the high complexing capacity of salt water.

3.2.1.3 Zinc

Zinc is rarely found as the free metal but occurs in a number of minerals – zinc blends, ZnS, smithsonite, $ZnCO_3$, willemite, Zn_2SiO_4, zincite, ZnO and others. Zinc is classified as a borderline element and can bind to inorganic ligands, organic ligands and particulates depending on the physical-chemical characteristics of the aquatic system. The most common oxidation state of Zn is (+2) (Moore et al., 1984).

Non-ferrous metal production and use account for 43% of zinc release to the atmosphere. Other important sources include wood combustion and waste incineration (Nriagu, 1979).

Toxicity of zinc to aquatic plants is highly variable. Acute toxicity of zinc to freshwater invertebrates is relatively low. Zinc is less toxic to fish than Hg, Cu, Ni and Pb.

3.2.1.4 Lead

Pb has stable (+2) and (+4) oxidation states. With the exception of nitrate and acetate, most Pb(+2) salts are insoluble in water. The behavior of Pb in natural water is a combination of precipitation equilibrium and complexing with inorganic and organic ligands. The degree of mobility of lead depends on the physical-chemical state of the complex formed (Moore et al., 1984).

The majority of lead deposited on land comes from mining. Atmospheric fallout is the most important source of lead in marine and freshwater.

Lead is toxic to humans. No organ system is immune to the effects of lead poisoning and the organ of most concern is the brain. The effects of lead poisoning on the brain are manifold and include delayed or reversed development, permanent learning disabilities, seizures, coma, and even death.

3.2.2 Metals Sorption from Water to Solid

The sorption of metals from water phase to solid phase includes matrix sorption and surface sorption. Matrix sorption can be described as exchange of constituents contained in water into the porous matrix of solid. Surface sorption is understood to be the accretion of solute atoms or molecules at the phase boundary. Surface sorption may occur by physical binding forces (van de Waals forces, physisorption), by chemical bonding, or by hydrogen bonding (chemisorption). While physisorption is reversible in most case, remobilization of constituents bound by chemisorption is difficult (Merkel et al., 2002).

3.2.3 Mathematical Description of the Sorption

There are a number of equations used to describe the experimental data for the interactions of metals in water with solid phase. They can be categorized into two types: empirical equations (sorption isotherm) and mechanistic models (Merkel et al., 2002).

3.2.3.1 Empirical Models

The most commonly used empirical models are linear regression isotherm (Henry isotherm), Langmuir isotherm and Freundlich isotherm as following:

Henry isotherm is defined as:

$$q = K_d \cdot C \qquad (1)$$

In which q (mg/g) is the mass of the metal sorbed, C (mg/L) is concentration of the metal in water and K_d (L/mg) is partition coefficient. A major disadvantage of this model is there is no upper limit to the sorption.

The Langmuir isotherm (Langmuir, 1918) is defined as:

$$q = \frac{N_m \cdot K \cdot C}{1 + K \cdot C} \qquad (2)$$

In which K is sorption constant and N_m is the maximum sorption capacity. The Langmuir isotherm was developed to describe sorbents with a limited number of sorption sites on their surface (Langmuir, 1918).

The Freundlich isotherm (Freundlich, 1906) is defined as:

$$q = K \cdot C^{\beta} \tag{3}$$

In which K and β are fitting parameters. The Freundlich isotherm is based on a model of a multi-layer coating of the solid surface assuming that all sites with the largest binding energy are occupied first and with increasing grade sites with lower binding energy being occupied later. For this model there is no upper limit to sorption, either.

The extended and combination forms of Langmuir and Freundlich isotherm include Sips isotherm, Redlich-Peterson isotherm, competitive Langmuir isotherm, and competitive Freundlich isotherm as follows:

Sips isotherm (Sips, 1948) is defined as:

$$q = \frac{N_m \cdot K \cdot C^{\beta}}{1 + K \cdot C^{\beta}} \tag{4}$$

Redlich-Peterson isotherm (Redlich et al., 1959) is defined as:

$$q = \frac{N_m \cdot K \cdot C}{1 + K \cdot C^{\beta}} \tag{5}$$

Competitive Langmuir isotherm (Adamson, 1990) is defined as:

$$q_i = \frac{N_m \cdot K_i \cdot C_i}{1 + \sum_{k=1}^{n} K_k \cdot C_k} \tag{6}$$

Competitive Freundlich isotherm (Sheindorf et al. 1981) is defined as:

$$q_i = K_i \cdot C_i \cdot (\sum_{k=1}^{n} a_{ik} \cdot C_k)^{n-1} \quad (7)$$

In which the definition of q, C, N_m, K, β are same as above. a_{ik} is interaction coefficient of metal species i to k.

3.2.3.2 Mechanistic Models

At the present time most of the widely used mechanistic geochemical modeling are of two types: ion exchange which includes simple ion exchange model and power exchange function model and surface complexation models including Diffuse Double-Layer Model, Constant-Capacitance Model, Triple-Layer Model (Langmuir, 1997). In general ion exchange models are used for the major ions in natural systems rather than for minor and trace components (Chen et al., 2002).

3.2.4 Metal Adsorption Onto Apatite

Apatite materials and their interaction with metals are the primary focus in this dissertation. In nature, the apatite mineral structure conforms to the 6/m class of minerals with hexagonal crystal structure and the generic formula $Me_5(XO_4)_3Z$ where Me is Ca, Sr, Ba, Cd, or Pb, X= P, As, V, Mn, or Cr; and Z= OH, F, Cl, or Br. The family includes the minerals abukumalite, britholite, carbonate apatite, chlorapatite, dahllite, ellestadite, fermorite, fluorapatite, francolite, hydroxyapatite, mimetite, pyromorphite, svabite, vanadinite, and wilkeite (Nriagu and Moore, 1984).

Apatites have been very well characterized with respect to surface properties and are capable of reacting with heavy metals through both surface sorption reactions and precipitation reactions (Traina and Laperche, 1999; Somasundaran and Wang, 1984; Chander and Fuerstenau, 1984; Singh et al., 2001; Monteil-Rivera et al., 1999; Bailliez et al., 2004; Fuller et al., 2003; Fedoroff et al., 1999). Generally, divalent metals such as Cd,

Cu, Ni, and Zn will undergo sorption to the hydroxyapatite surface at low metal cation concentrations, form solid solutions (e.g. $(Me,Ca)_5(PO_4)_3OH$) at concentrations around metal apatite saturation, and pure metal precipitates on the hydroxyapatite surface at concentrations above metal precipitate saturation (Misra et al., 1984; Xu et al., 1994). The sorption of these divalent metal ions is considered to take place mainly via ion exchange with Ca^{2+} of apatite lattice (Suzuki et al., 1981). Peld et al.(2004) found that for Zn^{2+} and Cd^{2+} sorption onto synthetic Ca-apatite ion-exchange with Ca^{2+} is the dominant mechanism. Prasad, et al.(2004) studied a sedimentary phosphate material and summarize that for Cu and Zn solutions, ion exchange is dominant and for Pb the dissolution-with-precipitation mechanism is more predominant than ion-exchange. Other work has determined that at high metal (Pb) concentrations, hydroxyapatite and other apatite minerals dissolve, while a more thermodynamically favorable pyromorphite mineral ($Pb_5(PO_4)_3OH$) formed (Laperche *et al*., 1996; Ma *et al*., 1994; Ma *et al*., 1995). This later type of reaction mechanism would be preferred over an ion exchange reaction because of the greater geochemical stability of the pure crystalline reaction product.

XRD analysis demonstrated that North Carolina Phosphate interacted with Cr were predominated by chromium phosphate minerals ($Cr(PO_3NH_3)_2NO_3$-$6H_2O$, $CrPO_4$). These phosphate compounds are not the highly stable reaction products (Crannell et al., 2004).

Heavy metals have been shown to react with apatite minerals by first forming a poorly-crystalline solid solution, which slowly transforms to the purer, more highly crystalline products. The sorption reactions for heavy metals on apatite surfaces are very fast (on the order of hours) and somewhat reversible. By contrast the crystallization of these sorbed metals and the metal precipitation reactions are slower (on the order of days to months) and less reversible (Kohn et al., 2002).

3.2.5 Metal Adsorption Onto Sediment

When metals are adsorbed onto sediment they may be partitioned into six fractions: dissolved, exchangeable, carbonate, iron-manganese oxide, organic and crystalline. Partitioning is affected strongly by variations in pH, redox state, organic content, and other environmental factors (Elder, 1989; Salomons, 1995). Wen et al.(1998) used surface complexation model (including Diffuse Double-Layer Model, Constant-Capacitance Model, Triple-Layer Model) to predict the adsorption behavior of natural sediment successfully.

3.2.6 pH Effect on Metal Sorption

The solution pH affects the surface charge of the adsorbent, the degree of ionization, and the speciation of the surface functional groups. Just a few metal ions (e.g. Na^+, K^+) are soluble to the same extent across the range of pH values of normal ground water. In general the dissolution and precipitation of metal ions in water are strongly pH dependent (Merkel et al., 2002). Sauve et al.(2000) summarized results from over 70 studies and found that for some divalent metal ions like Cu^{2+}, Zn^{2+}, Cd^{2+}, Pb^{2+} and Ni^{2+} the log of solid-liquid partition coefficients ($\log_{10} K_d$) are predicted using empirical linear regressions with pH. For Cu^{2+}, Zn^{2+} and Pb^{2+} when pH values approach 7, K_d values go to 10^3 to 10^4 Lkg^{-1}, which means that most of the metal is adsorbed on solid phase. Reddy et al. (1995) investigated soil samples from Wyoming and found that at near neutral pH, dissolved metal concentration in soil water extracts was dominated by DOC-metal complexes (DOC is dissolved organic carbon) and at low pH, dissolved metal concentration in soil water extracts was dominated by free ionic forms (e.g. Cu^{2+}, Zn^{2+}, Pb^{2+}).

3.3 Materials and Methods

3.3.1 Materials

The Sediment used in this experiment is Anacostia River sediment sampled from the Anacostia River capping project demonstration site (HSRC, 2004) in October, 2004. The first step was to tumble the sediment for 24 hours to achieve homogeneity. The average moisture content is around 51%.

The capping materials used are Play Sand, Florida Phosphate and Phosphil. Florida Phosphate, a powder like material, was collected from the IMC Agrico mine in Mulberry, Florida. Phosphil (a trade name) is a "waste" phosphate product from PCS-Phosphate, produced from oversized sand grained materials collected from the PCS-Phosphate Mine in Aurora, North Carolina and is used in Anacostia River demonstration capping site. These two phosphate materials were selected to represent naturally occurring phosphate minerals, which could affordably be used on a larger scale.

The particle size distribution of play sand and Florida Phosphate were investigated by sieve (USA standard sieve) analysis. Table 3-1 lists the results.

Table 3-1 Particle size distribution of play sand and Florida Phosphate

		Play sand	Florida Phosphate
Sieve #	d_50 (mm)	Wt%	Wt%
20/30	0.72	10.32	5.61
30/40	0.51	22.88	12.34
40/50	0.36	34.78	25.48
50/60	0.275	11.10	14.83
60/80	0.215	13.63	24.08
80/100	0.165	3.74	8.84
100/200	0.1125	3.55	8.81
Average diameter (mm)		0.39	0.31

(d_50: the average mesh size of two sieves)

The baseline metal concentrations in these materials and particularly the pore water metal concentration of the sediment are measured by ICP-MS and listed below (pore

water samples were obtained from the overlying water separated from the sediment after being centrifuged by Beckman J-6B Centrifuge):

Table 3-2 Baseline metal concentrations of sediment and capping materials

	Pore water in sediment (μg/L)	*Sediment(dry basis) (mg/kg)*	*Florida Phosphate (mg/kg)*	*Phosphil (mg/kg)*
Be	0	0.70	1.88	*0.963*
Mg	104000	3918.37	1480	2290
Al	86.2	18612.24	5480	2310
Ti	4.78	244.90	360	252
V	5.3	71.63	74.5	15.2
Cr	2.92	118.37	39.5	43.9
Mn	6580	422.45	189	15.2
Fe	11200	29183.67	6100	5240
Ni	130	257.14	60.9	38.1
Co	73.8	18.92	8.11	0.795
Cu	2.38	203.27	3.6	5.95
Zn	818	606.12	53.5	43.2
As	8.18	11.47	13.7	11.7
Se	3.5	2.90	4.78	2.77
Mo	8.48	1.57	4.78	5.2
Ag	0.134	22.45	0.385	0.374
Cd	0.682	4.73	2.66	4.22
Sn	0.184	2.14	5.09	1.83
Sb	5.12	0.22	2.08	0.716
Ba	144	312.24	94	63.9
Tl	0.0772	0.20	2.2	1.04
Pb	14.5	269	17.3	1.65

The porosities and densities of Florida Phosphate and Phosphil are measured by a simple method:

1) Add dry solid to a graduated cylinder and record the volume and weight of the solid, thus the bulk density can be calculated.

2) Add water to dry solid in the graduated cylinder until it reaches the top of solid layer. Porosity is the volume of added water dividing by the solid layer volume.

3) Particle density can be calculated from bulk density and porosity.

The results are shown below:

Table 3-3 Physical characteristics of phosphorite materials

	Porosity	*Particle density (g/cm^3)*	*Bulk density (g/cm^3)*
Florida Phosphate	0.4	2.61	1.96
Phosphil	0.4	2.56	1.93

There are four metal species investigated in this study. They are Cr(+3), Cu(+2), Zn(+2) and Pb(+2) obtained by dissolution and dilution of the following chemicals ordered from *SIGMA-ALDRICH* respectively.

$CrCl_3$, chromium (III) chloride, CAS number: 10025-73-7, purity ≥98%

$Cu(NO_3)_2$, copper (II) nitrate, CAS number: 19004-19-4, purity ≥99.999%

$Zn(NO_3)_2$, zinc nitrate, CAS number: 10196-18-6, purity ≥98%

$PbCl_2$, lead (II) chloride, CAS number: 7758-95-4, purity ≥98%

3.3.2 pH and Temperature

The ambient temperature of the experiment is 25 °C. The equilibrium pH values range from 4-6 (varied with the concentrations of metal solution) and the average value is around 5. PHREEQC 2.12.5.669 model was used to check if there is any metal species precipitation at this pH condition and predict the dissolved metal ion speciation. PHREEQC version 2 is a computer program written in the C programming language that is designed to perform a wide variety of low-temperature aqueous geochemical calculations. Table 3-4 and 3-5 are the PHREEQC simulation results of the metal speciation in distilled water at pH 5.0.

Table 3-4 Cu speciation in Mono-element (Cu(II)) solution

Speciation	Molarity(mol/L)	%
Cu(II)(total)	1.54E-02	
Cu^{2+}	1.53E-02	99.286
$Cu_2OH_2^{2+}$	4.69E-05	0.304
$CuOH^+$	8.81E-06	0.057
$Cu(OH)_2$	1.55E-06	0.010
$Cu(OH)_3^-$	1.11E-14	0.000
$Cu(OH)_4^{2-}$	3.61E-22	0.000

Table 3-5 Metal speciation in tetra-element (Cr(III), Cu(II), Zn(II), Pb(II)) solution

Speciation	Molarity(mol/L)	%		Speciation	Molarity(mol/L)	%
Cr(III)(total)	1.89E-02			**Cu(II) (total)**	1.54E-02	
$Cr(OH)^{2+}$	1.29E-02	68.134		Cu^{2+}	1.54E-02	99.611
Cr^{3+}	4.56E-03	24.178		$Cu_2(OH)_2^{2+}$	2.47E-05	0.160
$Cr(OH)_2^{+}$	1.44E-03	7.641		$CuOH^{+}$	5.94E-06	0.038
$Cr(OH)_3$	8.08E-06	0.043		$Cu(OH)_2$	9.22E-07	0.006
CrO_2^{-}	2.59E-11	0.000		$Cu(OH)_3^{-}$	7.35E-15	0.000
$Cr(OH)_4^{-}$	1.02E-11	0.000		$Cu(OH)_4^{2-}$	3.12E-22	0.000
Zn(II)(total)	1.50E-02	%		**Pb(II)(total)**	9.47E-04	%
Zn^{2+}	1.50E-02	100.000		Pb^{2+}	9.46E-04	99.894
$ZnOH^{+}$	8.27E-07	0.006		$PbOH^{+}$	8.62E-07	0.091
$Zn(OH)_2$	7.20E-10	0.000		Pb_2OH^{3+}	5.02E-08	0.005
$Zn(OH)_3^{-}$	3.00E-16	0.000		$Pb(OH)_2$	2.54E-11	0.000
$Zn(OH)_4^{2-}$	1.02E-23	0.000		$Pb_3(OH)_4^{2+}$	1.47E-14	0.000
				$Pb(OH)_3^{-}$	3.84E-17	0.000
				$Pb(OH)_4^{2-}$	1.89E-23	0.000

From these two tables we can see almost all metals are dissolved in solution. Cu, Zn and Pb exist as free ions dominantly in water solution. Most Cr exists as complex ion $Cr(OH)^{2+}$ and free ion Cr^{3+}.

3.3.3 Isotherm Measurement Procedure

- The metal solutions are made by diluting the stock chemicals in distilled water with pH value of 7.3.
- Put W(i) grams of solid (phosphate, Phosphil and sand are dry; Sediment is kept in original wet form) in a 50 mL polypropylene centrifuge tube containing C(i) mg/L metal ion solution (i=1..n, n is the total number of data points in isotherm); make the final solution volume in centrifuge tubes to 50 mL.

  W(i) ranges from 0.4 to 0.6 g; C(i) ranges from 1000 to 0.1 mg/L;
- Put all the 50 mL centrifuge tubes in a reciprocating shaker and shake for 24 hours;

- For the sand, phosphate and Phosphil systems, precipitation occurred after relatively short time (several hours) and the solid and water separated pretty clearly. Therefore, a clear water sample could easily be obtained. For the sediment system, the centrifuge tubes are centrifuged using Beckman J-6B Centrifuge for 10 minutes at 3500 rpm, 2520 g. After this the sediment and water are separated clearly and a clear water sample can be obtained.
- Measure metal concentrations C(i) and C(i)' of all the water samples obtained from the above process using ICP-MS (Perkin Elmer ELAN 9000). Four-point calibration is employed to construct the standard curve for ICP-MS. The concentrations used in these calibration solutions are 20, 50, 100, 500 μg/L. The internal standards used are Sc, Ge, Y, Ln, Bi with concentration of 20 μg/L. The measuring method parameters of ELAN 9000 are: dwell time 50 ms, sweeps/reading 20, 3 replicates for each sample, sample flush time 20s, flush pump speed 48 rpm, read delay 20s, read pump speed 24rpm, wash time 45 s, and wash pump speed 48 rpm.
- Calculate the solid phase concentrations by mass balance:

  $\Delta C(i) = C(i) - C(i)'$, (8)

  The change of solid phase concentration, i.e. the metal sorbed by solid is given by

  $$\Delta Cs(i) = \left[\frac{50 - W(i)/\rho}{1000} * \Delta C(i) \right] \Big/ W(i) \quad mg/g, \tag{9}$$

  ρ is the density of solid;

  Then solid phase concentration $Cs(i) = Cs0 + \Delta Cs(i)$ (10)

  $Cs0$ is the original metal concentration in solid, which is measured separately by metal digestion, following ICP-MS.

3.4 Results and Discussion

The isotherms under acidic conditions (average pH value 5.0) with different materials and metal species are shown in Figure 3-1 through Figure 3-20, where the amount of metal species adsorbed per unit dry weight of solid materials are plotted as the function of equilibrium metal concentration in water phase. Two series of experiments are carried out. One is mono-element system, i.e. Cu(+2) and Cr(+6) with Florida Phosphate and Anacostia River Sediment and another is tetra-element system (Cr(+3), Cu(+2), Zn(+2), Pb(+2)) with sand, Florida Phosphate, Phosphil and Anacostia River sediment.

The isotherm data of sand is too scattered to achieve reasonable fitting, which is probably due to the fact that sorption of metals in sand is much weaker than that in apatite and sediment. For other materials it was found that most isotherms are better fitted by Langmuir isotherm rather than Freundlich isotherm (The fitting processes were carried out using Origin®5.0). Langmuir equation has two forms. One is

$$Ws = \frac{a \cdot C}{1 + b \cdot C} \tag{11}$$

Where Ws (mg/g) is the mass sorbed, C (mg/L) is the water phase concentration at equilibrium. a (L/g) and b (L/mg) are fitting parameters. When C goes to zero, $Ws \to a \cdot C$, a becomes the gradient of the linear approximation of Langmuir isotherm.

Another form is:

$$Ws = \frac{W_m \cdot K \cdot C}{1 + K \cdot C} \tag{12}$$

Where K (L/mg) is sorption constant, W_m (mg/g) is the maximum sorption capacity or saturation concentration (as $C \to +\infty, Ws \to W_m$) and when it is divided by respective metal atomic weight A it can be transferred to N_m (mmol/g). Obviously $K = b$, $W_m = a / K$, $N_m = W_m / A$.

All Langmuir models fitted here use equation (11) to obtain parameters a and b first and then transfer to N_m and K. It can be easily seen from equation (12) that Ws increases with K when C and N_m are unchanged. That means K reflects how dramatically the isotherm curve approaches saturation concentration.

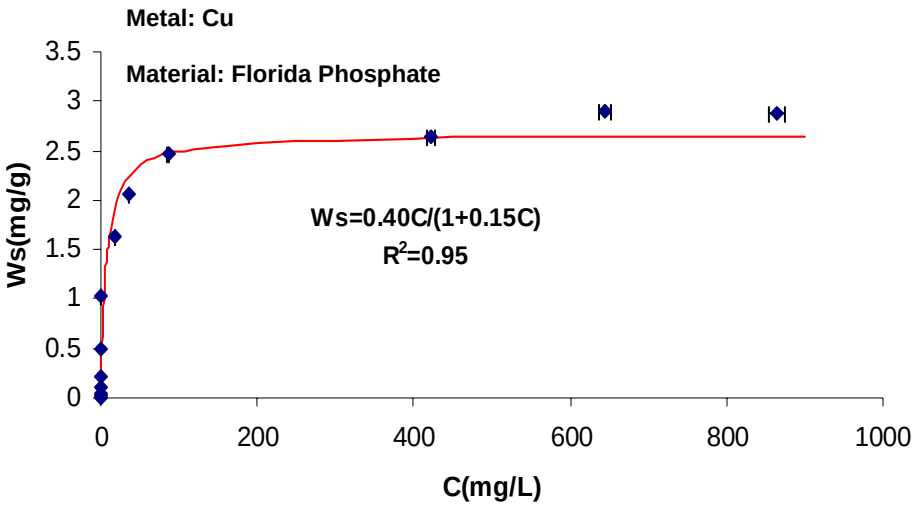

Figure 3-1 Cu(+2) Isotherm in Florida Phosphate (Mono-element system)

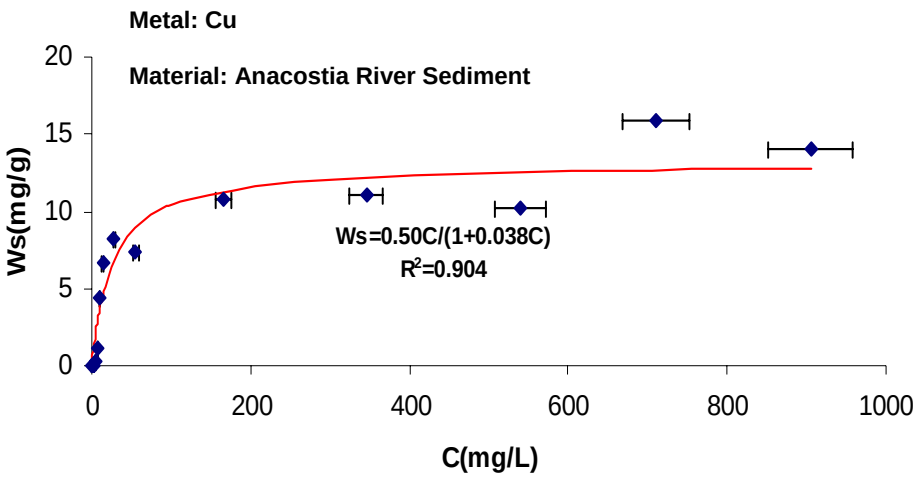

Figure 3-2 Cu(+2) Isotherm in Anacostia River Sediment (Mono-element system)

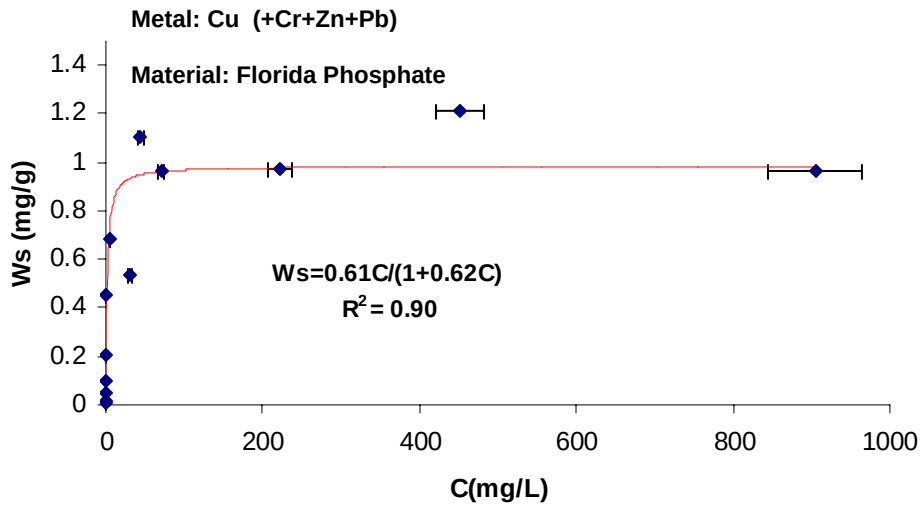

Figure 3-3 Cu(+2) Isotherm in Florida Phosphate (Tetra-element system)

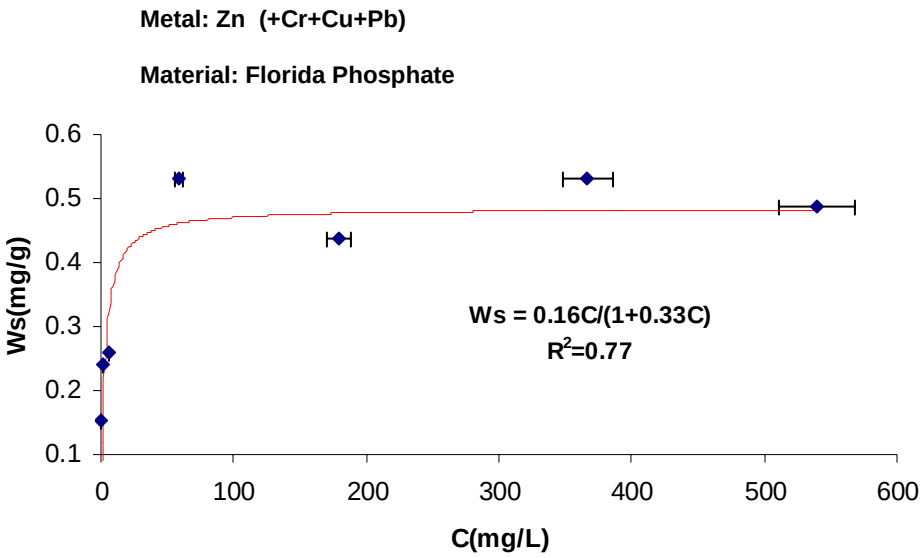

Figure 3-4 Zn(+2) Isotherm in Florida Phosphate (Tetra-element system)

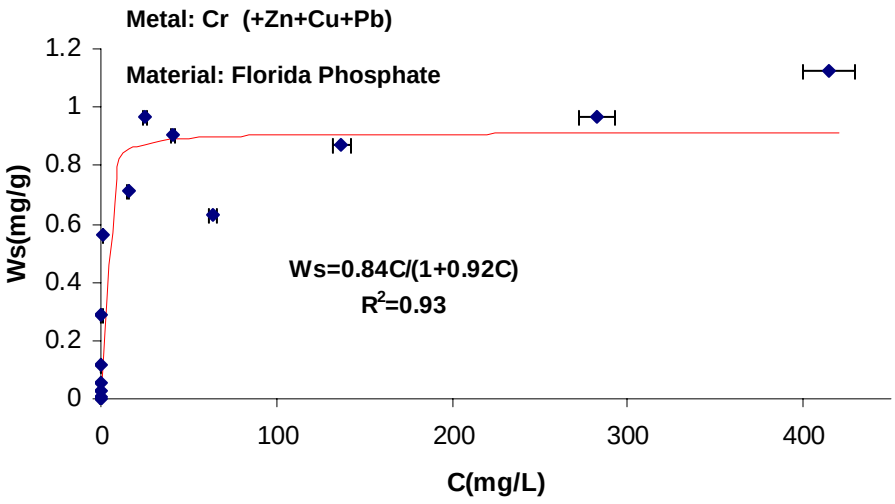

Figure 3-5 Cr(+3) Isotherm in Florida Phosphate (Tetra-element system)

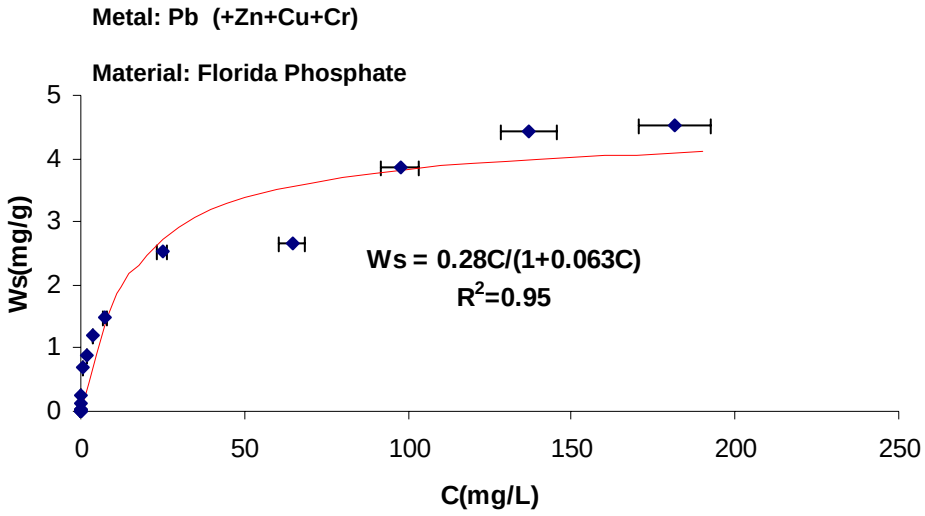

Figure 3-6 Pb(+2) Isotherm in Florida Phosphate (Tetra-element system)

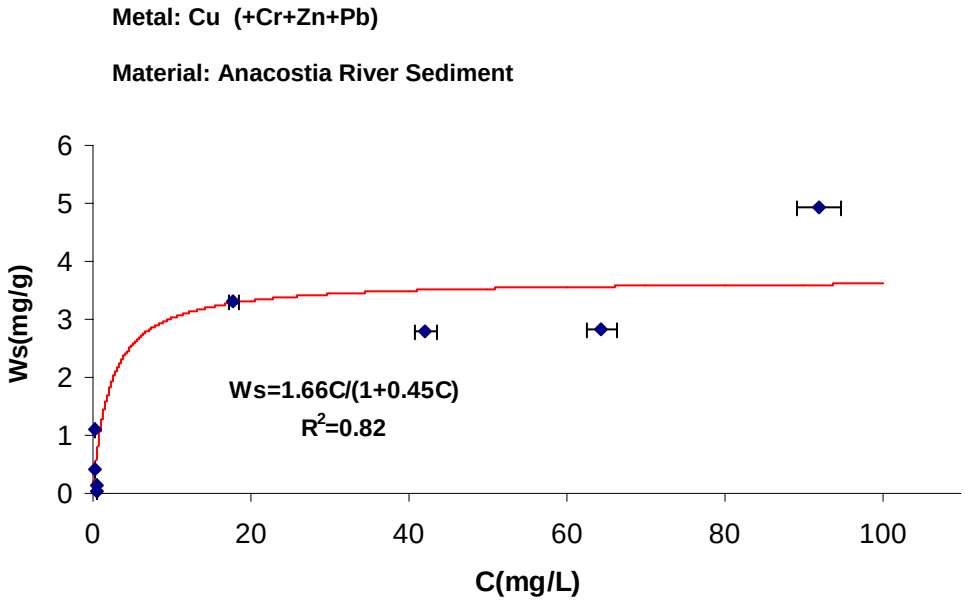

Figure 3-7 Cu(+2) Isotherm in Anacostia River Sediment (Tetra-element system)

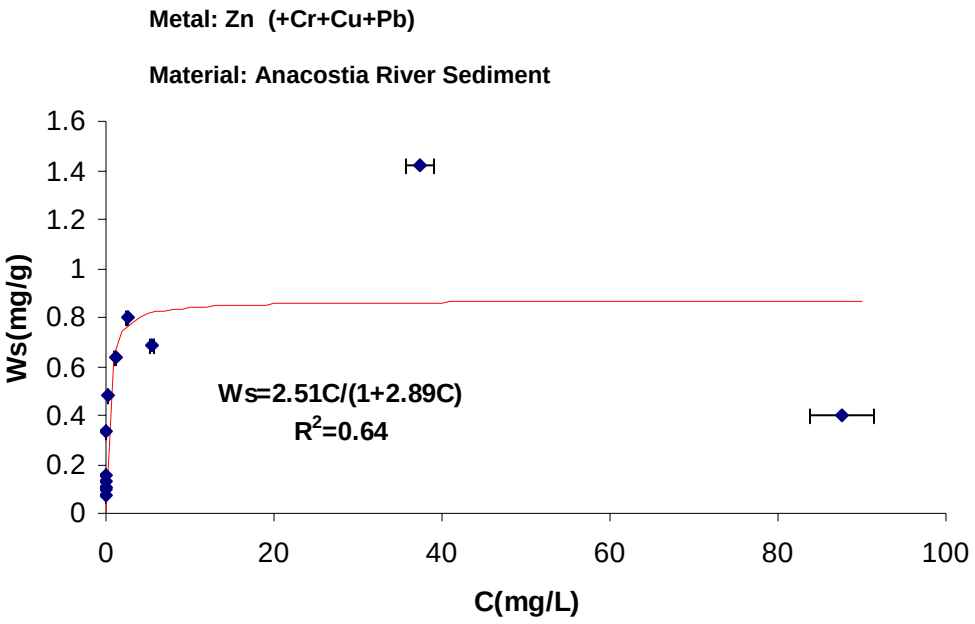

Figure 3-8 Zn(+2) Isotherm in Anacostia River Sediment (Tetra-element system)

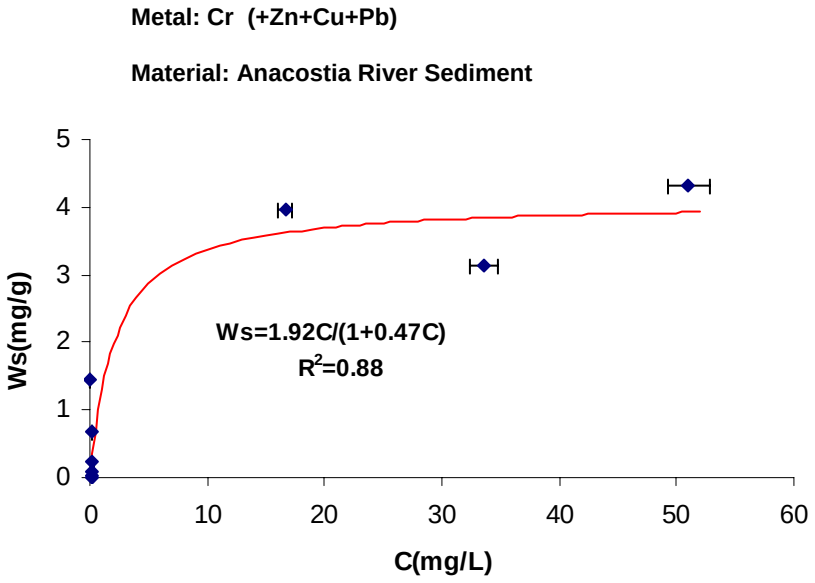

Figure 3-9 Cr(+3) Isotherm in Anacostia River Sediment (Tetra-element system)

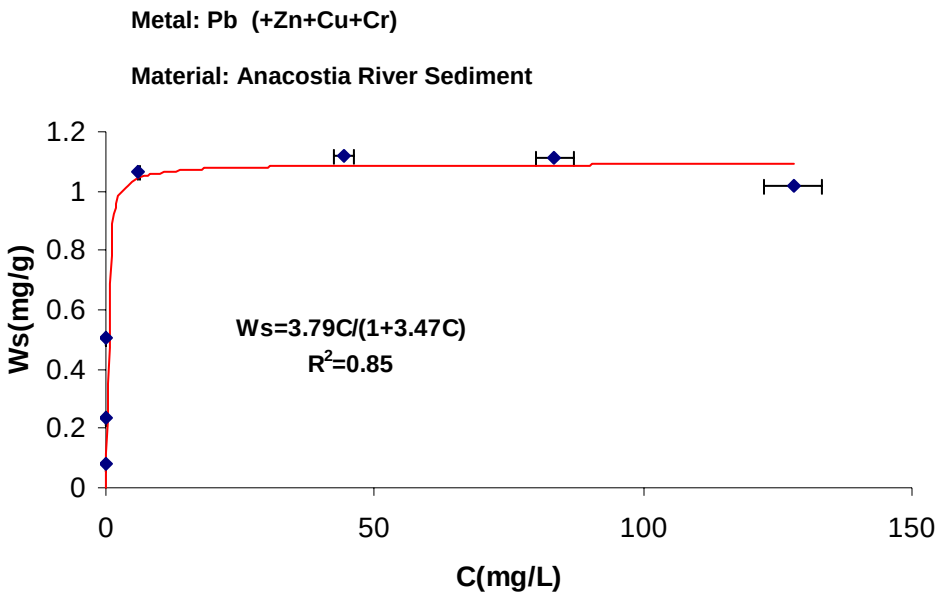

Figure 3-10 Pb(+2) Isotherm in Anacostia River Sediment (Tetra-element system)

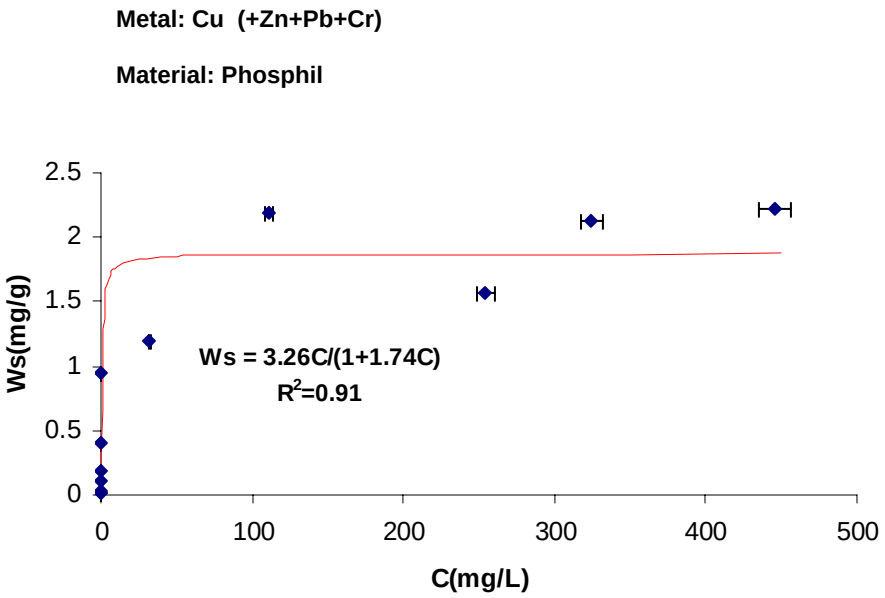

Figure 3-11 Cu(+2) Isotherm in Phosphil (Tetra-element system)

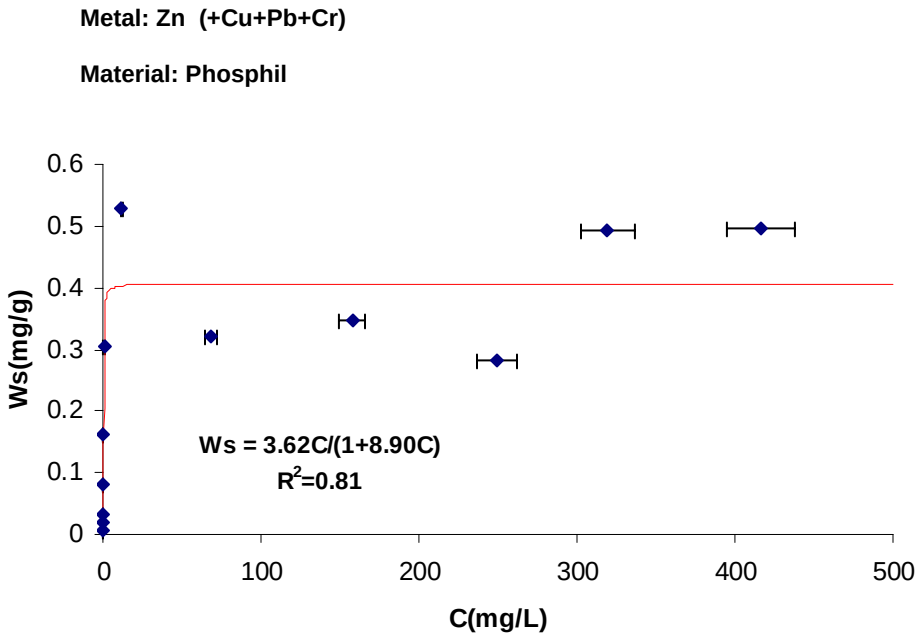

Figure 3-12 Zn(+2) Isotherm in Phosphil (Tetra-element system)

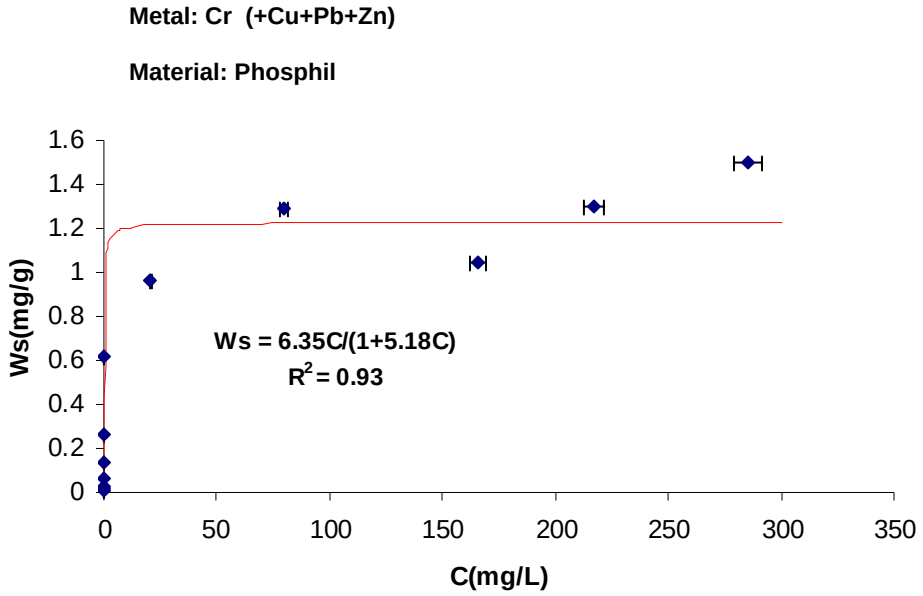

Figure 3-13 Cr(+3) Isotherm in Phosphil (Tetra-element system)

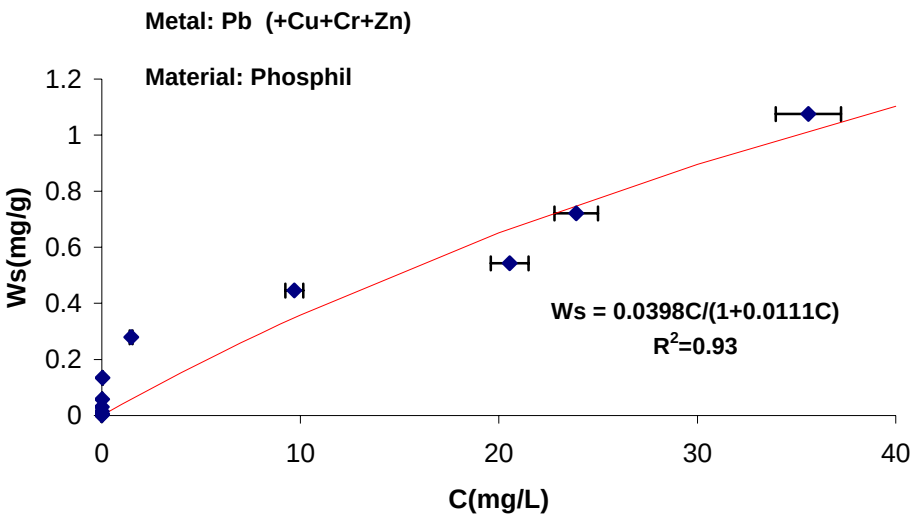

Figure 3-14 Pb(+2) Isotherm in Phosphil (Tetra-element system)

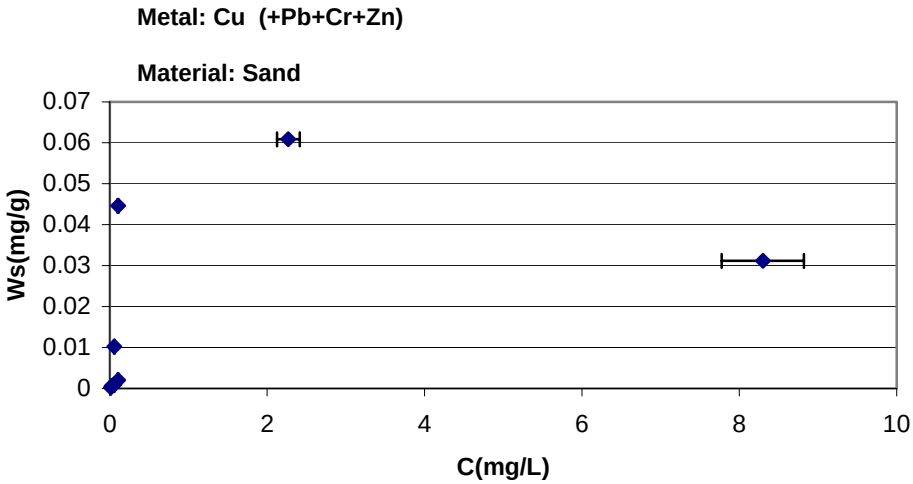

Figure 3-15 Cu(+2) Isotherm in sand (Tetra-element system); Maximum sorption capacity is 0.05 mg/g

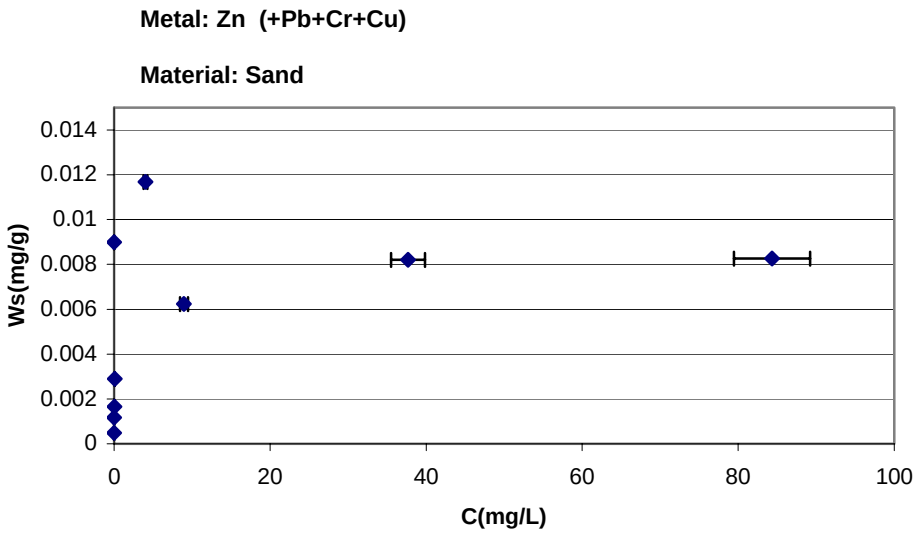

Figure 3-16 Zn(+2) Isotherm in sand (Tetra-element system); Maximum sorption capacity is 0.008 mg/g

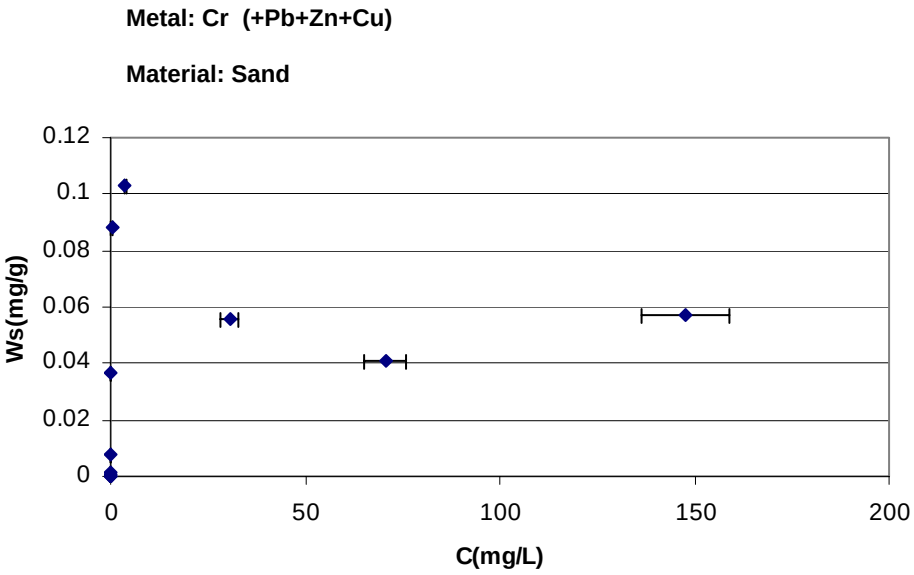

Figure 3-17 Cr(+3) Isotherm in sand (Tetra-element system); Maximum sorption capacity is 0.06 mg/g

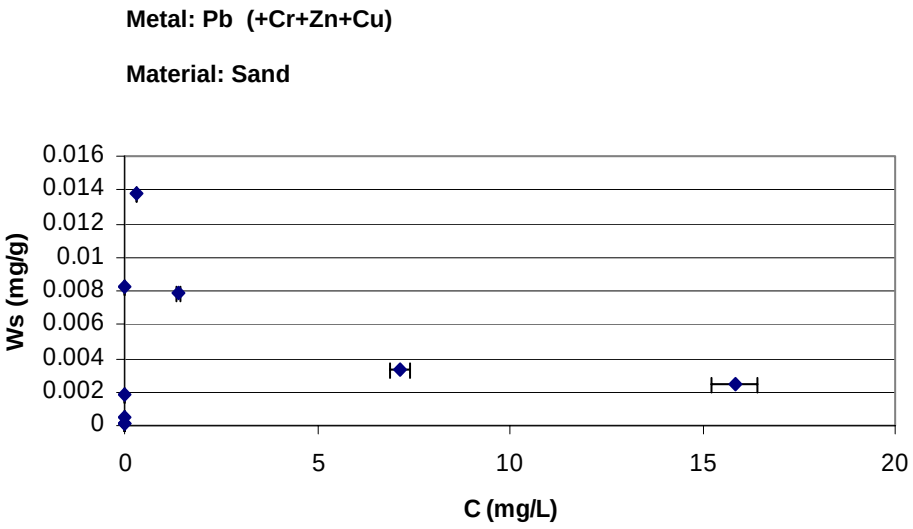

Figure 3-18 Pb(+2) Isotherm in sand (Tetra-element system); Maximum sorption capacity is 0.006 mg/g

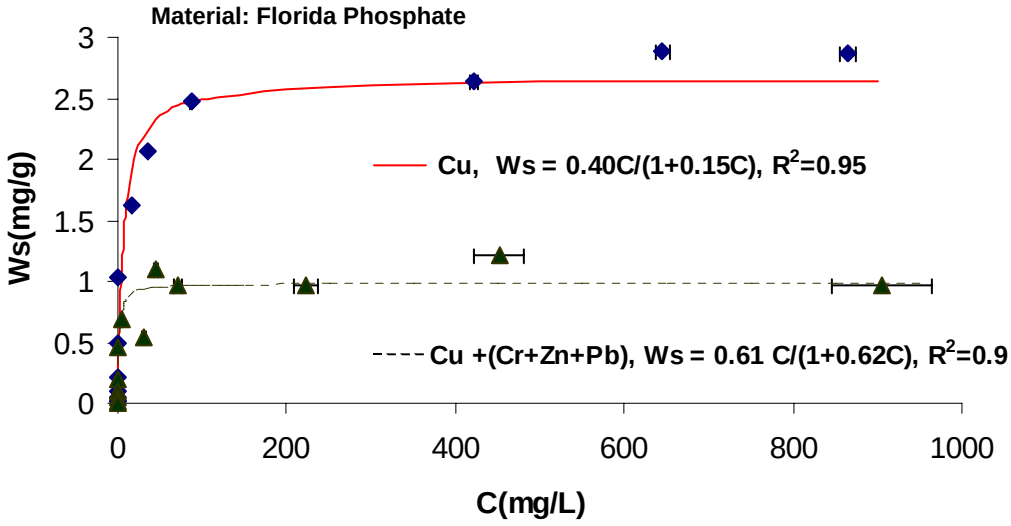

Figure 3-19 Comparison of Cu(+2) isotherm in Florida Phosphate in mono and tetra-element systems

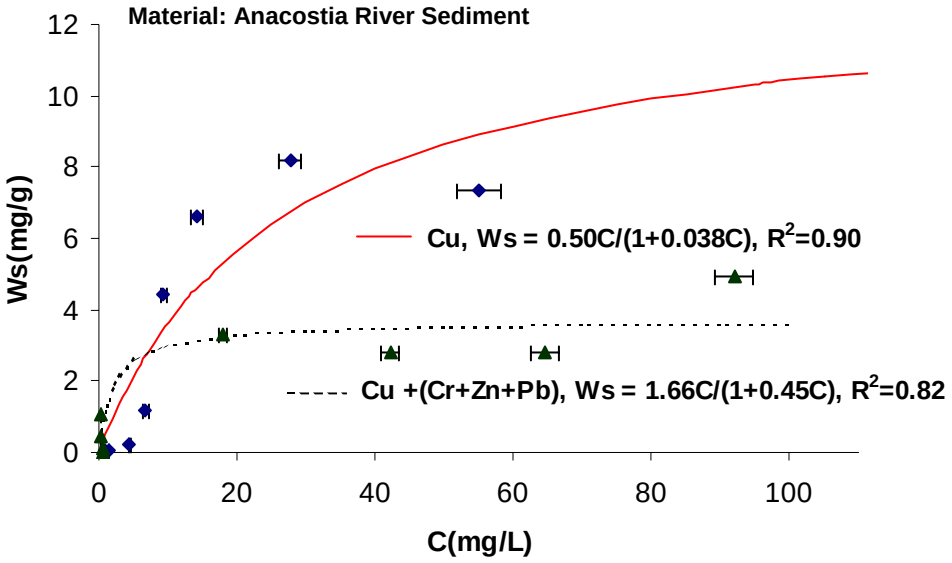

Figure 3-20 Comparison of Cu(+2) isotherm in Anacostia River Sediment in mono and tetra-element systems

Sand appears to very easily reach the maximum sorption capacity. Comparison with apatite materials and sediment shows that its ability of metal sorption can be neglected. This is most likely due to the fact that sand is dominated by quartz (SiO_2) (Crannell et al., 2004) which is not reported to have strong affinity to metals. The metal affinity order for sand is determined by maximum sorption capacity, which is Cr > Cu > Zn > Pb. This order is just the reverse order of atomic number.

Table 3-6 Langmuir parameters of different materials

		Anacostia River Sediment				Florida Phosphate				Phosphil			
		Wm	Nm	K	R^2	Wm	Nm	K	R^2	Wm	Nm	K	R^2
Cu	1	13.16	0.207	0.038	0.90	2.667	0.0420	0.15	0.95				
	2	3.689	0.058	0.45	0.82	0.9839	0.0155	0.62	0.90	1.874	0.0295	1.74	0.91
Cr	2	4.085	0.0786	0.47	0.88	0.9130	0.0176	0.92	0.93	1.226	0.0236	5.18	0.93
Zn	2	0.8685	0.0133	2.89	0.64	0.4848	0.00741	0.33	0.77	0.4067	0.00622	8.9	0.81
Pb	2	1.092	0.00527	3.47	0.85	4.444	0.0215	0.063	0.95	3.586	0.0173	0.0111	0.93

Wm: mg/g; Nm: mmol/g; K: L/mg; R^2: fitting parameter.
1: mono-element system
2: tetra- element system

From the Figure 3-19, 3-20 and table 3-3 it can be seen that competitive adsorption strongly affects the copper sorption in the tetra-element systems. In tetra-element system the sorption of copper is much weaker than that in mono-element system. When adding up the maximum sorption capacity Nm of four elements of tetra-element systems to Nm2 and comparing this with the corresponding Nm value of mono-element system (defined as Nm1) it is found that for sediment Nm1 > Nm2 and for Florida Phosphate Nm2 > Nm1. This implies that metal species in tetra-element system in Florida Phosphate may be adsorbed on a second layer. This does not necessary contradict the traditional mono-layer coverage assumption of the Langmuir equation because mathematically Langmuir model is essentially based on the presumption of limited number of adsorption site, not mono layer.

A couple of observations can be made for the sequences of maximum sorption capacity Wm of tetra-element systems from the isotherms and the Table 2-3:

- For Cr, Cu, the sequence is Sediment > Phosphil > Florida Phosphate
- For Zn, the sequence is Sediment > Florida Phosphate $\approx$ Phosphil
- For Pb, the sequence is Florida Phosphate > Phosphil > Sediment
- For Florida Phosphate, the sequence is Pb > Cu > Cr >Zn
- For Phosphil, the sequence is Pb > Cu > Cr >Zn
- For Anacostia Sediment, the sequence is Cr > Cu > Pb >Zn

For Cr, Cu and Zn Anacostia River sediment has the maximum sorption capacity. Among all four materials investigated, the Anacostia River sediment has smallest particle size and highest organic content. It is reported that organic matter is the most important sorbent that controls the activity of Cu^{2+}, Zn^{2+}, Cd^{2+} and Ni^{2+} in sandy soil while Pb is an exception with strong adsorption on iron hydroxide (Weng et al., 2001).

For Pb, apatite materials demonstrate extraordinary adsorption ability, which is consistent with other researcher's observations (Kaplan and Knox, 2004). There is also some XRD analysis indicating the formation of pure pyromorphite minerals ($Pb_5(PO4)_3OH$) when Pb is removed from solution by phosphorite materials (Crannell, et al., 2001).

In the case of Florida Phosphate, the ionic radius appears to determine the maximum sorption capacity order of Pb > Cu > Zn. The ionic radius of Pb^{2+},Ca^{2+}, Cu^{2+}, Zn^{2+} are 1.20 Å, 0.99 Å, 0.96 Å, 0.74 Å respectively. It has been reported that in the ion-exchange process, larger multivalent ions are more effectively removed than smaller ones (Christopher et al., 2002). This might be the reason for the maximum sorption capacity order of Florida Phosphate.

3.5 Summary

The isotherms of four metal species (Cr(+3), Cu(+2), Zn(+2), Pb(+2)) with 3 capping materials (Florida Phosphate, Phosphil, sand) and Anacostia River sediment under acidic condition are obtained. The Langmuir isotherm fits the isotherm data reasonably well. Under neutral pH condition most of these four metal species have low dissolved concentrations in water (lower than 1 ppm) implying that no isotherm with high water phase concentration will exist under neutral pH condition.

Among all the materials and metals tested, sand has a significantly lower sorption capacity. This suggests that apatite materials are much better capping materials than sand in terms of metal retardation. Two apatite materials have best sorption ability for Pb. Phosphil has greater sorption capacity for Cr, Cu and Zn than Florida Phosphate and has just slightly less sorption capacity for Pb. For all materials tested Zn has the smallest sorption capacity.

3.6 References

Adamson, A.W. *Physical Chemistry of Surface*, 5th ed., Wiley-Interscience: New York, 1990.

Bailliez, S., Nzihou, A., Beche, E., and Flamant, G. (2004) Removal of lead (Pb) by hydroxyapatite sorbent. *Process Safety and Environmental Protection*. 82: 175-180.

Celis, R., Hermosin, M.C., Cornejo, J., Heavy Metal Adsorption by Functionalized Clays, *Environ. Sci. Technol*. 2000, 34, 4593-4599

Chander, S. and D.W. Fuerstenau (1984) Solubility and interfacial properties of hydroxyapatite: a review, pp. 29-49. In: (D.N. Misra, ed.) *Adsorption and Surface Chemistry of Hydroxyapatite*. Plenum, N.Y.

Chen, Z and Anderson, G, 2002, *Environmental Applications of Geochemical Modeling,* Cambridge, pp138.

Christopher, J.; Gabelich, T. D.; Tran, I. H.; Suffet, M. Electrosorption of Inorganic Salts from Aqueous Solution Using Carbon Aerogels. *Environ. Sci. Technol*. 2002, *36* (13), 3010.

Crannell, B.S., T.T. Eighmy, L.G. Butler, F.K. Cartledge, E. Emery, C. Willson, D.D. Reible, and M. Yin (2001) *Phosphate-Based Heavy Metal Stabilization and Reactive Barrier Technologies for Contaminated Sediments and Dredged Materials*. Final NOAA/CICEET Project Report, UNH, Durham, N.H., 177 pp.

Crannell, B.S., Eighmy, T., Willson, C., Reible, D., Yin, M., "Pilot-Scale Reactive Barrier Technologies for Containment of Metal-Contaminated Sediments and Dredge Materials," A Final Report Submitted to the NOAA/UNH Cooperative Institute for Coastal and Estuarine Environmental Technology (CICEET), 2004.

Elder, J.F., 1989, Metal biogeochemistry in surface-water systems-A review of principles and concepts: *U.S. Geological Survey Circular* 1013, 43 p.

Fedoroff, M., Jeanjean, J., Rouchaud, J.C., Mazerolles, L. (1999) Sorption kinetics and diffusion of cadmium in calcium hydroxyapatites. *Solid State Sci.* T1:71-84.

Freundlich, H. M. F. Over the adsorption in solution, *J. Phy. Chem*. 1906, 57, 385.

Fuller, C.C., Bargar, J.R., and Davis, J.A. (2003) Molecular-scale characterization of uranium sorption by bone apatite materials for a permeable reactive barrier demonstration. *Environ. Sci. Technol.* 37:642-4649.

HSRC (Hazardous Substance Research Centers) South & Southwest, "Anacostia River Advanced Capping Demonstration Project Overview", 2004, http://www.hsrc-ssw.org/ana-index.html.

Jaworski, J.F., *Effects of chromium, alkali halides, arsenic, asbestos, mercury, cadmium in the Canadian environment*, National Research Council of Canada Publication No.NRCC. 17585 of the Environmental Secretariat, Ottawa, Canada, 1980.

Kaplan, D.I. and Knox, A.S., Enhanced Contaminant Desorption Induced by Phosphate Mineral Additions to Sediment, *Environ. Sci. Technol*. 2004, 38, 3153-3160

Ko, D.C.K, Porter, J.F., McKay, G., Mass Transport Model for the Fixed Bed Sorption of Metal Ions on Bone Char, *Ind. Eng. Chem. Res.* 2003**,** *42,* 3458-3469

Kohn, M.J., Rakovan, J., and Hughes, J.M. (2002) Phosphates: Geochemical, Geobiological, and Materials Importance. In: (Ribbe, P.H., ed.) *Reviews in Mineralogy and Geochemistry.* Vol. 48. Mineralogical Society of America, Washington, D.C.

Langmuir, I. The adsorption of gases on plane surfaces of glass, mica and platinum, *J. Am. Chem. Soc*. 1918, 40, 1361.

Langmuir, D., 1997. *Aqueous environmental geochemistry*, Prentice-Hall, Inc., New Jersey, USA, 343-395.

Laperche, V., Logan, T.J., Gaddam, P., and Traina, S.J. (1997) Effect of apatite amendments on plant uptake of lead from contaminated soil. *Environ. Sci. Technol*. 31:2745-2753.

Ma, Q.Y., Logan, T.J., Traina, S.J., and Ryan, J.A. (1994) Effects of NO_3^-,Cl^-, F^-, SO_4^{2-}, and CO_3^{2-} on Pb^{2+} immobilization by hydroxyapatite. *Environ. Sci. Technol.* 28: 408-418.

Ma, Q.Y., Logan, T.J., and Traina, S.J. (1995) Lead immobilization from aqueous solutions and contaminated soils using phosphate rocks. *Environ. Sci. Technol.* 29: 1118-1126.

Merkel, B.J., Planer-Friedrich, B., *Groundwater Geochemistry* (Springer Berlin Heidelberg New York, 2002)

Misra, D.N. and R.L. Bowen (1984) Interaction of zinc ions with hydroxyapatite, pp. 179-192. In: (D.N. Misra, ed.) *Adsorption and Surface Chemistry of Hydroxyapatite*. Plenum, N.Y.

Mohan, D, Singh, K.P, Singh, V, K, *Ind. Eng. Chem. Res.* 2005**,** *44,* 1027-1042

Monteil-Rivera, F., Masset, S., Dumonceau, J., Fendorf, M., and Jeanjean, J. (1999) Sorption of selenite ions on hydroxyapatite. *J. Mat. Sci. Lett.* 18: 1143-1145.

Moore, J.W and Ramamoorthy. S, *Heavy Metals in Natural Waters* (Springer-Verlag, 1984).

Niragu, J.O., 1979. Copper in the atmosphere and precipitation. In: J.O. Nriagu (Ed), *Copper in the environment*, Part I, Ecological cycling. Wiley, New York.

Niragu, J.O., 1979. Global inventory of natural and anthropogenic emissions of traces metals to atmosphere. *Nature* 279: 409-411.

Nriagu, J.O. and Moore, P.B. (1984) *Phosphate Minerals*, Springer-Verlag, Berlin.

Peld, M., Tonsuaadu, K., Bender, V., Sorption and Desorption of Cd^{2+} and Zn^{2+} Ions in Apatite-Aqueous Systems, Environ. *Sci. Technol*. 2004, 38, 5626-5631

Prasad, M and Saxena, S, Sorption Mechanism of Some Divalent Metal Ions Onto Low-Cost Mineral Adsorbent, *Ind. Eng. Chem. Res.* 2004, *43,* 1512-1522

Reddad, Z., Gerente, C., Andres, Y., Cloirec, P.L., Adsorption of Several Metal Ions onto a Low-Cost Biosorbent: Kinetic and Equilibrium Studies, *Environ. Sci. Technol*. 2002, 36, 2067-2073

Redlich, O., Peterson, D. L. A useful adsorption isotherm, *J. Chem. Phy*. 1959, 63, 1024.

Reddy, K.J., Wang, L., Gloss, S. P., Solubility and mobility of copper, zinc and lead in acidic environments, *Plant and Soil*, 171: 53-58, 1995.

Salomons, W., 1995, Environmental impact of metals derived from mining activities: Processes, predictions, prevention: *Journal of Geochemical Exploration*, v. 52, p. 5-23.

Sauve, S., Hendershot, W. and Allen, H.E., Solid-Solution Partitioning of Metals in Contaminated Soils: Dependence on pH, Total Metal Burden, and Organic Matter, *Environ. Sci. Technol*. 2000, 34, 1125-1131

Sheindorf, C. and Rebhun, M. (1981) "A Freundlich-type isotherm." *Journal of Colloid and Interface Science*, 79 (1), 136-142.

Singh, S.P., Ma, L.Q., Harris, W.G. (2001) Heavy Metal; Interactions with Phosphatic Clay Sorption and Desorption Behavior. *J. Environ. Qual.* 30.6:1961-1968.

Sips, R. On the structure of a catalyst surface, *J. Chem. Phy*. 1948, 16, 490.

Somasundaran, P. and Y.H.C. Wang (1984) Surface chemical characteristics and adsorption properties of apatite, pp.129-149. In: (D.N. Misra, ed.) *Adsorption and Surface Chemistry of Hydroxyapatite.* Plenum, N.Y.

Suzuki, T.; Hatsushika, T.; Hayakawa, Y. Synthetic hydroxyapatites employed as inorganic cation-exchangers. *J. Chem. Soc., Faraday Trans.* 1981, *77*, 1059-1062.

Traina, S.J. and Laperche, V. (1999) Contaminant bioavailability in soils, sediments, and aquatic environments. *Proc. Natl. Acad. Sci.* 96: 3365-3371.

Wen, X., Du, Q., Tang, H., Surface Complexation Model for the Heavy Metal Adsorption on Natural Sediment, *Environ. Sci. Technol.* 1998, 32, 870-875

Weng, L., Temminghoff, E.J., and Riemsdijk, W.H.V., Contribution of Individual Sorbents to the Control of Heavy Metal Activity in Sandy Soil, *Environ. Sci. Technol. 2001, 35, 4436-4443*

Xiao, B. and Thomas, K.M., Competitive Adsorption of Aqueous Metal Ions on an Oxidized Nanoporous Activated Carbon, *Langmuir* 2004**,** *20,* 4566-4578

Xu, Y. and F.W. Schwartz (1994) Lead immobilization by hydroxyapatite in aqueous solutions.*J. Contam. Hydrol.* 15: 187-206.

Xu, Y., Schwartz, F.W., and Traina, S.J. (1994) Sorption of Zn^{2+} and Cd^{2+} on hydroxyapatite surfaces. *Environ. Sci. Technol.* 28:1472-1480.

Yin, M., C.S. Willson, and D.D. Reible, 2004, Investigation of Heavy Metal Migration from Contaminated Sediment to Capping material using XRF, presented at the 2004 AICHE Annual Meeting, November 7-12, 2004, Austin, TX.

Chapter 4

Metal Migration in Sediment and Capping Materials Investigated by ICP-MS

4.1 Introduction

Among various capping materials batch pH-leaching experiments have demonstrated that phosphorite-based barriers are more effective to immobilize heavy metals compared with conventional capping materials (e.g. sand). From the results of transport column experiments under natural conditions (using contaminated field sediment as source of migration) we can not differentiate the metal migration characteristics of different metals and materials within reasonable time scales (Crannell et al., 2004). This is mainly due to the contaminated metals concentration in field sediment is relatively low. At this low concentration range the sorption isotherm can be approximated as linear and the retardation factor is high. The sorption isotherm experiments shown in chapter 3 indicate that when extended to a larger concentration range most of the data can be fitted well by Langmuir isotherm. With this different sorption isotherm the migration should be different. Although usually this the contaminated metals in field sediment will not go to this high level, in some pollution accident the metal migration at high concentration will be of interest.

Various methodologies have been utilized in previous studies of metal migration. One of them is observing the metal breakthrough curve produced by metal solution flow through chromatographic columns packed by the materials of interest (Voegelin, et al., 2002; Ko et al., 2003). Another type involves DGT and DIFS techniques (Ernstberger et al., 2002). Tokunaga measured Se and Cr(VI) diffusion profile directly by micro-XANES (Tokunaga, et al., 1998, 2001).

In this study, relatively high concentration metal solutions were placed atop a solid layer and migration was allowed to occur over the time scale of days. The metal migration profiles are measured by slicing the migration columns followed by ICP-MS analysis of each slice. This method takes advantage of two properties of ICP-MS: the ability to detect lower metal concentrations and the ability to detect greater number of elements. The method is destructive and has worse spatial resolution than the method using synchrotron X-ray technique. This is a complementary experiment to the experiment involving XRF technique.

4.2 Materials and Methods

4.2.1 Materials

The sediment and capping materials used in this experiment are defined in Chapter 3.

The metal solutions are made by dilution of metal reagents described in Chapter 3 by distilled water. The pH value and ambient temperature are same as those in the experiments described in section §3.3.2.

4.2.2 Apparatus

The ends of 60 mL polypropylene syringes were cut off. As showed in Figure 4-1, the pistons are pulled to the nearly full-open position. Solid materials were placed on top of the pistons and metal solutions ponded over the solid layer. The cut-off ends of the syringes were sealed by Parafilm® to prevent water evaporation.

4.2.3 Procedure

- The mixed solution of Cr^{3+}, Cu^{2+}, Zn^{2+} and Pb^{2+} is prepared by dissolving and diluting the corresponding reagents into distilled water with PH value of 7.3. The final pH value of the solution is around 5.

- Pull the piston to nearly opening position and put 30 mL distilled water over the piston.
- Load the solid media from the cut-off end into syringe and agitate it with water to make sure solid media is water saturated; make the volume of water layer on top of the solid layer 50 mL.
- Let the syringe stand still until the overlying water become clear.
- Use pipette to gently introduce concentrated metal solution to water layer and then agitate the water layer slowly to make the disturbance on the interface minimum.
- After a given time of metal diffusion, agitate the pond solution and extract a water sample for ICP-MS analysis. Then push the piston toward the cut-off end until certain thickness (1.76 mm or 3.52 mm) of solid layer is extruded out of the syringe. Cut this extruded layer out by blade and continue this extrude-cut procedure until the whole solid layer is sectioned. Each section is processed by nitric acid digestion and subsequently analyzed by ICP-MS.

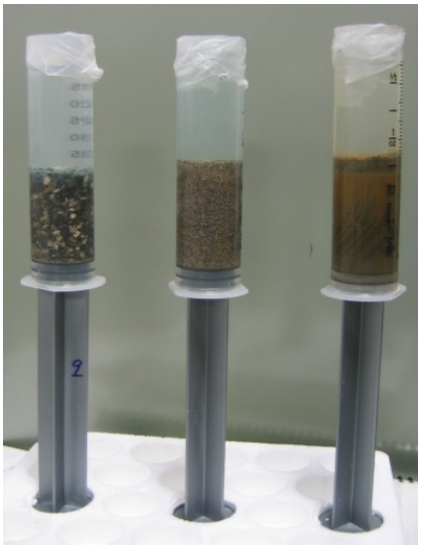

Figure 4-1 Metal transport columns

4.2.4 Analysis Techniques

An Anton Paar microwave digester was used for the total element acid digestion. The procedure follows the standard method EPA 3051. ICP-MS (Perkin Elmer ELAN 9000) is used to measure metals concentrations in water. The measuring parameters are same as those described in chapter 2. Methods for ICP-MS analysis are fully described by EPA 200.8 and EPA 6020. The detection limits (method detection limit) of ICP-MS for selected metals in pore water and soil are listed in Table 4-1:

Table 4-1 Detection limits of ICP-MS for soil and pore water

	Water		*Soil*	
Element	Detection limit	Reference	Detection limit	Reference
Cr	1 µg/L	EPA 200.8	1 µg/gm	EPA 200.8
Cu	1 µg/L	EPA 200.8	1 µg/gm	EPA 200.9
Zn	1 µg/L	EPA 200.8	1 µg/gm	EPA 200.10
Pb	0.1 µg/L	EPA 200.8	0.1 µg/gm	EPA 200.11

4.3 Results and Discussion

The migration profiles of different metal species in different materials are shown in Figure 4-2 to Figure 4-13, where the total metal concentrations (including solid phase and water phase) are plotted as the function of the depth below the solid-water interface. The migration profiles of four metal species (Cr^{3+}, Cu^{2+}, Zn^{2+} and Pb^{2+} in a mixed water solution) in three materials (Phosphil, Florida Phosphate and Anacostia River Sediment) at three time spans (1 day, 5 days and 9 days) are obtained. The metal concentration of pond solution at each time interval is also recorded in each figure. The error bars come from three replicate measurements of the water sample produced by acid digestion of solid sample.

From Chapter 3 we know sand has little sorption of the metal species being studied, this implies that when metal ion solution flow through sand layer most of the metals will

remain in water phase. Then if using the same procedure as above to slice the transport column of sand significant loss of metal induced by loss of pore water is expected to occur during slicing process. A nondestructive analysis technique is desirable to measure the metal transport profile in sand.

4.3.1 Quality Control: Mass Balance Verification

In principle, the metal migrated into the solid layer should be equal to the metal depleted from water solution. Table 4-2 lists metal gain in solid and depleted from water layer and the ratio of them. This is the data set for day 9 columns. The metal gain in solid is the integral of transport profile after subtracting baseline concentration. The integration is numerically approximated by rectangle method. The metal depleted from water is simply calculated by the difference in concentrations between day zero and day nine.

The mass balance verification results for Phosphil are worse than the other two materials. This is most likely due to its heterogeneity considering Phosphil is an oversized sand grained material.

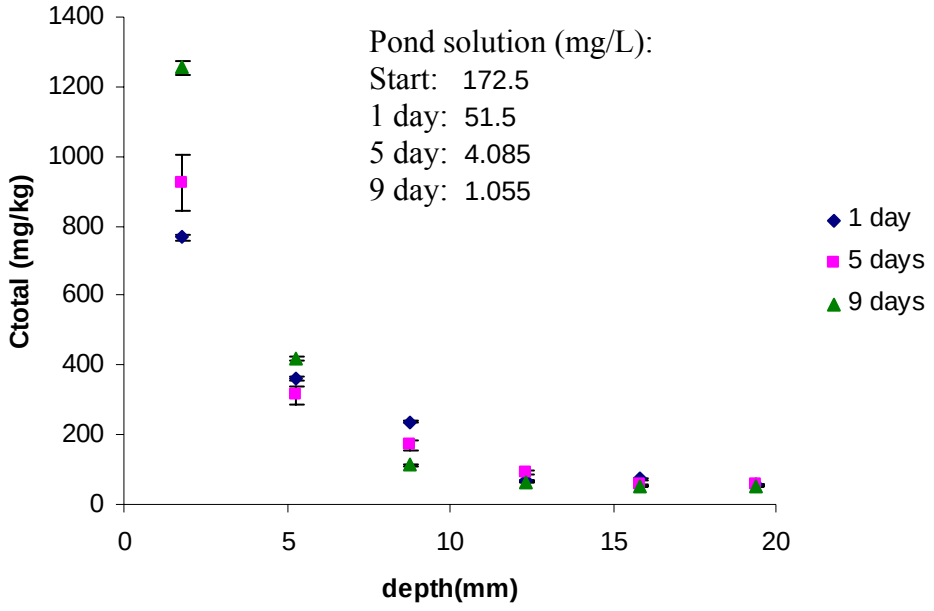

Figure 4-2 Cr^{3+} Transport profile in Phosphil

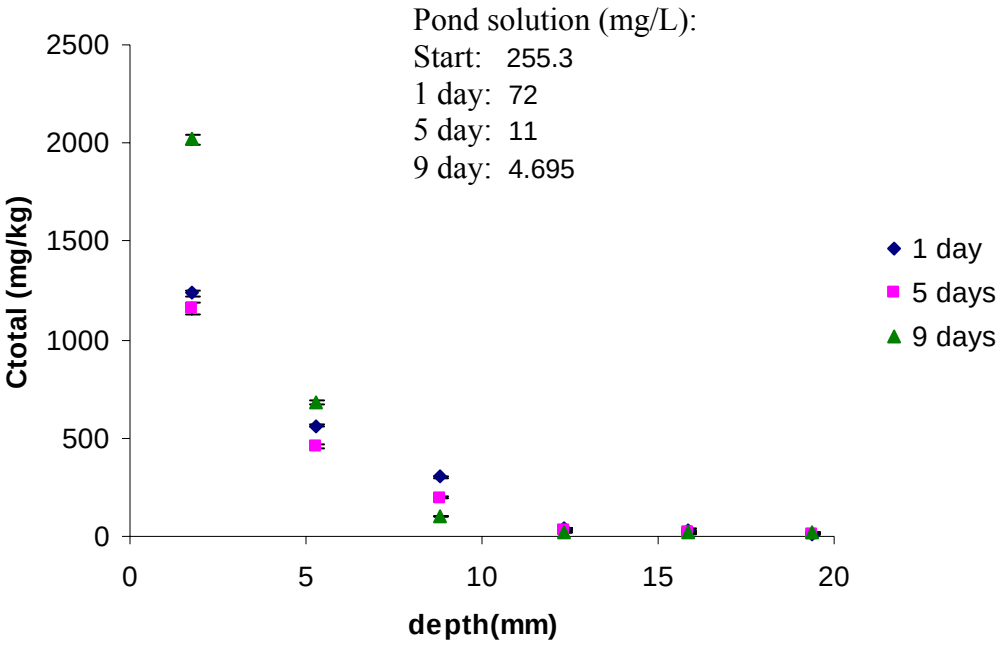

Figure 4-3 Cu^{2+} Transport profile in Phosphil

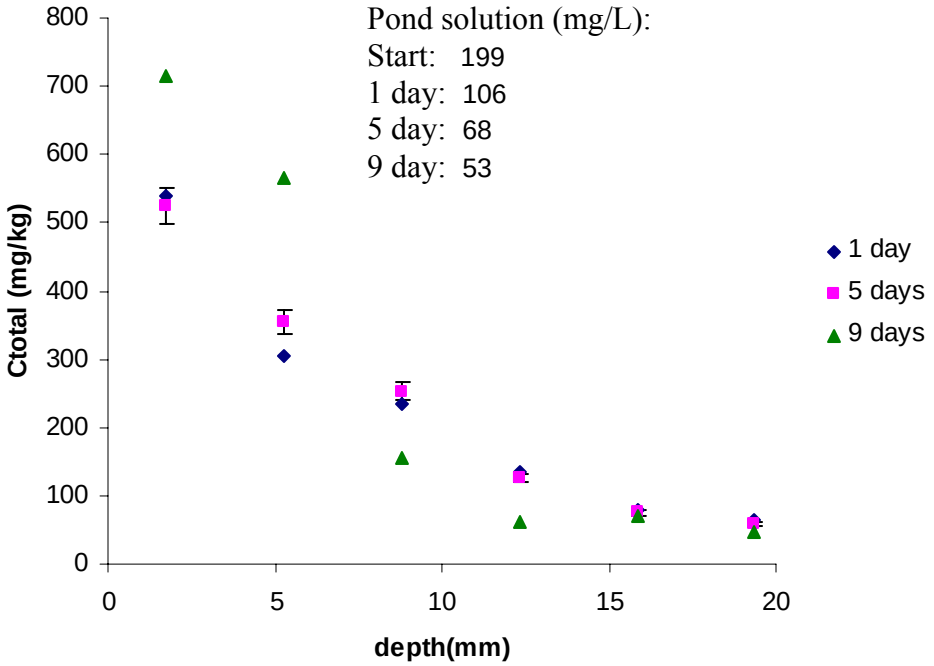

Figure 4-4 Zn^{2+} Transport profile in Phosphil

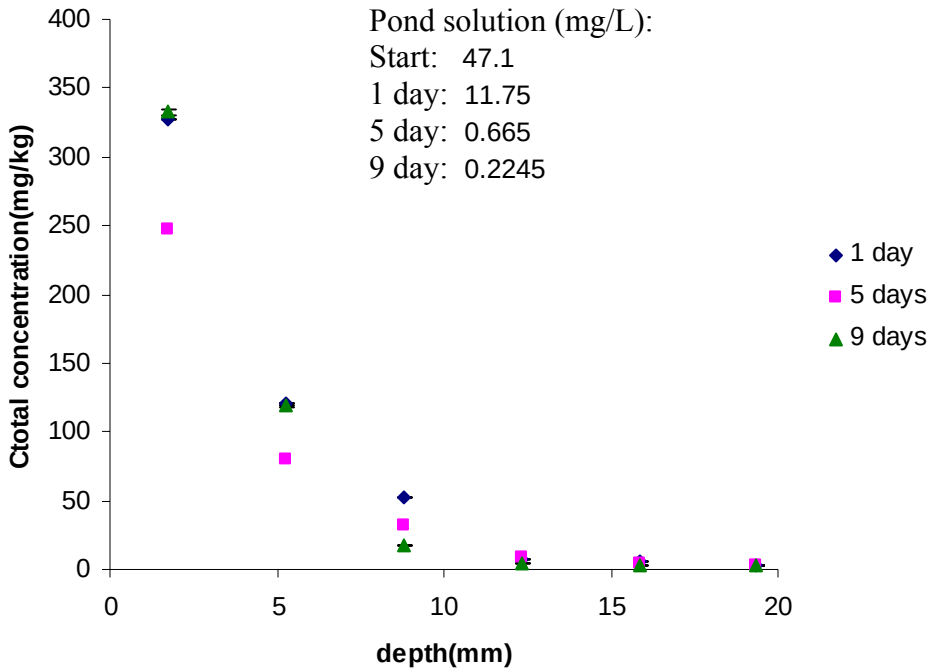

Figure 4-5 Pb^{2+} Transport profile in Phosphil

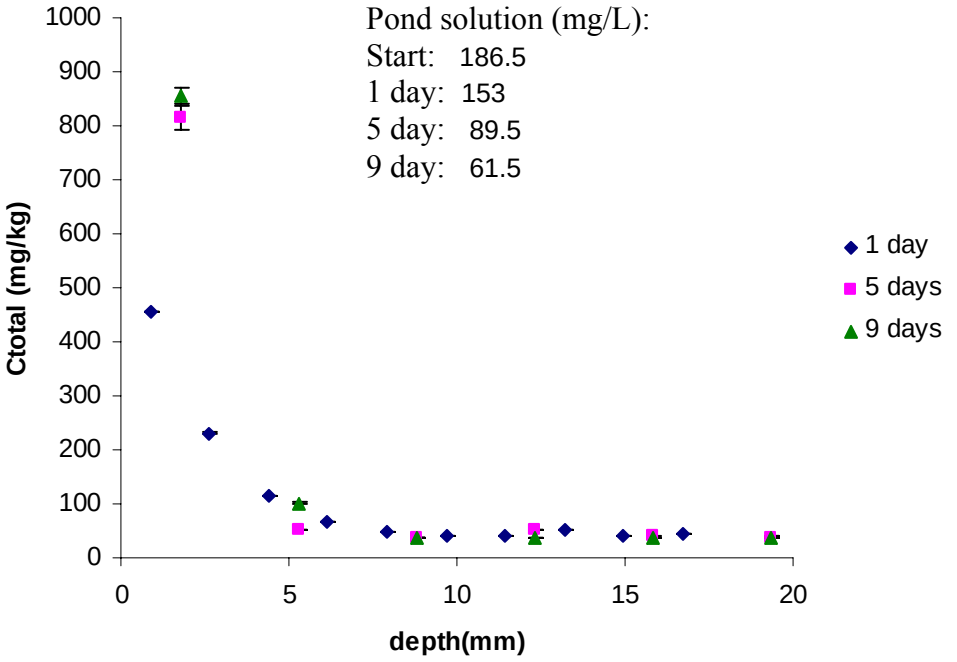

Figure 4-6 Cr^{3+} Transport profile in Florida Phosphate

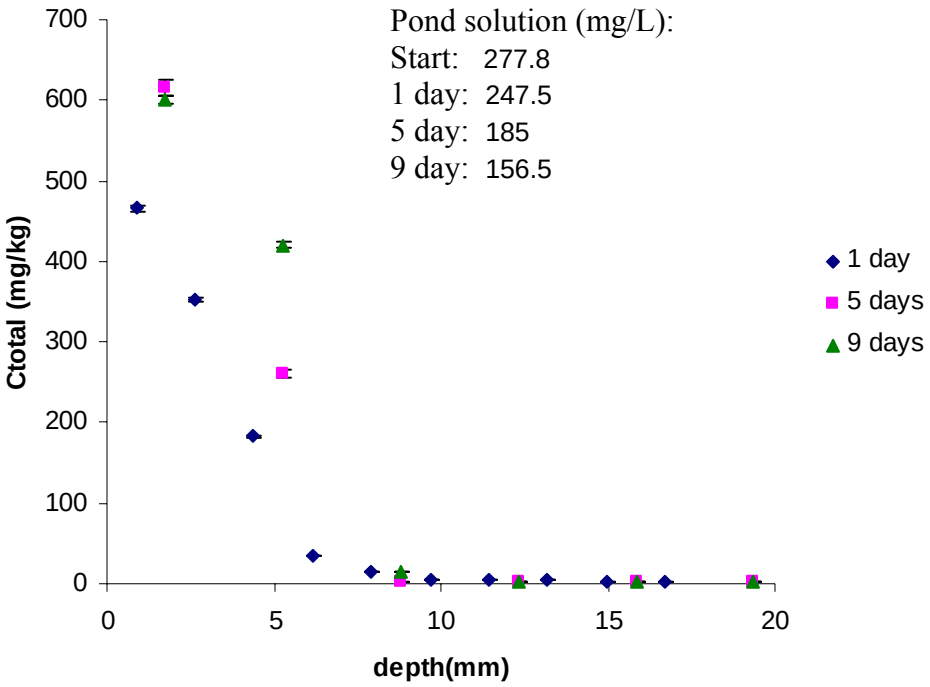

Figure 4-7 Cu^{2+} Transport profile in Florida Phosphate

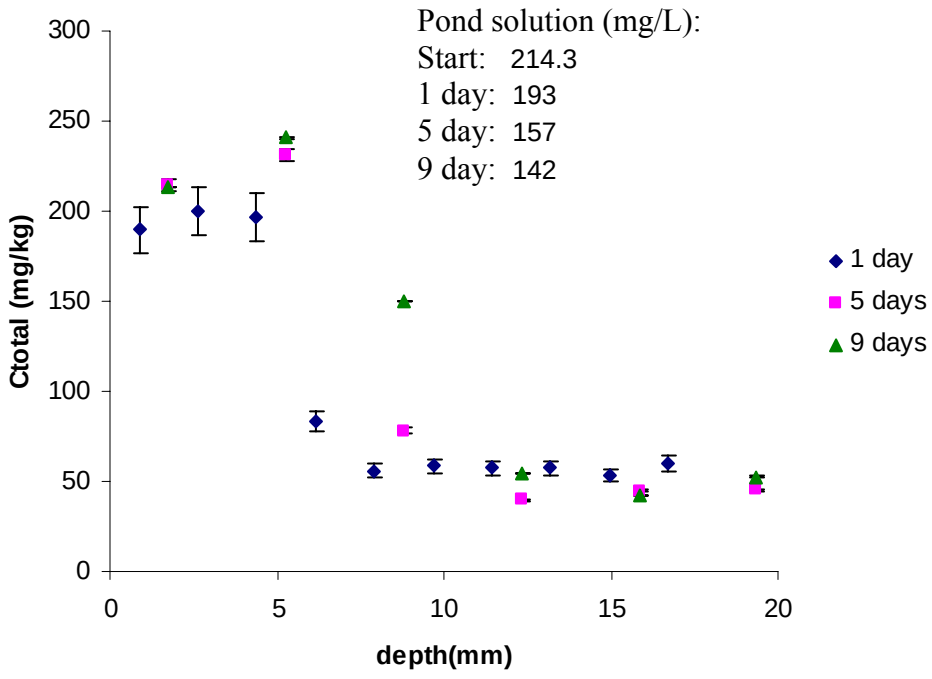

Figure 4-8 Zn^{2+} Transport profile in Florida Phosphate

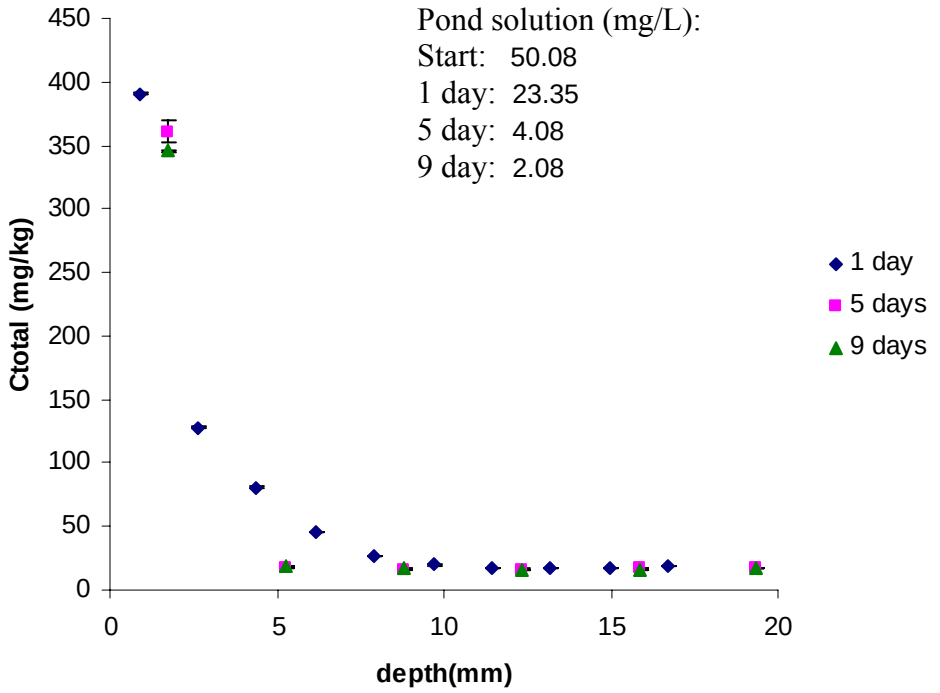

Figure 4-9 Pb^{2+} Transport profile in Florida Phosphate

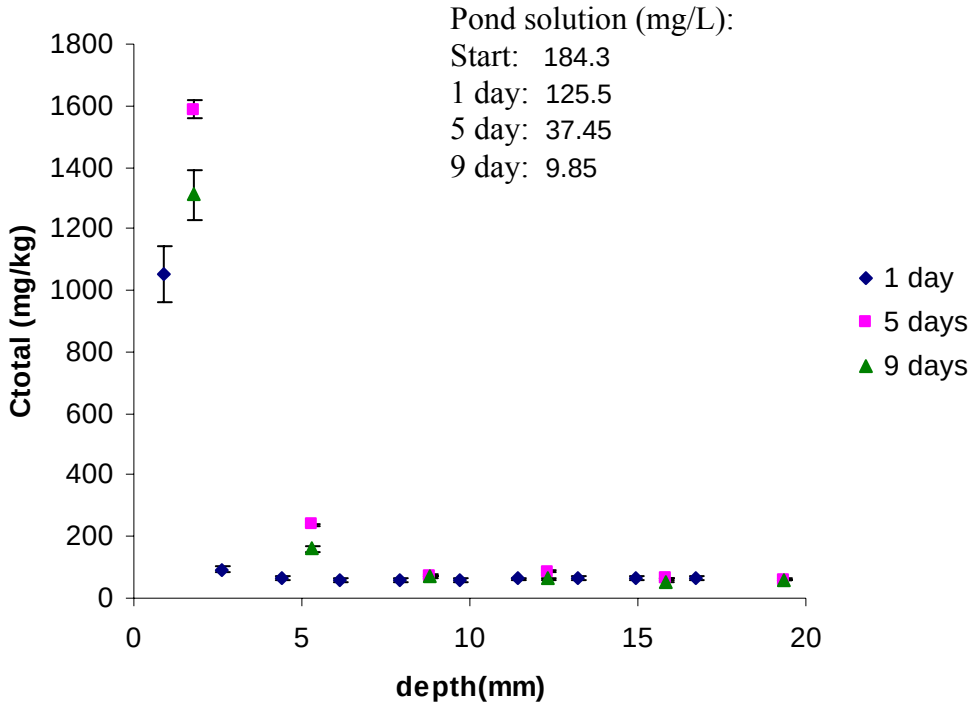

Figure 4-10 Cr^{3+} Transport profile in Anacostia River Sediment

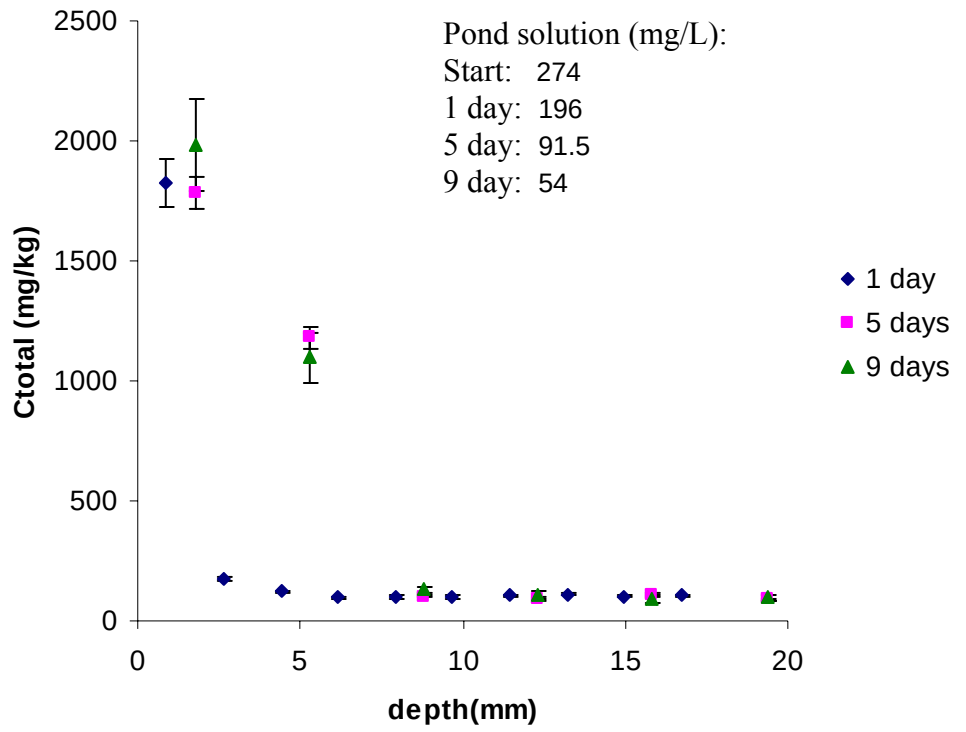

Figure 4-11 Cu^{2+} Transport profile in Anacostia River Sediment

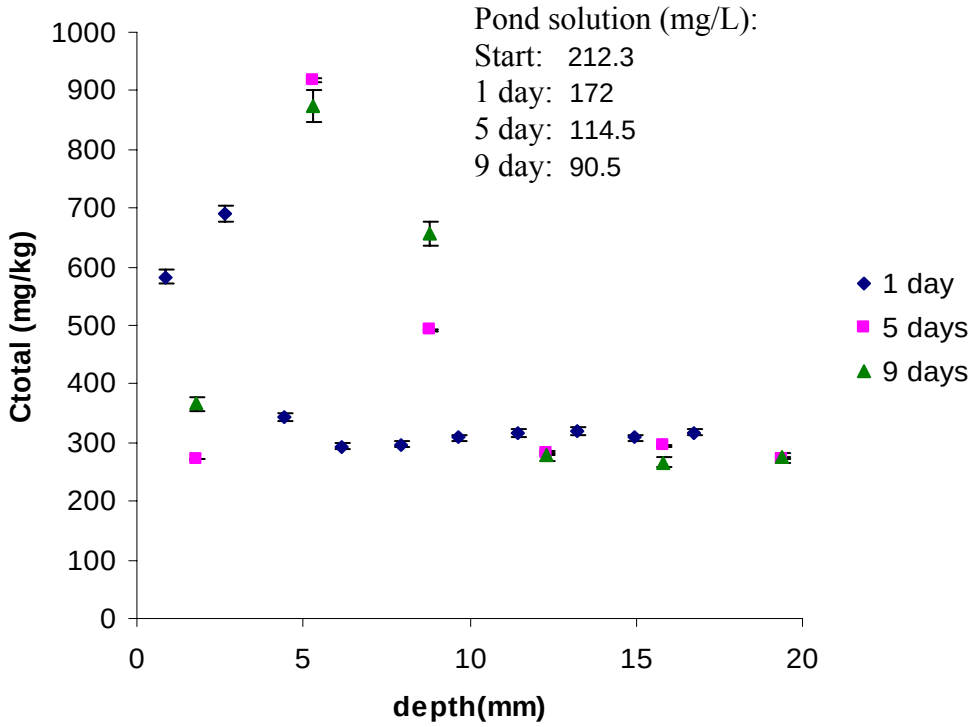

Figure 4-12 Zn^{2+} Transport profile in Anacostia River Sediment

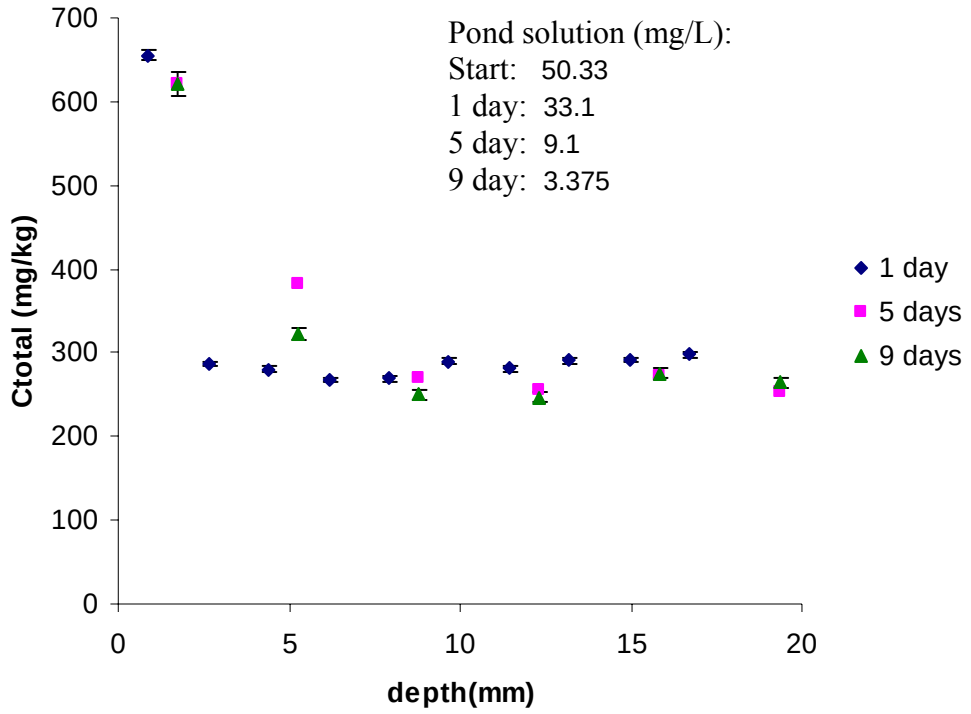

Figure 4-13 Pb^{2+} Transport profile in Anacostia River Sediment

Table 4-2 Mass balance verification

		gain in solid (mg)	Depleted from water (mg)	ratio
Phosphil	Cr	6.27	6.86	0.91
	Cu	10.5	6.86	1.52
	Zn	5.4	4.01	1.35
	Pb	1.77	1.23	1.44
Florida Phosphate	Cr	3.36	3.37	1.00
	Cu	3.87	3.33	1.16
	Zn	1.91	1.97	0.97
	Pb	1.28	1.22	1.04
Sediment	Cr	3.92	4.78	0.82
	Cu	8.31	6.06	1.37
	Zn	3.08	3.35	0.92
	Pb	1.49	1.25	1.19

4.3.2 Migration of Different Metals

To compare the migration behavior of different metals in same material the absolute concentrations are normalized by their own maximum and minimum concentrations in corresponding transport profiles. Thus these normalized profiles can be put together for

comparison. These comparisons are shown from Figure 4-14 to Figure 4-16 for metal migration in Phosphil, Florida Phosphate and Anacostia River, respectively.

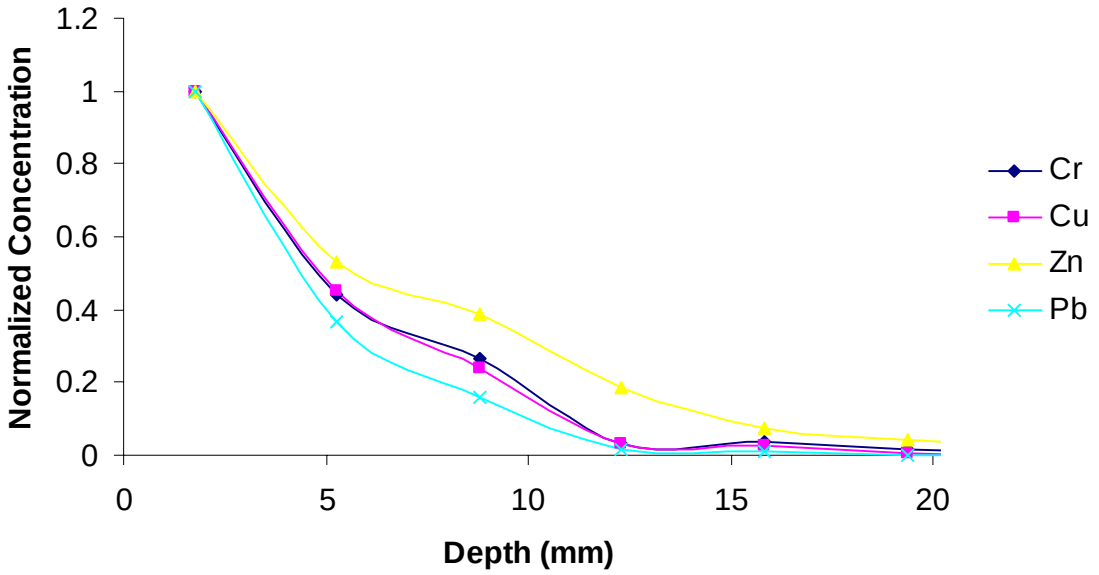

Figure 4-14 Metal Transport in Phosphil (9 day)
(Zn>Cr≥Cu>Pb)

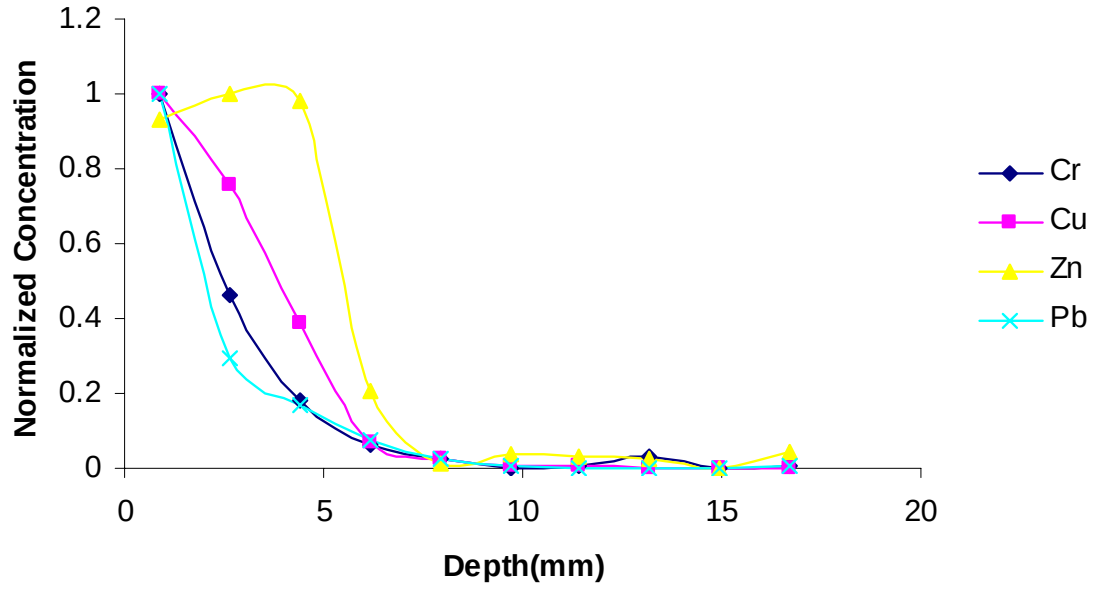

Figure 4-15 Metal Transport in Florida Phosphate (9 day)
(Zn>Cu>Cr>Pb)

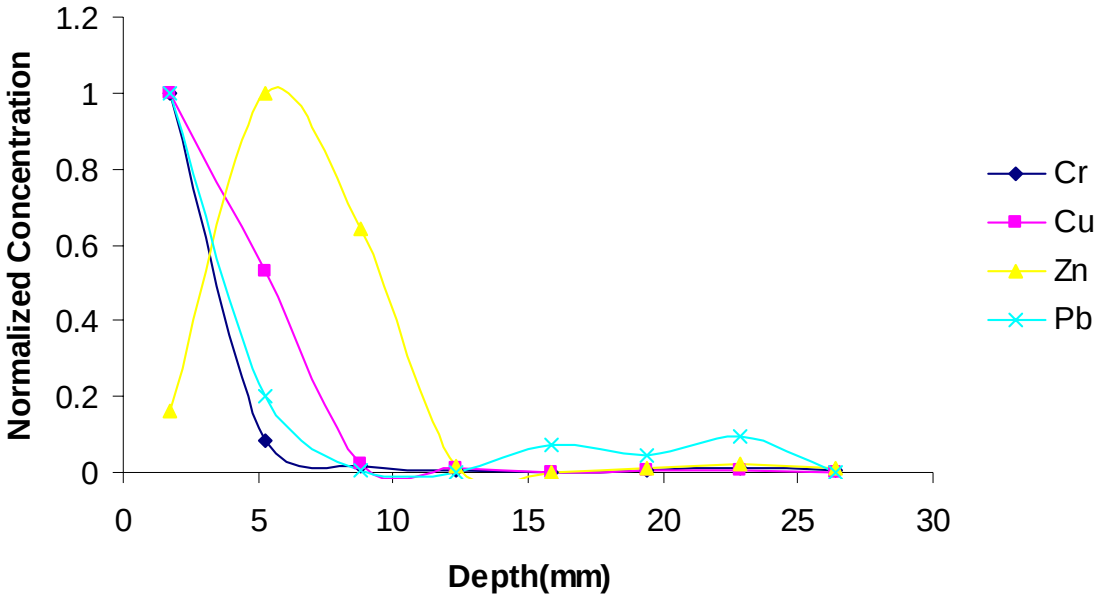

Figure 4-16 Metal Transport in Anacostia River Sediment (9 days) (Zn>Cu>Pb>Cr)

A couple of observations can be made from Figure 4-14 to Figure 4-16:

- For Phosphil, the sequence of migration speeds is Zn > Cr ≥ Cu> Pb which is exactly same as the reverse order of maximum adsorption capacity (W_m) measured by sorption isotherm experiment (see §3.4**)**.
- For Florida Phosphate, the sequence of migration speeds is Zn > Cu> Cr> Pb which is also consistent with the reverse order of maximum adsorption capacity (W_m) measured by sorption isotherm experiment is Zn > Cu ≈ Cr > Pb.
- For Sediment, the sequence of migration speeds is Zn > Cu > Pb ≥Cr. The reverse order of maximum adsorption capacity (W_m) measured by sorption isotherm experiment is Zn > Pb > Cu >Cr. Except for Pb the orders of other three element are consistent.

4.3.3 Migration in Different Materials

Similar comparisons of the normalized profiles of same metal in different materials were made. No statistically significant difference was observed.

4.3.4 Metal Depleted From Pond Solution Taken Up By Solid Phase

After 9 days migration, the metals were dramatically depleted from pond solution. Table 4-3 lists the decreases in the metal concentrations in pond solution.

Table 4-3 Metal depleted from pond solution (9 days)

	Phosphil	Florida Phosphate	Sediment
Cr	96.57%	66.67%	94.66%
Cu	98.16%	43.71%	80.40%
Zn	72.82%	33.64%	57.51%
Pb	99.50%	95.56%	93.10%

For Phosphil, from small to large the order of these percentages is Zn, Cr, Cu, Pb; For Florida Phosphate it is Zn, Cu, Cr, Pb; For sediment, it is Zn, Cu, Pb, Cr. Notice that these are the exactly same orders of corresponding migration speeds which means in these systems the more the solid layer uptakes metal the slower that metal migrates in solid.

4.4 Summary

The migration profiles of four metal species in three materials are measured by ICP-MS. The maximum spatial resolution that can be reached by this method is 1.32 mm. The method also has a high detection limit (ppb level) and good element coverage. However, the slicing process is destructive and makes this method not suitable for samples with high metal pore water concentrations such as the case of sand. The migration of metal in solid phase is highly correlated with the metal depleted from pond solution and maximum sorption capacity measured in sorption isotherm experiment.

4.5 References

Crannell, B.S., Eighmy, T., Willson, C., Reible, D., Yin, M., "Pilot-Scale Reactive Barrier Technologies for Containment of Metal-Contaminated Sediments and Dredge Materials," A Final Report Submitted to the NOAA/UNH Cooperative Institute for Coastal and Estuarine Environmental Technology (CICEET), 2004.

Ernstberger, H., Davison, W., Zhang, H., Tye, A., Young, A., Measurement and Dynamic Modeling of Trace Metal Mobilization in Soils Using DGT and DIFS, *Environ. Sci. Technol*. 2002, 36, 349-354

Ko, D.C.K, Porter, J.F., McKay, G., Mass Transport Model for the Fixed Bed Sorption of Metal Ions on Bone Char, *Ind. Eng. Chem. Res.* 2003*, 42,* 3458-3469

Tokunaga, T. K.; Sutton, S. R.; Bajt, S., Nuessle, P, Shea-Maccarthy, G, 1998, Selenium diffusion and reduction at the water-sediment boundary: micro-XANES spectroscopy of reactive transport, *Environ. Sci. Technol.,32*, 1092-1098.

Tokunaga, T. K., Wan, J., Firestone, M. K.; Hazen, T. C.; Schwartz, E., Sutton, S. R., Newville, M., 2001, Chromium diffusion and reduction in soil aggregates, *Environ. Sci. Technol, 35,* 3169-3174.

Voegelin, A.; Vulava, V. M.; Kretzschmar, R., 2001, Reaction-Based Model Describing Competitive Sorption and Transport of Cd, Zn, and Ni in an Acidic Soil, *Environ. Sci. Technol., 35,* 1651-1657.

Voegelin, A, Scheinost, A, Buhlmann, K, Barmettler, K and Kretzschmar, R, Slow Formation and Dissolution of Zn Precipitates in Soil: A Combined Column-Transport and XAFS Study, *Environ. Sci. Technol*. 2002, 36, 3749-3754

Chapter 5

Metal Migration in Sediment and Capping Materials Investigated by Synchrotron X-ray Fluorescence

5.1 Introduction

In Chapter 4, metal migration profiles from a ponded water solution into sediment and capping materials were studied by slicing the solid layer vertically and analyzing the total metal concentration in each slice by ICP-MS. A major drawback to this method is that it will destroy the samples so that migration profiles at different time intervals have to be measured in different sample columns. This leads to difficulties when comparing the migration profiles at different time intervals because it is difficult to ensure that the sample columns are identical. A second limitation of this experimental technique is that it is hard to avoid pore water loss during the slicing process. Accurate concentration measurements rely on the assumption that most of the metals are absorbed on the solid phase. While this is mostly true for sediment and apatite, it is not the case for sand. Third, the spatial resolution of this slicing method is limited to 1-2 mm. A fourth limitation is that the time resolution is limited to 1 day (i.e., the time it takes to slice, prepare and analyze the samples). Therefore, if the migration profile changes significantly within hours then the slicing method cannot catch up. All these factors suggest that a nondestructive, high spatial and time resolution detection technique is desirable for higher quality data. Synchrotron X-ray fluorescence meets all these requirements.

Synchrotron X-ray Fluorescence (XRF) is a mature multi-element detection technique with high spatial and time resolution. From 2001 to 2003 the metal concentration profiles of a number of diffusion cells containing similar sediment and capping materials had been measured by synchrotron XRF and this technique proved to

be suitable for measuring these types of metal migration profiles in sediment and capping materials (Yin, et al., 2004). Tokunaga et al. (1998) investigated Selenium diffusion and reduction at the water-sediment boundary using synchrotron micro-XANES spectroscopy. Using the same technique they (Tokunaga et al., 2001) also investigate the Chromium diffusion and reduction in soil aggregate.

The experiments in chapter 4 provide a preliminary test of column metal migration experimental at high concentration range. In this chapter, the migration profiles of similar columns with different packing method were measured by synchrotron XRF in the DCM beamline at CAMD.

5.2 Materials and Methods

5.2.1 Materials and Sample Preparation

The sediment and capping materials (sand and apatite) used in these experiments are the same as those in Chapter 3. The ponded solution is also made by the same way, except that the concentrations are different.

The polypropylene tubes used in Chapter 4 are too thick for the XRF scanning directly since the thick tube walls will attenuate a large fraction of the incident x-rays. To achieve optimum XRF spectra, the migration core was packed in thin polyethene tubing (thickness on the order of μm's) and supported by a hard polypropylene cylinder cut in half.

The migration cores are made by essentially the same steps in Chapter 4 with two differences. One is after metal solution is ponded on top of the solid layer, the top of the polyethene tubing is sealed by a thermal sealer instead of sealed by Parafilm®. The second is that the length of the ponded solution on top of the solid matrix is around 11 cm; more than twice the water depth as in the polypropylene syringes used in Chapter 4.

5.2.2 XRF Instrumentation and Experiment Setup

The XRF analysis was carried out at the double crystal monochromator (DCM) beamline at CAMD. The AUTOCAD drawing of the CAMD DCM beamline is shown in Figure 4-3.

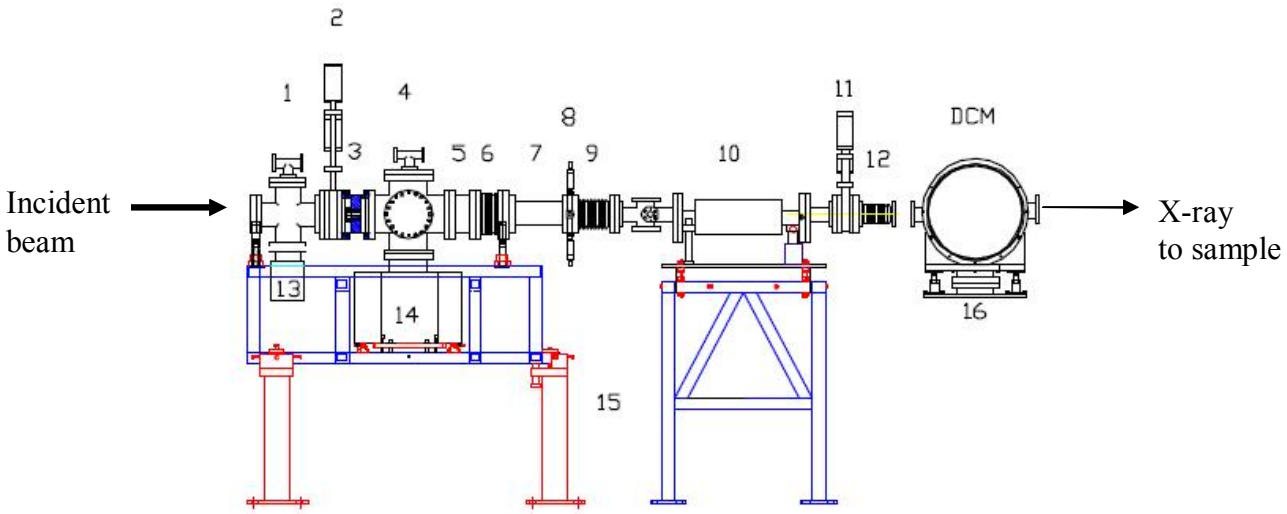

Figure 5-1. DCM beamline at CAMD

The whole beamline, including DCM, is under high vacuum with the pressures increasing from left to right. A differential ion pump (10) separates the high vacuum part of the beamline (to the left) from the lower vacuum part on the right. The typical vacuum levels are 10^{-7} torr in the DCM and 10^{-9} torr to the left. The white light enters the beamline from the left. A Kapton window on the right window of the DCM separates it from the sample chamber. The beamline is mounted on a very stable base (15) to reduce vibrations. A removable thin window (11) separates the main beamline from the DCM. It is removed during normal operation to keep the flux at the maximum and kept closed while the beamline is not in use. The window material is typically a low Z (absorption) material, such as beryllium or aluminum. During sample loading, several pneumatically operated valves (e.g., 2) have to be closed.

The beam that emerges from the DCM is usually several mm across and a few mm in height. It can be adjusted by moving the slits (11). The total flux will depend on the dimensions of the beam.

The DCM acts as a filter, removing all the radiation except the wavelength satisfying Bragg's law and its multiples. If the two crystals are parallel to each other, the X-rays also emerge parallel to the incident x-rays. The energy resolution of a double crystal monochromator is better than a single crystal. Particularly for short wavelengths (< 0.5 Å), the beam is also better collimated than a slit system. The crystals can be moved independently of each other. Si 400 crystals were used in the DCM and the crystals were tuned to 10 keV; above the K-edge of Cr, Cu and Zn but below the L-edge of Pb so that no Pb peaks will be excited.

The intensity of the beam right after the DCM (I_0) was monitored via a gas ionization chamber placed in the x-ray beam. There was a set of four jaw slits positioned before the sample to reduce the size of the x-ray beam to 6 x 0.5 mm, which is a compromise between acquisition time (300 seconds) and spatial resolution. The sample is placed in motor stage that is controlled by a LabView® program running on Mac G4 computer. The motor stage can move vertically with precision 10^{-3} mm. The stage was positioned at 45° from the incident beam and the detector. This puts the Ge detector 90° from the incident beam (See Figure 5-2). A 13 element ultra low energy Ge diode detector was used to collect all data. This energy dispersive detector allowed for the simultaneous detection of multiple metals. A multi-channel analyzer was used to collect and integrate the signal pulses. The detector was calibrated prior to each operation cycle so that signal peaks were displayed at the appropriate energies using a radioactive iron isotope of known wavelength.

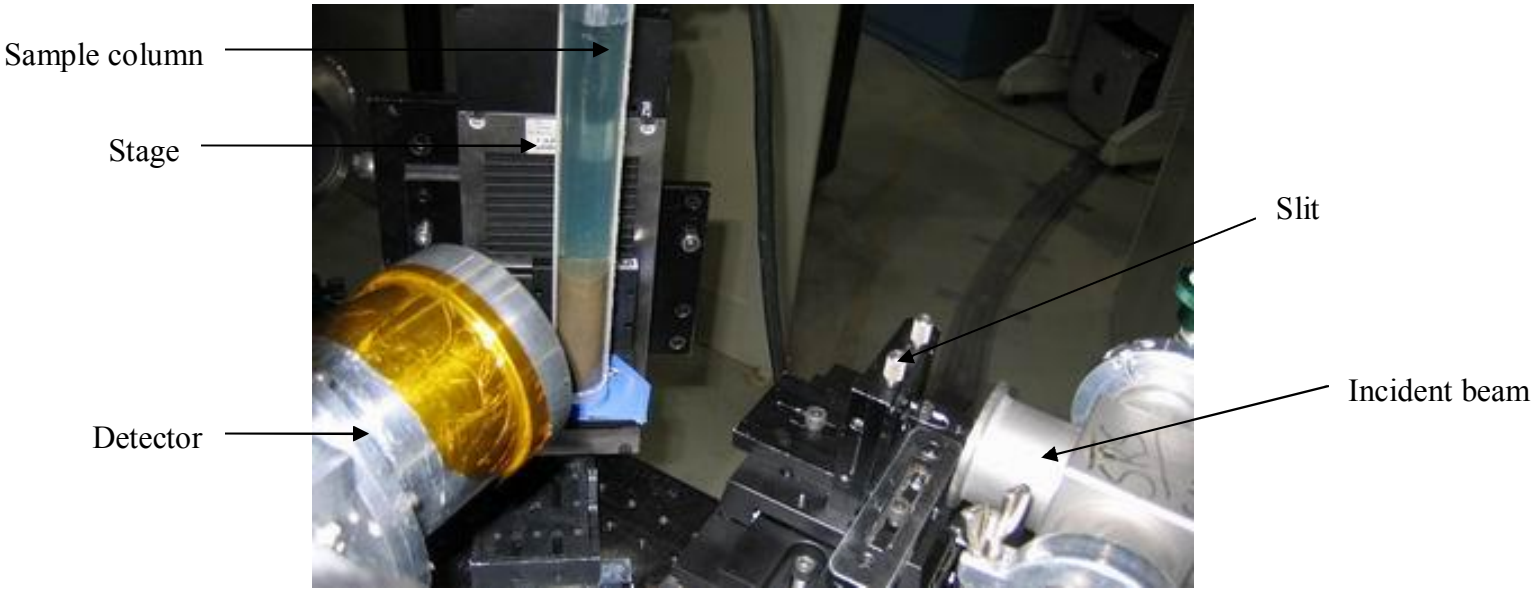

Figure 5-2. Experiment setup in DCM beamline

5.2.3 XRF Experiment Procedure and Data Processing

Before XRF scanning the crystal of the double crystal monochromator was tuned to 10 keV; in other words the incident energy on the sample was 10 keV. The slit positioned before the sample was aligned with the x-ray beam so that the center part of the beam, with the highest photon flux, passed through the slit and the slit was adjusted to reduce the outcoming beam size to 6 x 0.5 mm. These adjustments are made by using x-ray sensitive burn paper to "visualize" the x-ray beam.

Burn paper was also used in the scanning process to determine the vertical position of the water-solid interface in the migration core by using the fact that the x-ray fluorescence spectrum of burn paper has a significant characteristic peak at 4.5 keV (Ti Kα). First the burn paper was placed on the sample column so that the burn paper covers only the solid side and the edge of the paper is just at the water-solid interface. The stage (and sample) is then moved vertically and the column is scanned at different points. This results in a fluorescent spectrum at each point. If the spectrum has a significant peak at

4.5 keV that means the beam is hitting on solid side otherwise it is hitting on the waterside. By this trial and error procedure the water-solid interface position can be determined accurately.

The transport columns were scanned at times 1 day, 5 days and 9 days from the beginning of the transport. Prior to scanning, the top of the tubing was opened and the ponded metal/water solution was mixed to achieve homogeneity. After that, a pipette was used to extract a 20 μL water sample from the middle of the metal solution for later ICP-MS analysis for metal concentrations. At the beginning of each day's scanning a standard metal solution was scanned first and the concentration of this metal solution was measured by ICP-MS afterward.

Once the XRF spectra are obtained the data processing procedure is same as that described in 2.3.5.

5.3 Results and Discussion

5.3.1 XRF Spectra and Spectra Reproducibility

The metal concentrations at each point of metal migration profiles are obtained from the XRF spectra taken at that point. In general there are 11 major peaks in the spectra of the materials studied in this chapter (sand, sediment, Florida Phosphate). In addition to the Kα and Kβ peaks, there is an excitation peak of 10 keV. All these are summarized in the following table:

Table 5-1 Energies of major spectral peaks in spectra

Element	Kα (keV)	Kβ (keV)
Ca	3.7	4.0
Cr	5.4	5.9
Fe	6.4	7.0
Cu	8.0	8.9
Zn	8.6	9.6
Excitation peak	10	

Figure 5-3 is a typical spectrum from the Florida Phosphate core following migration of the metals. Notice the overlap between the Cu Kβ and Zn Kα peaks. As described in the previous section, Peakfit® was used to deconvolute these two peaks and obtain the integrals under the respective peaks. Practically, the sum of the integrals of Kα and Kβ peaks of each element represents the concentration of that element. However, in our experiments it was found that the use of only the Kα peak leads to almost identical migration profiles.

Pb Lα and Lβ peaks at 10.5 keV and 12.6 keV (energies of Pb Kα and Kβ are even higher) are beyond the energy of excitation peak so that Pb cannot be detected in this XRF setup. Tuning the excitation peak at 10 keV is based on two considerations. One is the low beam intensity at high-energy range (intensity drops dramatically after Cu Kα, see Figure 2-1) at CAMD beam line. If the excitation peak is tuned beyond the Pb Kβ peak, the integration time for each scan will be much longer to achieve the same count rates. This will make the total beam time requirement unrealistic. Another consideration is based on this principle: the closer the excitation energy is to the absorption edge, the higher the intensity and sensitivity will be for the element of interest. In Figure 5-3 it is noticed that Cr peak is much lower than Zn and Cu peaks while the actual concentrations are not very different. If the excitation peak moves further to beyond Pb Kβ peak, these differences will be even bigger.

The CAMD beam intensity follows an exponential decline over time after each injection. The median value of the incident beam intensity (I_0) was used to normalize the spectra taken for each sample column profile. But I_0 cannot reflect the spectral change of incident beam that can also lead to different florescence spectra. Plus the sample columns

are on a vertically moving stage. Theoretically, all of these factors make it difficult to reproduce the spectra taken at each physical location. For each metal migration profile a certain point was selected to be scanned three times (the stage moves and back to the same location). As can be seen in Figure 5-4, excellent reproducibility was achieved. Error bars for each migration profile can be calculated from these three spectra taken at one location.

5.3.2 Metal Migration Profiles

Two types of metal migration profiles are measured. The first is of Cu migration from a copper (II) nitrate water solution into sand, Florida Phosphate and Anacostia River sediment. The second is of Cr, Cu and Zn migration from a mixed water solution of chromium (III) chloride, copper (II) nitrate, zinc nitrate and lead (II) chloride into the (0.5 mm thick). This makes for an extremely inhomogeneous sample and therefore, the profiles of Phosphil will not be presented here.

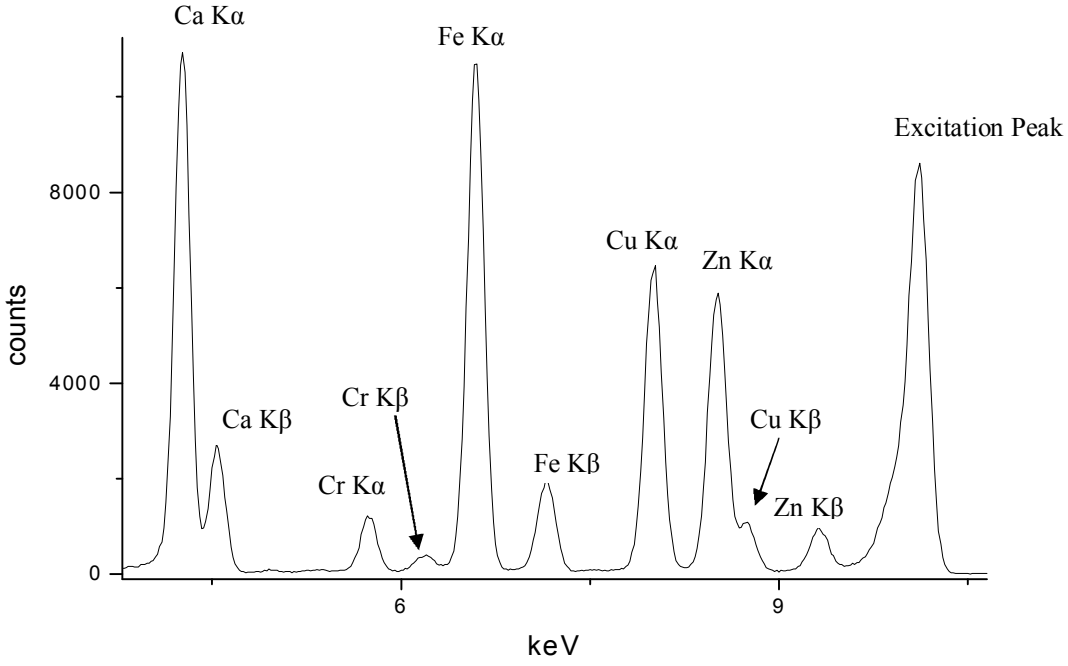

Figure 5-3 XRF spectra of Florida Phosphate (contaminated)

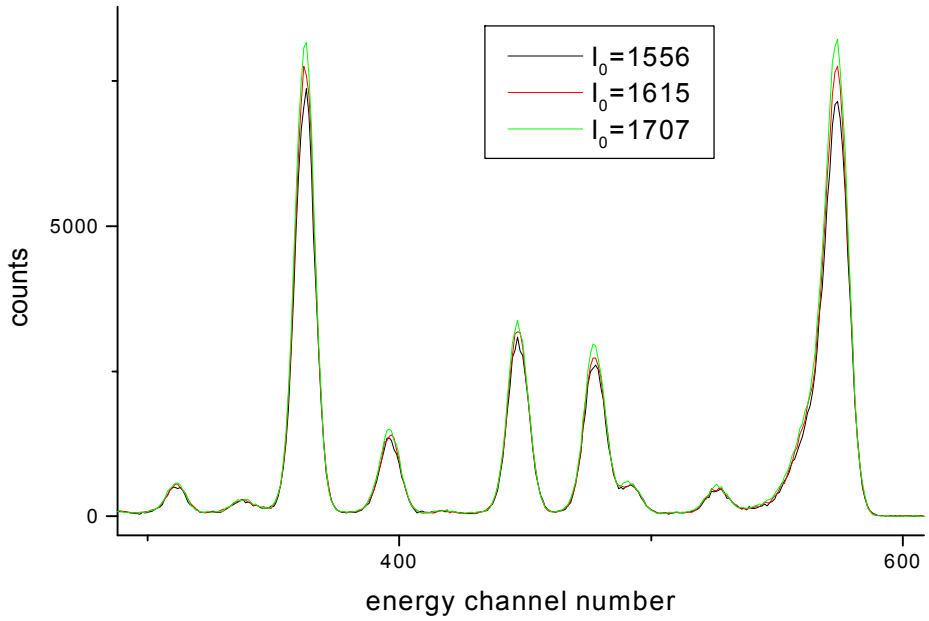

Figure 5-4 Reproducibility test: three XRF spectra of Florida Phosphate (contaminated) taken at same location at different times

Because minor position changes will result in significantly different responses in detector, the profiles measured at different days are calibrated with the relative concentration obtained from the spectra of standard metal solution mounted on the same sample holder taken at corresponding dates so that they can be put in a same plot to compare. For the apatite materials (e.g. Florida Phosphate) it was found that the Ca concentration (relative concentration obtained from spectra) in the solid phase is fairly stable during the metal migration process. Therefore, it is feasible to calibrate the profiles taken at different dates by the Ca concentration. The results of these two calibration methods turn out to be similar. Considering the second method only applies to apatite, all the profiles presented in this chapter are calibrated by the first method.

All the metal migration profiles shown in Figure 5-5 to Figure 5-15 are plotted as normalized concentration versus the depth below water-solid interface. Except for the profiles of sand, all the points in profiles are normalized to the first point of day 1 profiles.

Also shown on the plots is the concentration of the particular metal in the ponded solution at the beginning of the experiment and at each of the scanning times.

The migration speed can be represented by the penetration depth of that specific metal at certain time. Here, the penetration depth is defined as the distance from water-solid interface to the depth where the concentration decreases to 1% of the maximum concentration along the entire profile. A Summary of the penetration depth of different metals in Florida Phosphate and Anacostia River Sediment is given in Table 5-2.

Table 5-2 Penetration depth of metals

Penetration depth (mm)		Cr	Cu		Zn
			"Cu only"	"Cu in Mix"	
Florida Phosphate	Day 1	18.5	7	12.5	18.5
	Day 5	32.5	12	37.5	47.5
Anacostia Sediment	Day 1	7.5	7	7.5	10.5
	Day 5	8.5	10	10.5	17.5

5.3.2.1 Cu ("Cu only") Migration Profiles

Figure 5-5 and Figure 5-6 are the Cu migration profiles from overlying Cu^{2+} solution to Florida Phosphate and Anacostia River sediment. The profiles taken at three different dates (same sample column at 1, 5 and 9 days) are plotted together. The Cu concentrations of overlying solution at different dates are measured by ICP-MS and listed in each figure. For Sand the investigation of its day one profile reveals that Cu had already penetrated the whole 6 cm solid layer, which suggested that shorter time intervals (e.g. by hours) should be used to study the metal migration behavior in this experiment system.

It can be seen that there is no significant difference when comparing penetration depths of Florida Phosphate and sediment (both are 7 mm at day 1). However, the shape of the profiles and the changes in Cu concentration in the ponded solution seem to indicate that the sediment adsorbs more Cu than the phosphate. This is consistent with the isotherm experimental results presented in chapter 3.

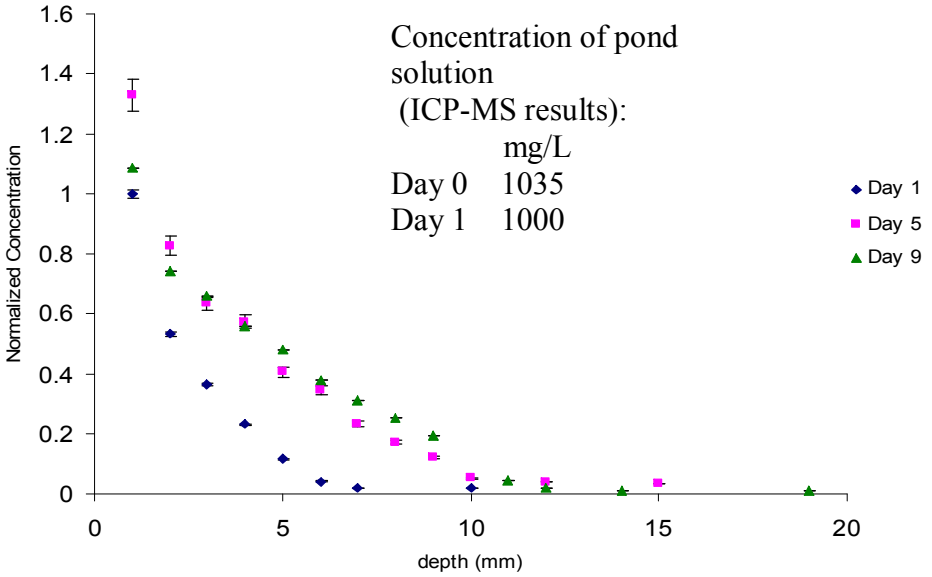

Figure 5-5 Cu^{2+}(Cu only) Migration in Florida Phosphate

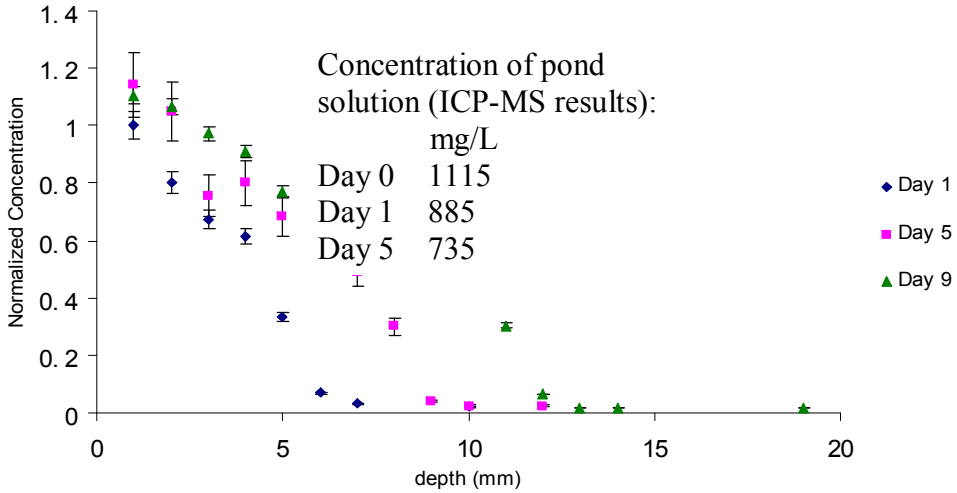

Figure 5-6 Cu^{2+}(Cu only) Migration in Anacostia River Sediment

5.3.2.2 Metal Migration Profiles from Mixed Metal Solution

The migration profiles of Cr, Cu and Zn from a mixed solution of Cr^{3+}, Cu^{2+}, Zn^{2+} and Pb^{2+} to sand, Florida Phosphate and Anacostia River sediment are shown from Figure 5-7 to Figure 5-15. For Florida Phosphate and sediment the calibration and normalization method are same with those in Cu only case. Due to unstable condition of CAMD beamline at day 9 only profiles at day 1 and day 5 are presented here.

Because of the rapid migration times in sand, the metal migration profiles in the sand samples (Figure 5-7 to 5-9) are measured at "time 0" (the time for scanning one point is 5 minutes), 1, 3 and 5 hours. During this scanning process the XRF setup was not modified and therefore, no calibration with spectra of standard solution is needed to compare profiles at different times. All migration profiles in sand are normalized to the first point of the 1 hour profile.

5.3.2.2.1 Migration of Different Metals

To compare different metal migration behavior in the "mixed metal" case the concentrations in each profile are normalized by its maximum and minimum concentrations (i.e. maximum to 1 and minimum to 0) and then they can be combined for comparison. Figure 5-16 and Figure 5-17 are the comparison of different metals' migration profiles at day 5 in Florida Phosphate and Anacostia River sediment.

It can be observed that the order of penetration depth for Florida Phosphate and Anacostia River sediment is Cr < Cu < Zn. The isotherm data in chapter 3 indicate that the order of maximum adsorption capacity of these two materials is Cr > Cu > Zn. Thus, the migration results are consistent with the isotherm data; i.e., higher adsorption results in slower migration.

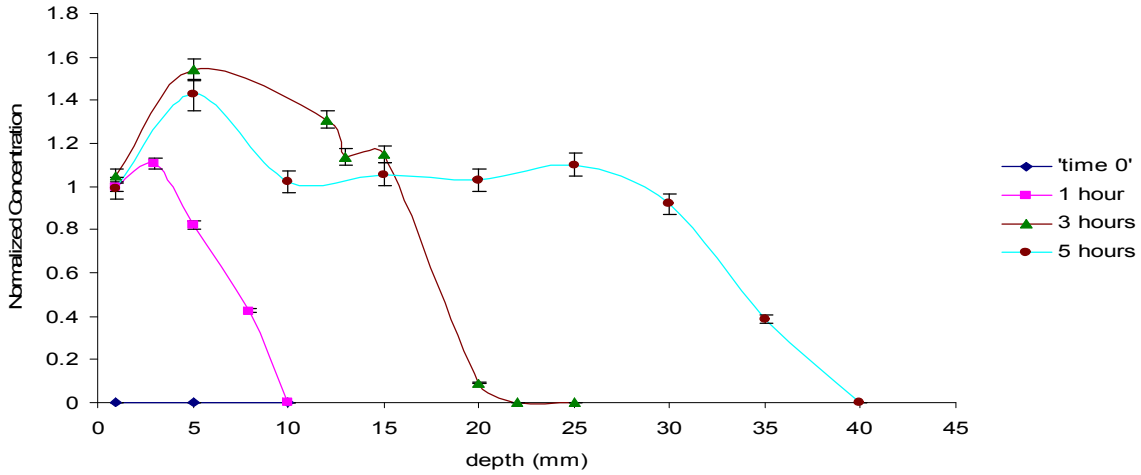

Figure 5-7 Cr^{3+}(in mixed metal solution) Migration in Sand

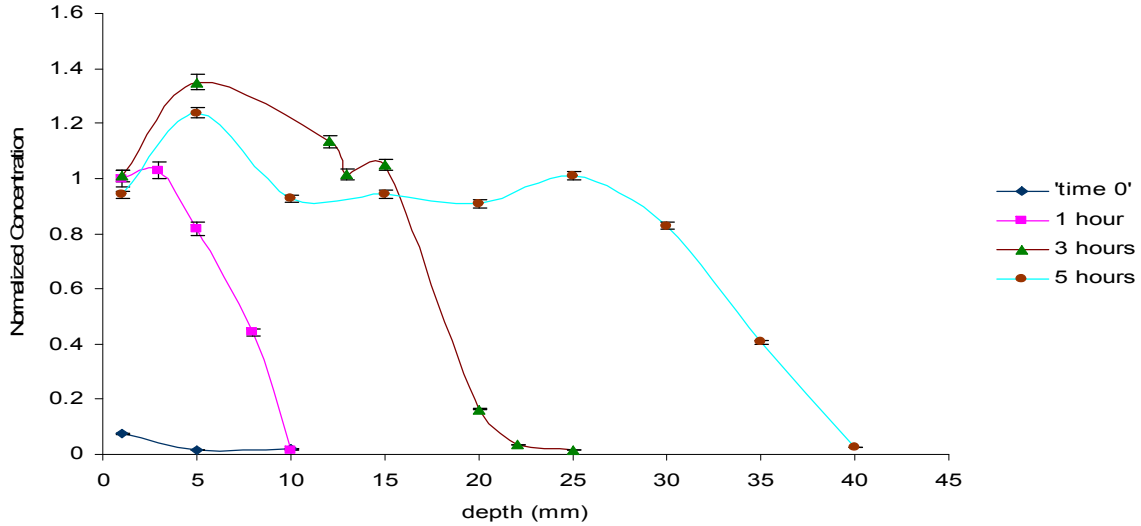

Figure 5-8 Cu^{2+} (in mixed metal solution) Migration in Sand

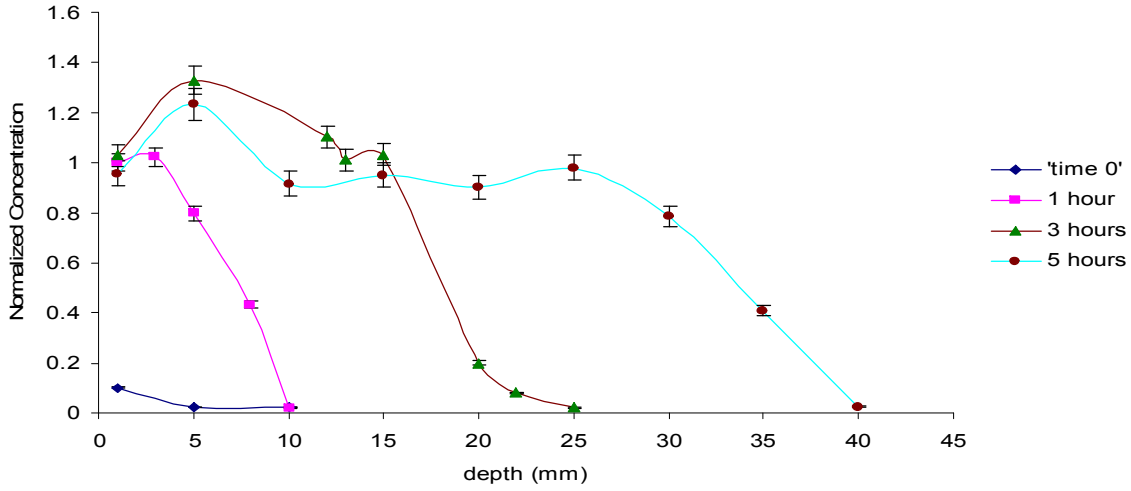

Figure 5-9 Zn^{2+} (in mixed metal solution) Migration in Sand

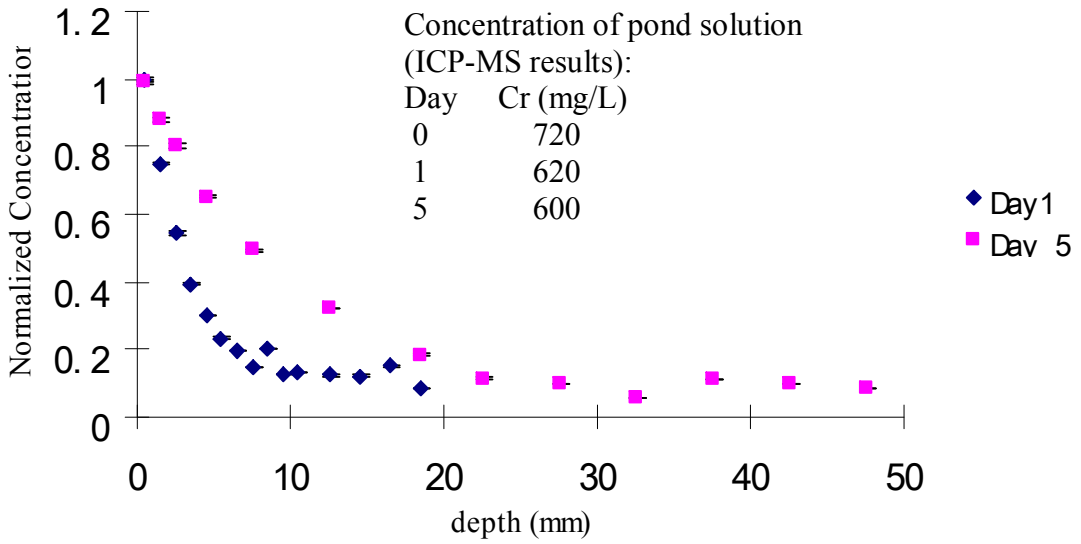

Figure 5-10 Cr^{3+} (in mixed metal solution) Migration in Florida Phosphate

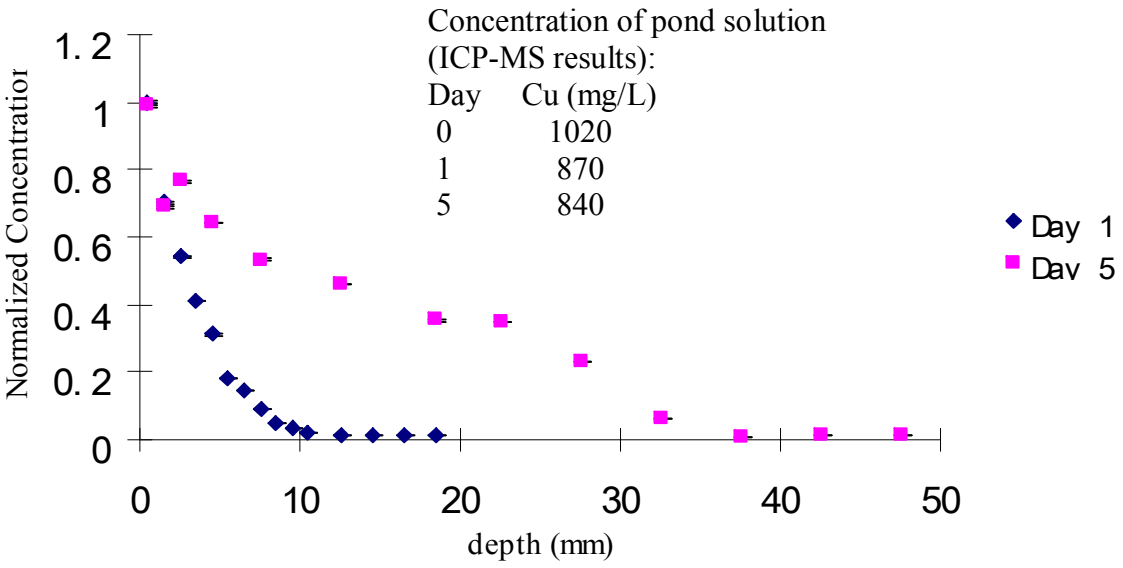

Figure 5-11 Cu^{2+} (in mixed metal solution) Migration in Florida Phosphate

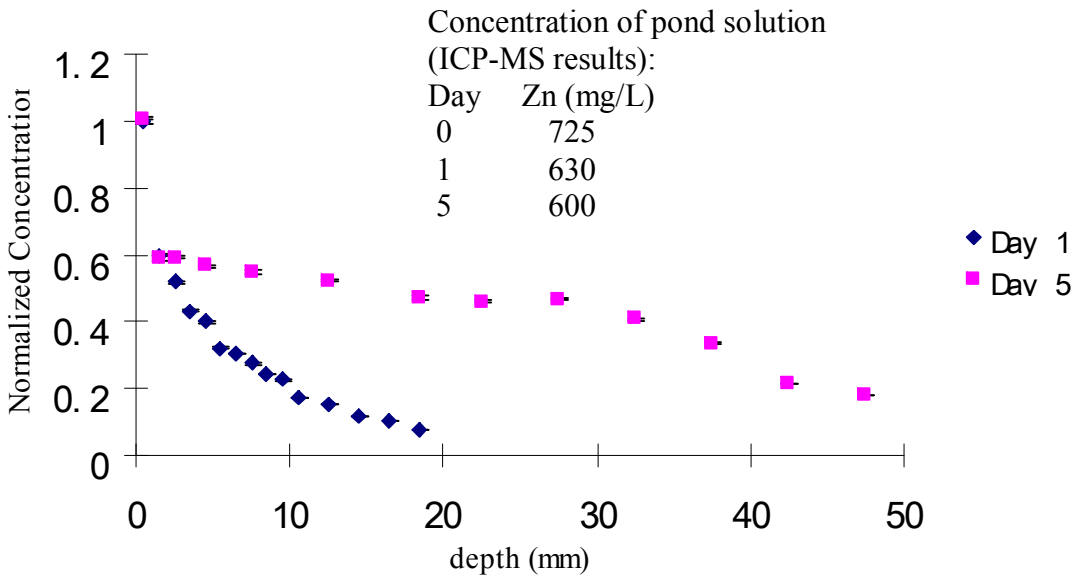

Figure 5-12 Zn^{2+} (in mixed metal solution) Migration in Florida Phosphate

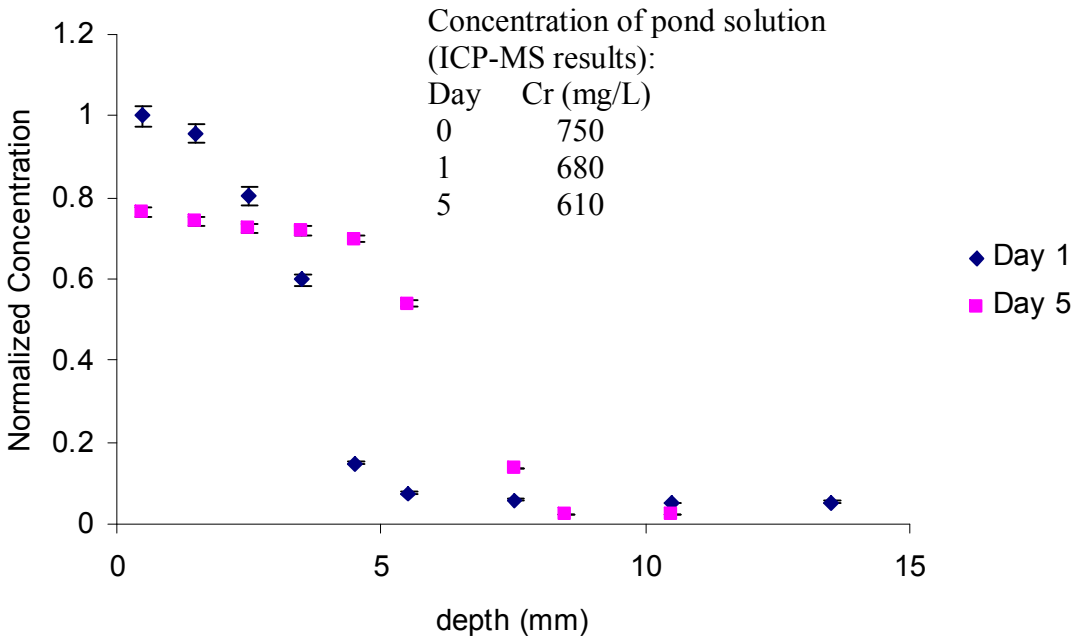

Figure 5-13 Cr^{3+} (in mixed metal solution) Migration in Anacostia River Sediment

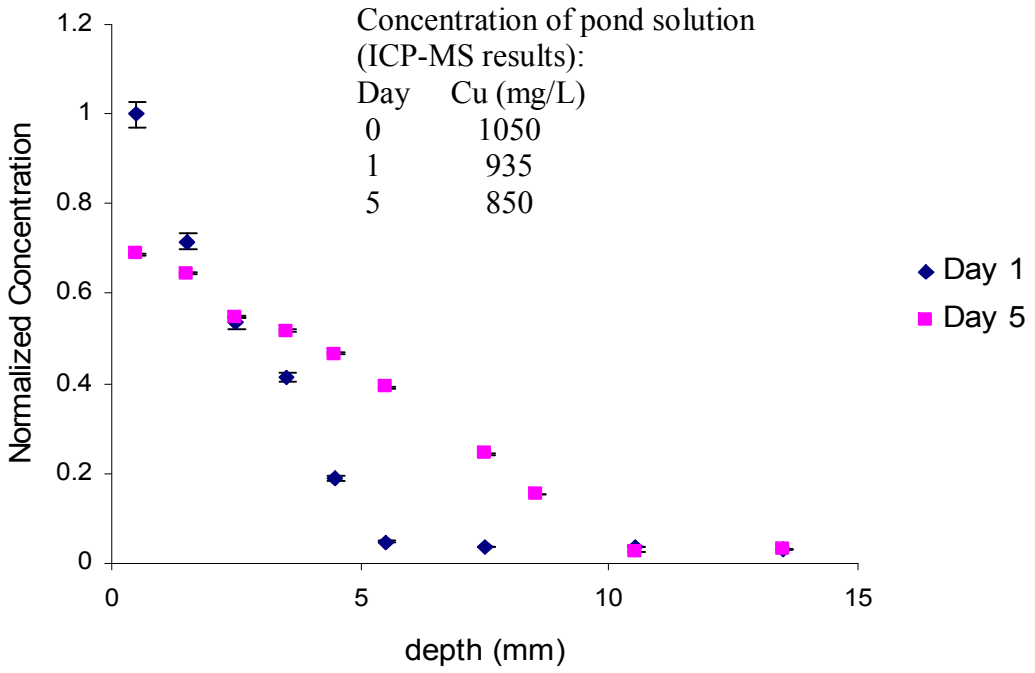

Figure 5-14 Cu^{2+} (in mixed metal solution) Migration in Anacostia River Sediment

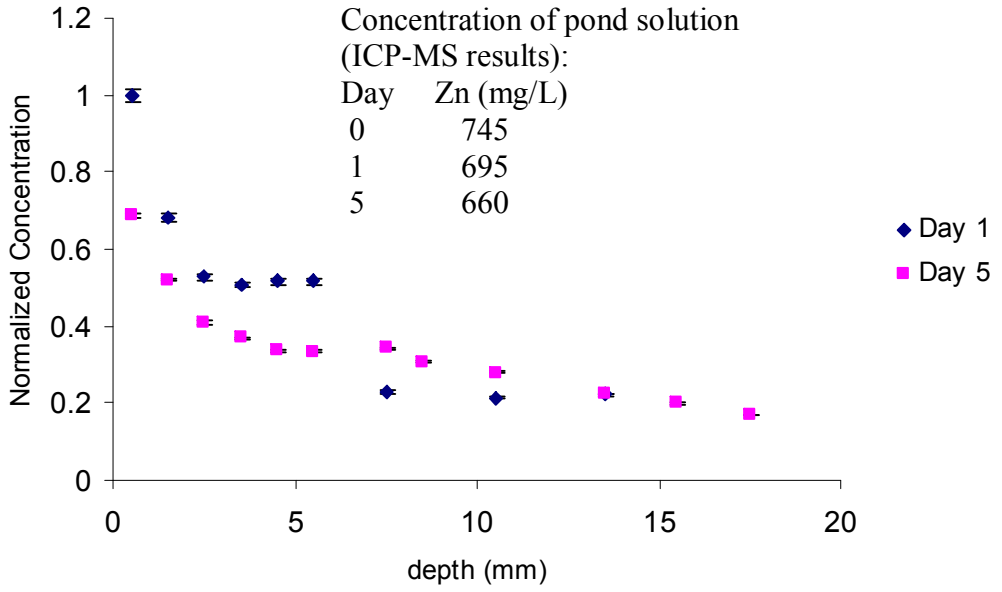

Figure 5-15 Zn^{2+} (in mixed metal solution) Migration in Anacostia River Sediment

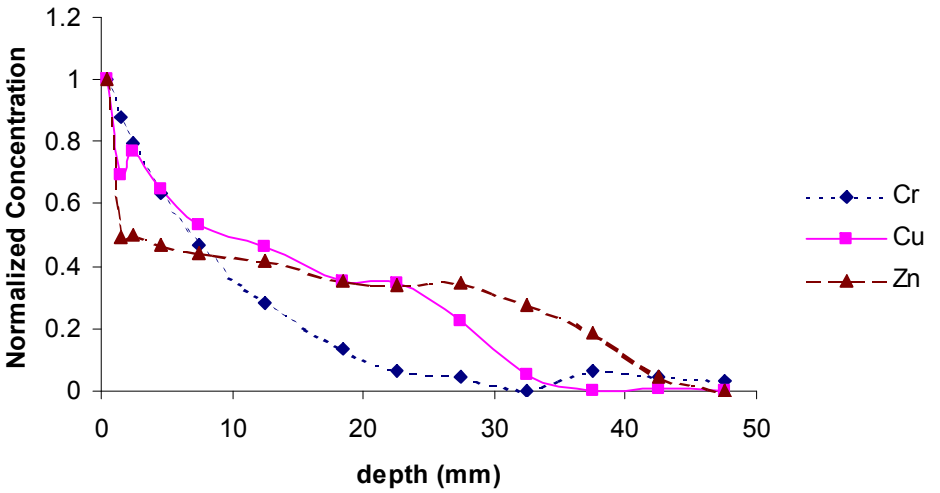

Figure 5-16 Comparison of different metals' migration in Florida Phosphate

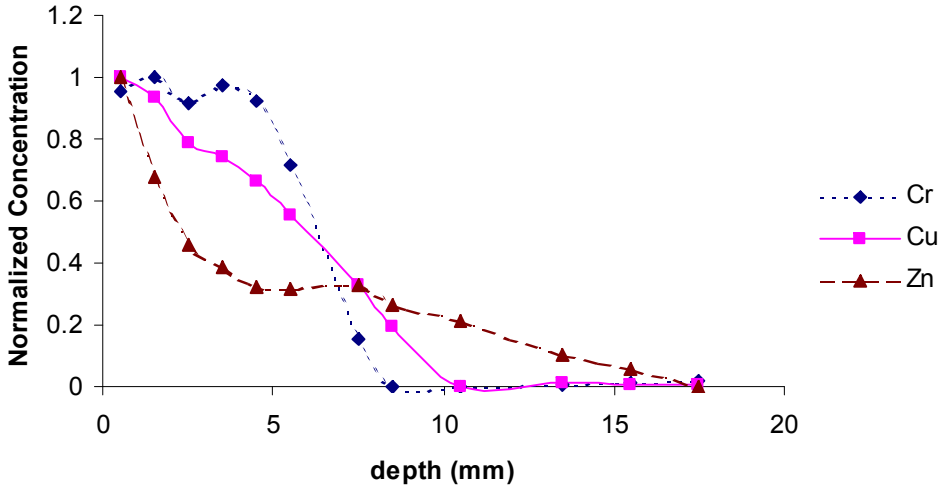

Figure 5-17 Comparison of different metals' migration in Anacostia River Sediment

For sand it can be noticed that the migration profiles of three metals are similar, which implies that because of very weak adsorption in sand (see isotherm data in chapter 3) the controlling factor for metal migration in sand is the porous structure.

5.3.2.2.2 Migration in Different Materials

After being normalized by their maximum and minimum concentrations (i.e. maximum to 1 and minimum to 0), the migration profiles at day 5 in Florida Phosphate and sediment are shown together for Cr, Cu and Zn respectively in Figure 5-18. From these figures it is pretty clear that these three metals migrate faster in Florida Phosphate than in Anacostia River sediment. For sand the migrations are much faster. All these three metals migrate around 10 mm in one hour in sand. Therefore the order of migration speed of these three metals in different materials is: Sand > Florida Phosphate > Anacostia River Sediment, which is consistent with the reverse order of maximum adsorption capacity presented in chapter 3. Recall from chapter 4 that it also takes days for these three metals migrate 10 to 20 mm in Phosphil. Thus, we can conclude that apatite is superior to sand with respect to retardation ability of Cr^{3+}, Cu^{2+} and Zn^{2+}.

5.3.2.3 Comparison of Cu^{2+} Migration in "Cu only" and "Cu in Mix" Cases

The Cu migration profiles at day 5 for "Cu only" and "Cu in Mix" in Florida Phosphate and sediment are shown together in Figure 5-19. It can be clearly seen that the Cu in the "Cu in Mix" case migrates much farther in Florida Phosphate than the Cu only case. This is consistent with corresponding isotherm data of maximum adsorption capacity (0.98 mg/g for "Cu in mix" versus 2.67 mg/g for "Cu only). For sediment no significant difference can be observed. From Figure 5-19 we also notice that migration of Cu in the "Cu only" Florida Phosphate sample is less than that in the sediment.

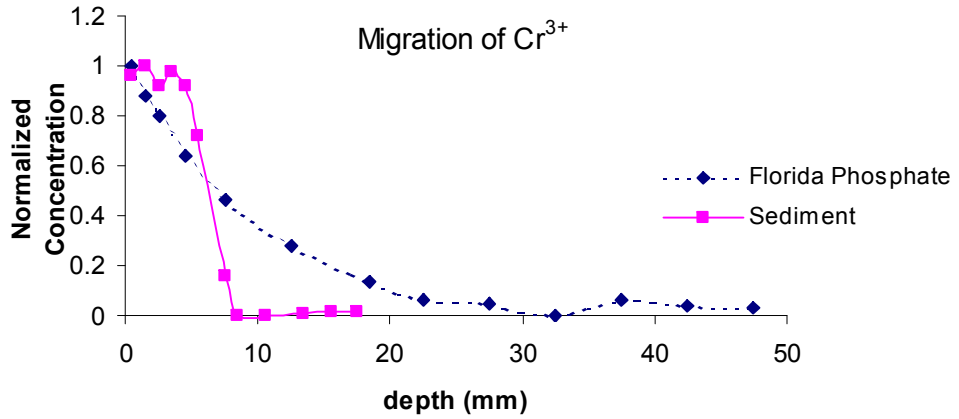

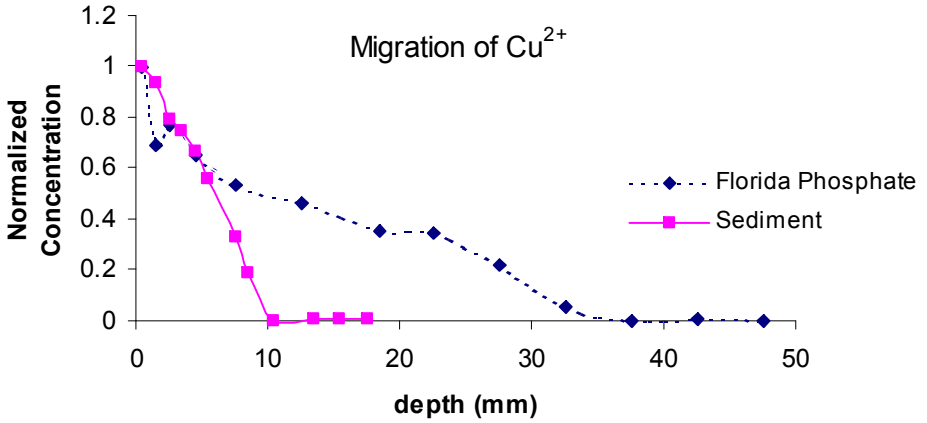

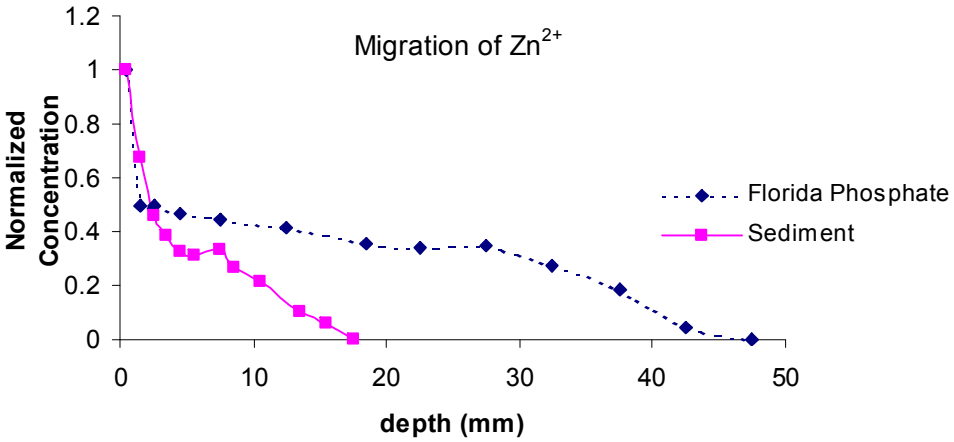

Figure 5-18 Comparison of metal's migration in different materials (day 5)

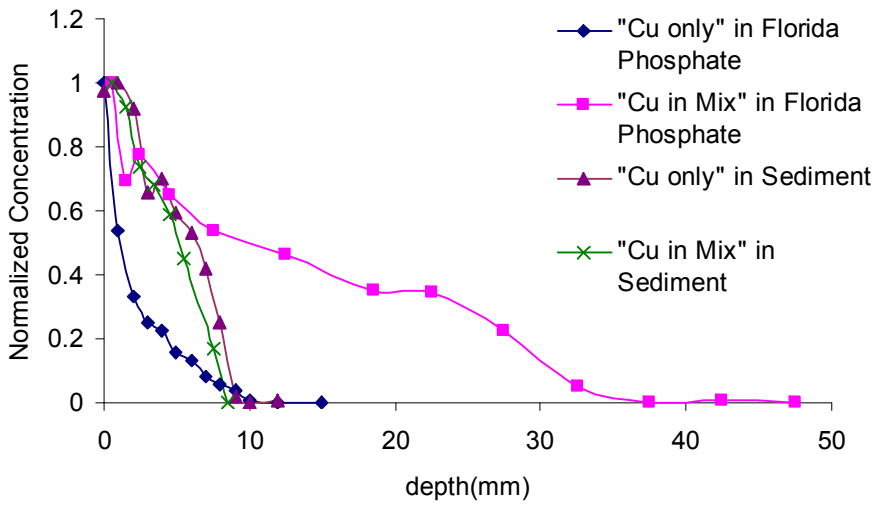

Figure 5-19 Comparison of Cu^{2+} migration in "Cu only" and "Cu in Mix" cases

5.4 Summary

Comparison of the migration speed of metals in the mixed solution case shows:

- For all these three metals, Sand > Florida Phosphate > Anacostia sediment
- For Florida Phosphate and Anacostia sediment, Zn > Cu > Cr
- These observations are consistent with corresponding isotherm data.

Comparing "Cu only" and "Cu in Mix" cases:

- For Florida Phosphate Cu in mixed metal solution migrates much faster, which is consistent with the corresponding isotherm data.
- No significant difference can be seen for sediment

From this set of experiments it is clearly shown that apatite materials are better capping materials than sand with respect to retardation for Cr^{3+}, Cu^{2+} and Zn^{2+}. It is also demonstrated that the high spatial resolution of synchrotron XRF helps improve the data quality of migration profiles comparing with the traditional sectioning method in chapter 4. Finally the high time resolution of synchrotron XRF makes the monitor of metal migration in sand in a time scale of hours possible.

5.5 References

Atlas, E.; Pytkowics, R.M., *Limnol. Oceanogr*. 1977, *22*: 290-300.

Crannell, B.S., Eighmy, T.T., Butler, L., Cartledge, F.K., Emery, E., Willson, C.S., Reible, D.D., and Yin, M., 2001, Reactive Barriers for Containment of Metals-Contaminated Dredged Materials: Diffusion Studies, Proceedings of the Beneficial Use of Recycled Materials in Transportation Applications Conference, Arlington, VA, November 13-15-2001

Crannell, B.S., Eighmy, T., Willson, C., Reible, D., Yin, M., "Pilot-Scale Reactive Barrier Technologies for Containment of Metal-Contaminated Sediments and Dredge Materials," A Final Report Submitted to the NOAA/UNH Cooperative Institute for Coastal and Estuarine Environmental Technology (CICEET), 2004.

Eighmy, T., Lee, 2001, Phosphate mineral-based reactive barrier containment system, *United States Patent*, Patent No.: 6290637 B1

Freeze, R.A.; Cherry, J.A. *Groundwater*. Prentice Hall, Englewood Cliffs, NJ. 1979.

Gao, Y, Kan, A, Tomson, M.B., 2003, Critical evaluation of desorption phenomena of heavy metals from natural sediments, *Environ. Sci. Technol.,* 37, 5566-5573.

Howe, J.A., Loeppert, R.H., Derose, V.J., Hunter, D.B., Bertsch, P.M., 2003, Localization and speciation of chromium in subterranean clover using XRF, XANES, and EPR spectroscopy, *Environ. Sci. Technol.,* 37, 4091-4097.

Janssens K., Adams F., and Rindby A., *Microscopic X-ray Fluorescence Analysis*, J.Weley, Chichester (2000).

Kaplan, D.I., Knox, A.S., 2004, Enhanced contaminant desorption induce by phosphate mineral additions to sediment, *Environ. Sci. Technol.,* 38, 3153-3160.

Liu, C., Jay, J.A., Ika, R., Shine, J.P., Ford, T.E., 2001, Capping efficiency for metal-contaminated marine sediment under conditions of submarine groundwater discharge, *Environ. Sci. Technol.,* 35, 2334-2340.

Liu, C., Jay, J.A., Ford, T.E., 2001, Evaluation of environmental effects on metal transport from capped contaminated under conditions of submarine groundwater discharge, *Environ. Sci. Technol.,* 35, 4549-4555.

Nathan, Y.; In: *Phosphate Minerals,* Nriagu, J.O.; Moore, P.B., Eds. Springer-Verlag, Berlin. 1984 pp. 275-291.

Pinzani, M.C.C., Somogyi, A., Simionovici, A.S., Ansell, S., Steenari, B.M., Lindqvist, O., 2002, *Environ. Sci. Technol.,* 36, 3165-3169.

Pyle, M.S., Nocerino, J.M., Deming, S.N., Palasota, J.A., Palasota, J.M., Miller, E, Hillman, D.C., Kuharic, C.A., Cole, W.H., Fitzpatrick, P.M., Watson, M.A., Nichols, K.D., 1996, Comparison of AAS, ICP-AES, PSA, and XRF in determining Lead and Cadmium in soil, *Environ. Sci. Technol.,* 30, 204-213.

Saile, V, 2002, properties of synchrotron radiation, *Applications of Synchrotron Radiation in Environmental Science, CAMD Summer School 2002.*

Scheinost, A.C., Kretzschmar, R., Pfister, S., Roberts, D.R., 2002, Combining selective sequential extractions, X-ray absorption spectroscopy, and principal component analysis for quantitative Zinc speciation in soil, *Environ. Sci. Technol.,* 36, 5021-5028.

Simpson, S.L., Pryor, I.D., Mewburn, B.R., Batley, G.E., Jolley, D, Considerations for capping metal-contaminated sediments in dynamic estuarine environments, 2002, *Environ. Sci. Technol.,* 36, 3772-3778.

Somasundaran, P.; Wang, Y.H.C. In: Misra, D.N. Ed. *Adsorption and Surface Chemistry of Hydroxyapatite.* Plenum, N.Y. 1984 pp.129-149.

Szulczewski, M.D., Helmke, P.A., Bleam, W.F., Comparison of XANES analyses and extractions to determine Chromium speciation in contaminated soils, 1997, *Environ. Sci. Technol.,* 31, 2954-2959.

Tantemsapya, N, Meegoda, J.N., 2004, Estimation of diffusion coefficient of chromium in colloidal silica using digital photography, *Environ. Sci. Technol.,* 38, 3950-3957.

Tokunaga, T. K.; Sutton, S. R.; Bajt, S., Nuessle, P, Shea-Maccarthy, G, 1998, Selenium diffusion and reduction at the water-sediment boundary: micro-XANES spectroscopy of reactive transport, *Environ. Sci. Technol., 32*, 1092-1098.

Tokunaga, T. K., Wan, J., Firestone, M. K.; Hazen, T. C.; Schwartz, E., Sutton, S. R., Newville, M., 2001, Chromium diffusion and reduction in soil aggregates, *Environ. Sci. Technol, 35,* 3169-3174.

Tokunaga, T. K.; Wan, J.; Pena, J.; Sutton, S. R.; Newville, M., 2004, Hexavalent Uranium Diffusion into Soils from Concentrated Acidic and Alkaline Solutions, *Environ. Sci. Technol., 38*, 3056-3062.

U.S. EPA *Selecting Remediation Techniques for Contaminated Sediment*s, 1993, EPA-823-B-93-001, U.S. EPA, Washington, D.C.

Van der Sloot, H.A.; Wijkstra, J.; Geusebroek, M. Isolation of a dredge spoil deposit with a self-forming seal on the interface of an alkaline reactant layer with dredge spoil. Netherlands Energy research Foundation, 1995, *ECN Report* ECN-C-95-071.

Voegelin, A.; Vulava, V. M.; Kretzschmar, R., 2001, Reaction-Based Model Describing Competitive Sorption and Transport of Cd, Zn, and Ni in an Acidic Soil**,** *Environ. Sci. Technol., 35,* 1651-1657.

Willson, C.S., The Use of Synchrotron Radiation in Environmental Science and Engineering: X-Ray Microtomography and X-Ray Absorption Spectroscopy, Proceedings of the 2002 Association of Environmental Engineering and Science Professors Meeting, August 9-11, 2002, Toronto, CA.

Yin, M., C.S. Willson, and D.D. Reible, 2004, Investigation of Heavy Metal Migration from Contaminated Sediment to Capping material using XRF, presented at the 2004 AICHE Annual Meeting, November 7-12, 2004, Austin, TX.

Chapter 6
Diffusive Modeling of Metal Transport in Capping Materials and Sediment

6.1 Introduction

The experiments described in previous chapters suggest that the sorption isotherms and the metals migration in apatite and sediment are highly correlated. Determining isotherms via batch equilibrium experiments is practically much easier than the dynamic migration experiments. It is attractive to predict the migration of metals with the use of the corresponding isotherms. When certain assumptions (e.g. local equilibrium) are met, the diffusion equation indicates that the metal migration profiles in porous media are impacted by the partitioning of metal between solid and aqueous phase (i.e. isotherm). A diffusive mass transport model for binary metals in bone char was developed by Cheung et al. (2003) based on Langmuir or Langmuir-Freundlich isotherm.

For the diffusion-advection equations when the Langmuir or Freundlich isotherm is introduced Serrano (2001) used series solution to approximate the analytical solution. But it becomes inapplicable when initial condition and one of the Langmuir parameters are large enough. These nonlinear and non-differentiable (when concentrations approaching zero) problems may also cause some numerical methods such as nonlinear solvers based on Newton's method designed for differentiable problems to fail (Fowler et al., 2003). Dawson et al. (1991) solved this nonlinear nonsmooth contaminant transport problem using a mixed finite element method. In this chapter a nonlinear diffusive model that uses a Langmuir isotherm is developed

to model the column transport experiments in chapter 5. A finite difference method is adopted to numerically solve this problem.

6.2 Diffusive Modeling

6.2.1 Development of Model

The metal transport experiments in chapter 3 and chapter 4 can all be modeled the same way: metal ions from water solution overlying the porous media migrate into the underlying porous media. The metal migration is modeled as diffusion in both the water and porous media. The major assumptions of the model are:

1. When metal ions in water interact with solid particles in porous media, local equilibrium will be achieved instantaneously.
2. The adsorption and desorption of metals in solid particles are reversible. This implies that there is no 'metal loss' due to irreversible precipitation in solid phase.
3. The interaction of metals and the plastic materials (polypropylene and polyethene) used in the transport column experiments can be neglected. Then according to the symmetric geometry of the columns used in those experiments, one dimensional diffusion can be assumed.
4. Metal migrations between solid particles occur through the water phase. There is no 'direct' migration from particle to particle.

Based on these assumptions we can develop the mathematical model as the following. From figure 6-1 we can see water solution of metal ions overlies a porous media. At the beginning, the metal concentrations in both water and solid layers are uniform with pore water concentrations C_high (mg/L) in water layer and

C_low (mg/L) in the solid layer respectively. When the experiment starts, metal ions diffuse from the water layer into the solid layer. The parameters in Figure 5-1 are defined as the following:

c : Concentration in water phase

D_w : Diffusivity of metal in water

ε : Porosity of porous media (solid layer)

a , b: the lengths of two layers

ρ_s : Particle density of solid

D_e : Effective diffusivity in solid layer (considering porosity)

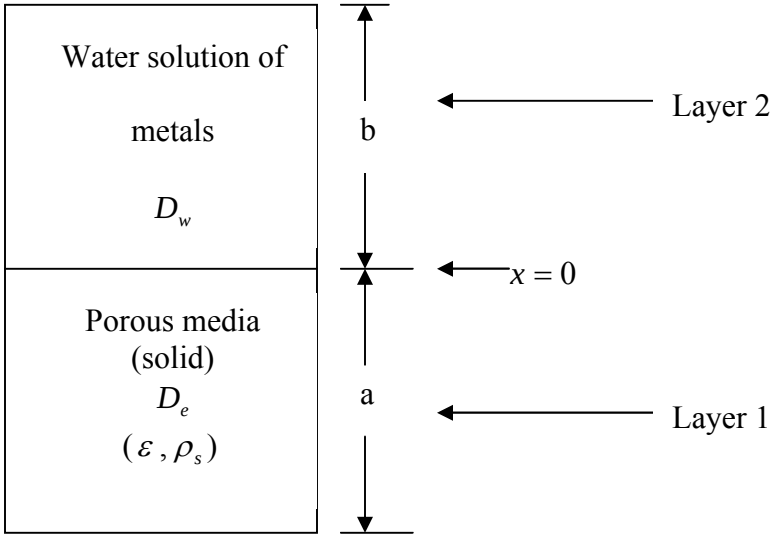

Figure 6-1 Scheme for 'pond' model

For simplicity, we model the pore water concentration c in both layers as a function of time and vertical position (x). The concentration in solid phase and total concentration can be easily calculated from pore water concentration according to isotherm.

From a mass balance and assuming no reaction, the diffusion equation for water layer is

$$\frac{\partial c}{\partial t} = D_w \cdot \frac{\partial^2 c}{\partial x^2} \tag{1}$$

For the solid layer the diffusion equation is

$$\frac{\partial c_{total}}{\partial t} = D_e \cdot \frac{\partial^2 c}{\partial x^2} \tag{2}$$

where

c_{total} is the total metal concentration including metal in pore water and solid phase, given by

$$c_{total} = \varepsilon \cdot c + (1-\varepsilon) \cdot \rho_s \cdot w_s(c) \tag{3}$$

in which $w_s(c)$ is the metal concentration in solid phase, a known function of pore water concentration c (e.g. Langmuir isotherm based on the isotherm experiments in chapter 2). Substituting (3) to (2) yields

$$\frac{\partial}{\partial t}(\varepsilon \cdot c + (1-\varepsilon) \cdot \rho_s \cdot w_s(c)) = D_e \cdot \frac{\partial^2 c}{\partial x^2} \tag{4}$$

For a medium containing a single mobile phase, the effective diffusivity may be estimated by the relationship derived by Millington and Quirk (1961):

$$D_e = D_w \varepsilon^{4/3} \tag{5}$$

Substituting (5) into (4) gives

$$\frac{\partial}{\partial t}(\varepsilon \cdot c + (1-\varepsilon) \cdot \rho_s \cdot w_s(c)) = D_w \varepsilon^{4/3} \cdot \frac{\partial^2 c}{\partial x^2} \tag{6}$$

Given the following initial and boundary conditions we can solve Equation (6) (governing equation) for the pore water concentration c in both layers as a function of time and vertical position (x). Assume the water-solid interface position is at $x = 0$, water layer is from 0 to b , and solid layer is from 0 to $-a$.

Initial Condition:

$$c(x,t) = C\_high \qquad -a \le x \le 0 \ , \ t = 0 \qquad (7)$$

$$c(x,t) = C\_low \qquad 0 < x \le b \ , \ t = 0 \qquad (8)$$

Boundary Condition:

Continuum boundary condition at interface $x = 0$:

$$c_1 = c_2 \qquad x = 0, t > 0 \qquad (9)$$

$$D_e \frac{\partial c_1}{\partial x} = D_w \frac{\partial c_2}{\partial x} \qquad x = 0, t > 0 \qquad (10)$$

(c_1 and c_2 are the concentrations in layer 1 (solid) and layer 2 (water) respectively)

Neumann boundary condition at both ends:

$$\frac{\partial c}{\partial x} = 0 \qquad x = b, t \ge 0 \qquad (11)$$

$$\frac{\partial c}{\partial x} = 0 \qquad x = -a, t \ge 0 \qquad (12)$$

Once the profile (along x) of pore water concentration c is obtained the total concentration profile can be calculated by equation (3).

6.2.2 Numerical Solution: Finite Difference Method

The solid phase concentration $w_s(c)$ in equation (6) can be obtained from isotherm experiment. It can be a Langmuir isotherm, or a Freundlich isotherm etc.

However sometimes it can not easily be regressed to certain analytical forms and just remains as a numerical 'table'. Therefore it is not typically feasible to obtain the analytical solution for equation (6). In this section a finite difference method is introduced to numerically solve equation (6).

6.2.2.1 Discretization of Model Equations and Boundary Conditions

Equation (6) can be rewritten as

$$f(c)\cdot\frac{\partial c}{\partial t}=\frac{\partial^2 c}{\partial x^2} \tag{13}$$

where

$$f(c)=\frac{\varepsilon+(1-\varepsilon)\cdot\rho_s\cdot\dfrac{\partial w_s}{\partial c}}{D_w\varepsilon^{4/3}} \tag{14}$$

Discretize (13) using an explicit method,

$$f(c_{i,j})\cdot\frac{c_{i,j+1}-c_{i,j}}{\Delta t}=\frac{c_{i+1,j}-2\cdot c_{i,j}+c_{i-1,j}}{\Delta x^2} \tag{15}$$

Where

$c_{i,j}$ denotes concentration at i th spatial point and j th time step, Δt is time step, Δx is spatial step.

The convergence for an explicit method is conditionally based on:

$$\Delta t\le 0.5\cdot f(c)\cdot(\Delta x)^2 \tag{16}$$

Using an implicit method to discretize equation (6) gives:

$$f(c_{i,j})\cdot\frac{c_{i,j+1}-c_{i,j}}{\Delta t}=\frac{c_{i+1,j+1}-2\cdot c_{i,j+1}+c_{i-1,j+1}}{\Delta x^2} \tag{17}$$

Assuming the solid layer is equally divided to N parts and water layer is equally divided to M parts. Then $\Delta x_1 = \frac{a}{N}$, $\Delta x_2 = \frac{b}{M}$ and boundary condition is:

At interface $$D_e \frac{c_{N,j} - c_{N-1,j}}{\Delta x_1} = D_w \frac{c_{N+1,j} - c_{N,j}}{\Delta x_2} \quad (18)$$

and at two ends $$c_{0,j} = c_{1,j} \quad (19)$$

$$c_{N+M-1,j} = c_{N+M,j} \quad (20)$$

The initial condition is:

$$c_{i,0} = C\_low \qquad i = 0 \cdots N,\ j = 0 \quad (21)$$

$$c_{i,0} = C\_high \qquad i = N+1 \cdots N+M,\ j = 0 \quad (22)$$

6.2.2.2 Verification of the Numerical Method: Comparison to Analytical Solution

To verify the finite difference model a comparison of its computation results to an analytical solution is made. First we need to simplify the model so that an analytical solution can be achieved. Assuming the metal concentration of the ponded water is constant C_h, the initial concentration in solid layer is C_0 and the solid layer has a constant partition coefficient K_d, then the analytical solution for the pore water concentration can be solved by Laplace transform and the result is:

$$c(x,t) = C_0 + (C_h - C_0) \cdot erfc\left(-\frac{x}{2 \cdot \sqrt{\frac{Dw \cdot \varepsilon^{4/3} \cdot t}{\varepsilon + (1-\varepsilon) \cdot \rho_s \cdot K_d}}}\right) \quad (23)$$

The finite difference algorithm is used to solve this simplified model and the result is compared with analytical solution.

Figure 6-2 to Figure 6-4 are three examples comparing the analytical solution and the finite difference method (FDM) results with spatial step decreasing from 0.25 mm

to 0.05 mm, respectively. For all these three examples, C_h = 1000, C_0 = 0.0003, discretion time step is 400 seconds and K_d =0.41. From the figures we can see the FDM result matches the analytical solution well. Variations decrease dramatically with a decreasing spatial step indicating convergence of the FDM algorithm. Here average relative variation is defined as the mean of Abs{(Cm-Ca)/Ca}. Cm concentration from FDM result, Ca is the concentration from analytical result.

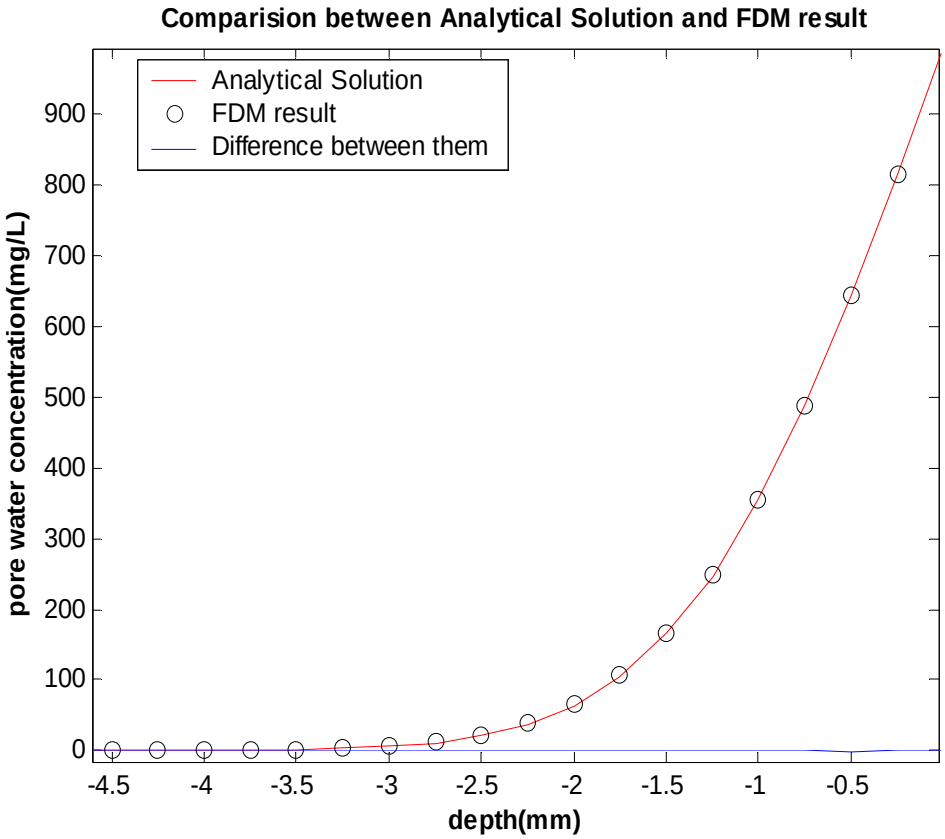

Figure 6-2 Comparison between analytical solution and FDM result (discretion spatial step Δx = 0.25 mm; average relative variation is 0.029)

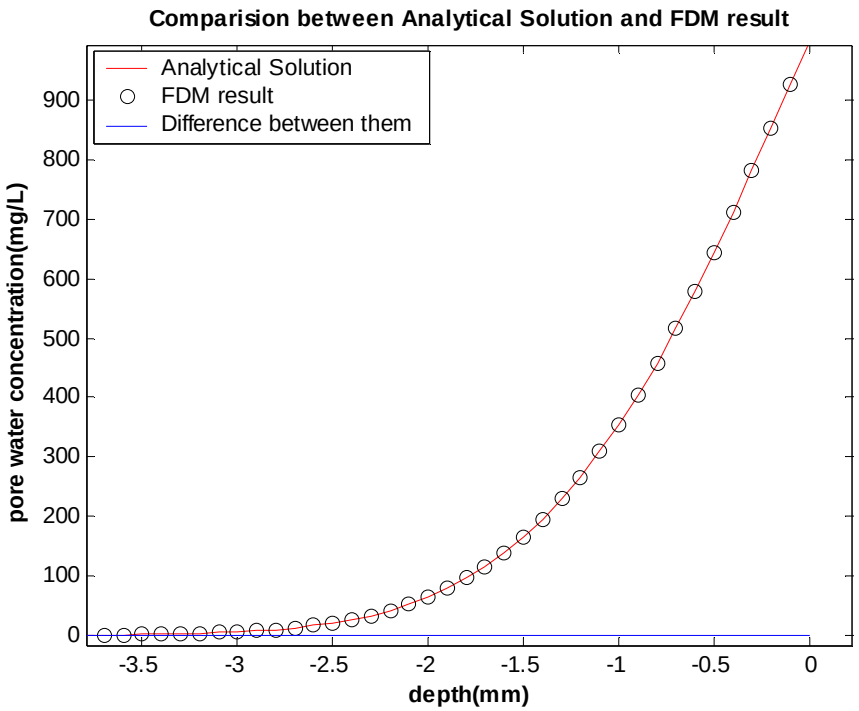

Figure 6-3 Comparison between analytical solution and FDM result (discretion spatial step Δx =0.1 mm; average relative variation is 0.0037)

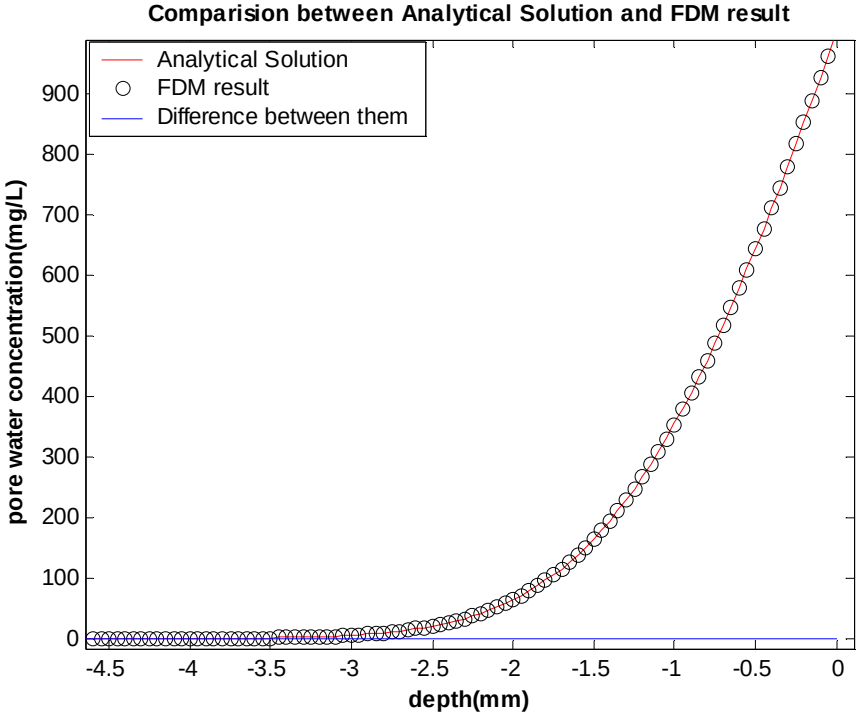

Figure 6-4 Comparison between analytical solution and FDM result (discretion spatial step Δx =0.05 mm; average relative variation is 0.00063)

6.2.3 Model Prediction and Sensitivity Analysis

Figure 6-5 is a typical result of this numerical modeling of the Cu diffusion (Mono-element system) in Florida Phosphate for 1 day, 5 days and 9 days. The solid-water interface is at $x = 0$. The water layer is in the region of $x > 0$ and the region of $x < 0$ denotes the solid layer. The plotted concentration is the pore water concentration so that the concentration is continuous across solid-water interface. It can be noted that the expansion length of diffusion in water layer is much larger than that in solid layer. This is because the diffusivity of Cu in water is much larger due to absence of the retardation of solid matrix. Table 6-1 gives the parameters used to calculate the diffusion profiles in Figure 6-5.

Table 6-1 Modeling parameters for Cu diffusion in Florida Phosphate

C_0 (mg/L)	H (mm)	W_m (mg/g)	K (L/mg)	ρ_s (g/L)	ε
1000	120	2.67	0.15	2600	0.4

The definitions of these parameters are:

C_0 : initial concentration in water layer;

H : length of water layer;

ε : porosity;

W_m : maximum sorption capacity (Langmuir parameter);

K : Langmuir parameter;

ρ_s : particle density;

Figure 6-6 is a "zoom in" of the solid layer in Figure 6-5. Based on the isotherm data in chapter 3, the total concentrations can be calculated from pore water concentrations by equation (3) (Figure 6-7). Notice that the shapes of the diffusion profiles of pore water and total concentrations are different. That is due to the nonlinearity of the Langmuir isotherm. At high concentrations, when pore water concentration increases the concentration in solid phase will not change accordingly. That is why the profile of total concentration increases slower from low to high concentration.

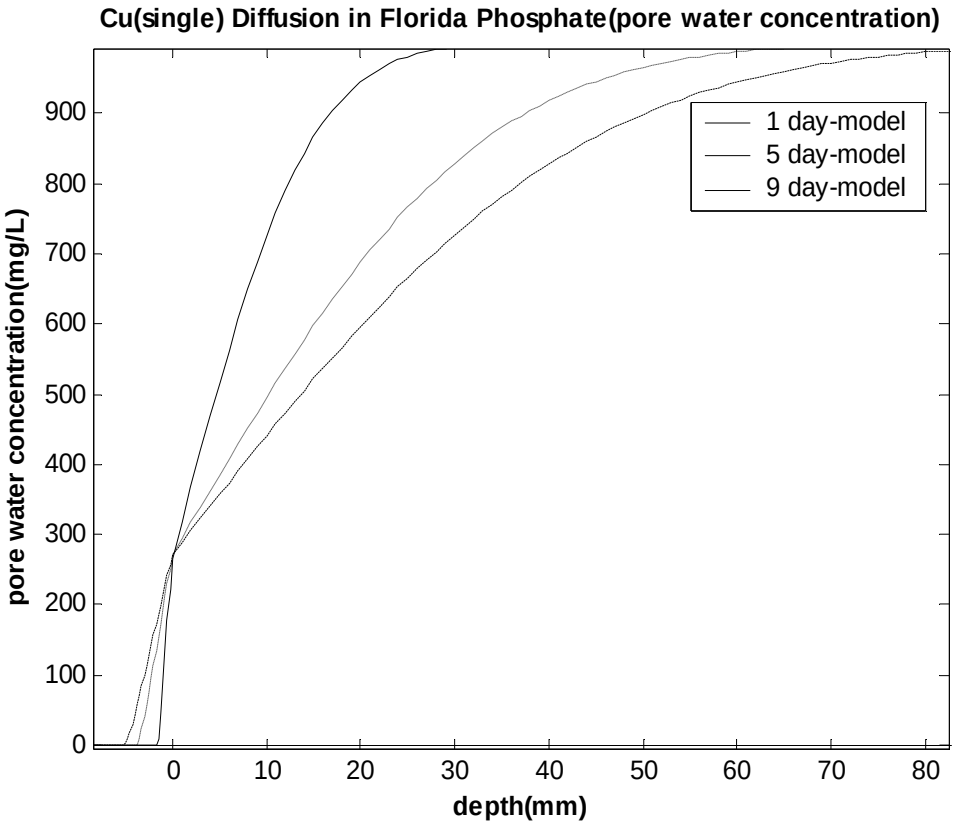

Figure 6-5 Cu Diffusion profiles in water layer and Florida Phosphate (Mono-element System)

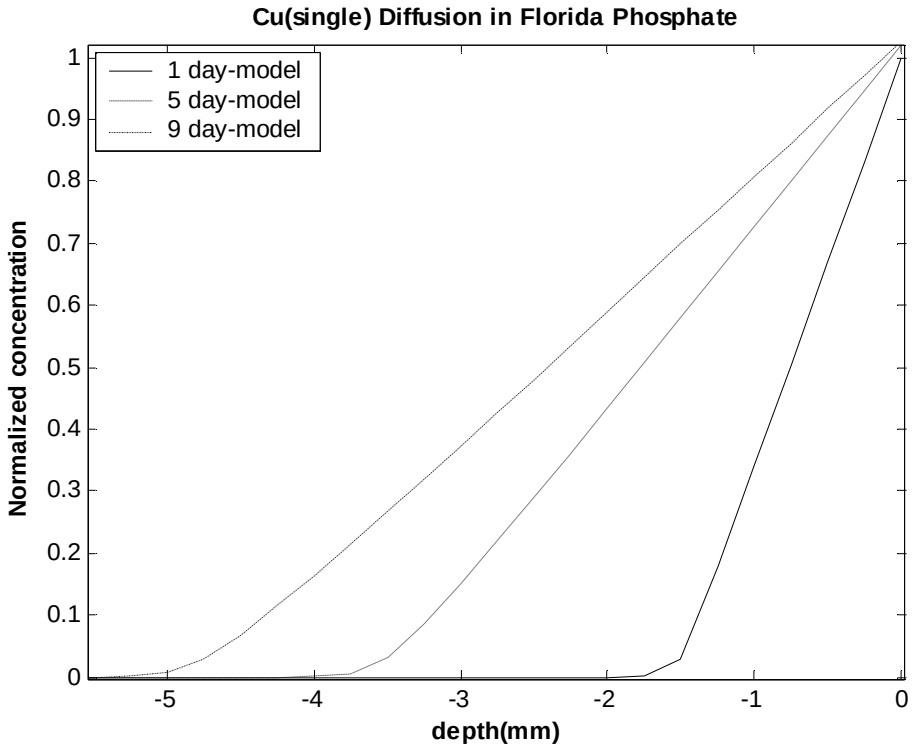

Figure 6-6 Cu Diffusion profiles (pore water concentration) in Florida Phosphate (Mono-element system)(concentration normalized to the first point of day one profile)

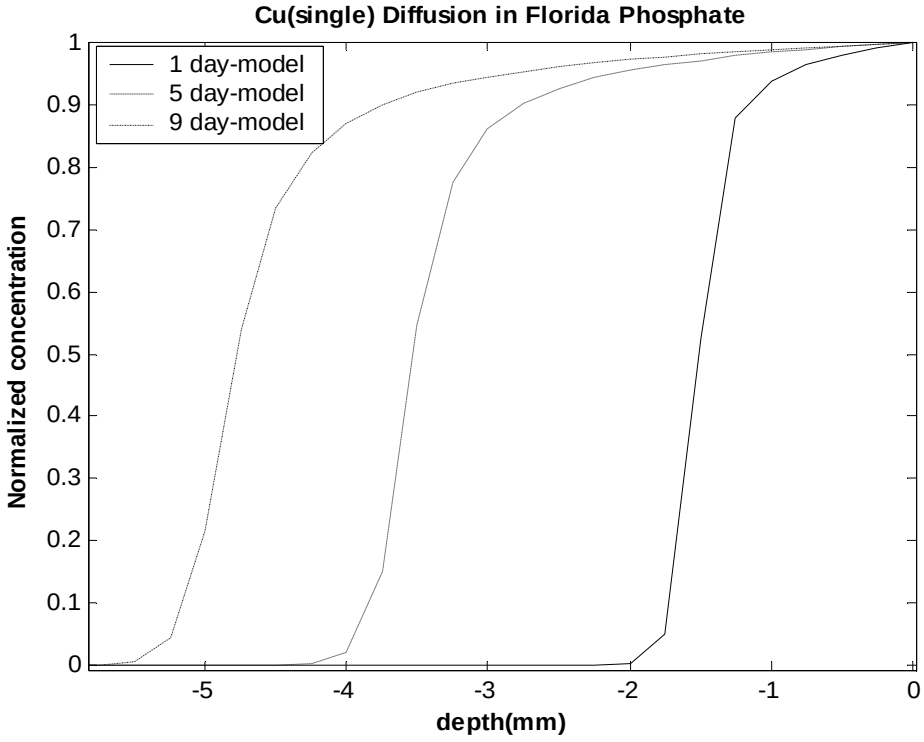

Figure 6-7 Cu Diffusion profiles (total concentration) in Florida Phosphate (Mono-element system) (concentration normalized to the first point of day one profile)

This model can also be used to estimate the effective retardation factor based on linear isotherm. First substitute the nonlinear isotherm data and calculate the penetration depth (defined in 5.3.2) at certain time interval and then compare with the linear model which assume constant retardation factor, by trail and error, the effective retardation factor can be found (e.g. for migration experiments with high concentration metal solution, model inferred retardation factors of Cu in tetra-element system were 0.46, 43, 100 for sand, Florida Phosphate and *Phosphil*®).

The major parameters affecting the diffusion profiles are those listed in table 6-1 (i.e. C_0 , H , W_m , K , ρ_s , ε). The other parameters vary little relatively in the experiment process. For example, the molecular diffusivity of metal in water is a linear function of temperature. $D_A = \frac{1.173 \cdot 10^{-16} T \sqrt{\phi \cdot M}}{\mu \cdot V_m^{0.6}}$ (Wilke and Chang, 1955), T is temperature, μ is viscosity of the solvent (which is related with T), ϕ and V_m is a solvent related parameter. Usually the temperature range in lab is 293 K to 303 K (20^0C to 30^0C). That means there will be only about 3% deviation in the molecular diffusivity.

Sensitivity analysis was done to evaluate how those parameters affect the diffusion profile. It is found that the shape of the diffusion profiles are all similar to those in figure 6-5 to figure 6-7 as the parameters change. The principle change in the profile is the penetration depth which is defined as the distance at which the concentration of metal decreases to the initial background concentration of solid layer. Figure 6-8 to Figure 6-13 are the plots of different values of those 6 parameters (C_0 , H , W_m , K , ρ_s , ε) versus penetration depths (d) for one day, respectively.

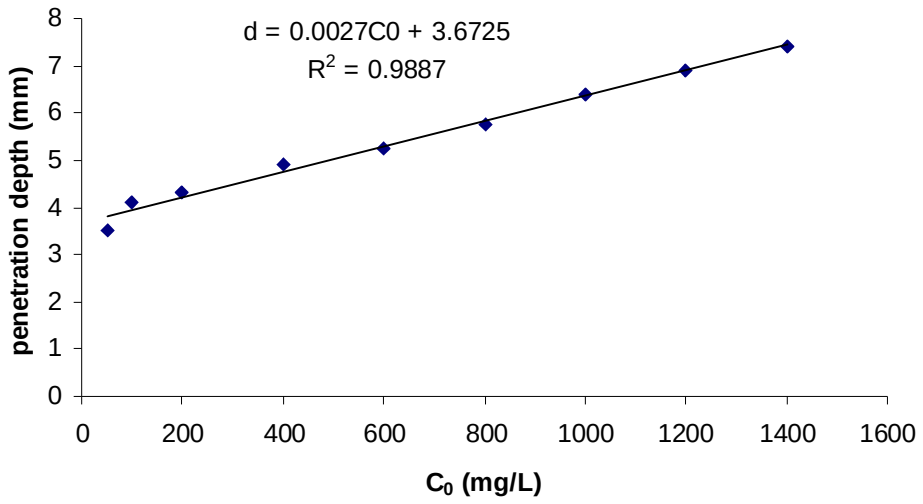

Figure 6-8 Sensitivity analysis: initial concentration in water layer (C_0) (H =120mm, W_m =2.67 mg/g, K =0.15 L/mg, ρ_s =2600 g/L, ε =0.4)

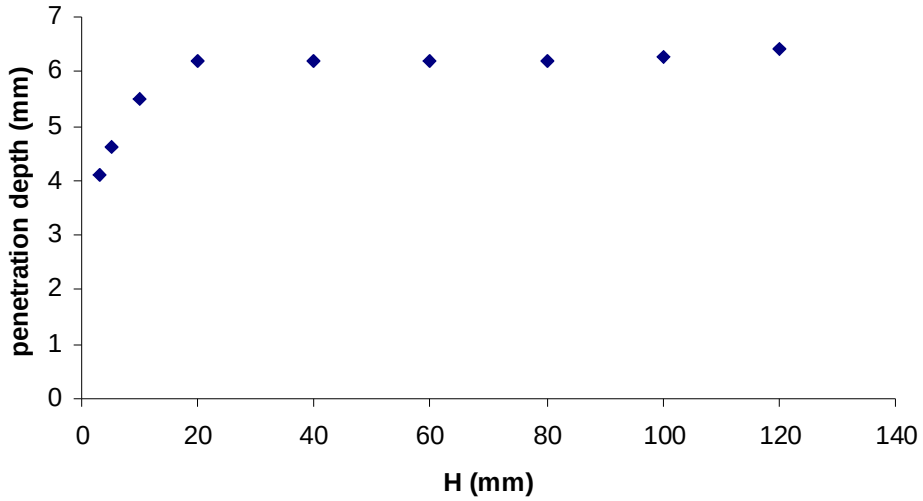

Figure 6-9 Sensitivity analysis: length of water layer (H) (C_0 =1000 mg/L, W_m =2.67 mg/g, K =0.15 L/mg, ρ_s =2600 g/L, ε =0.4)

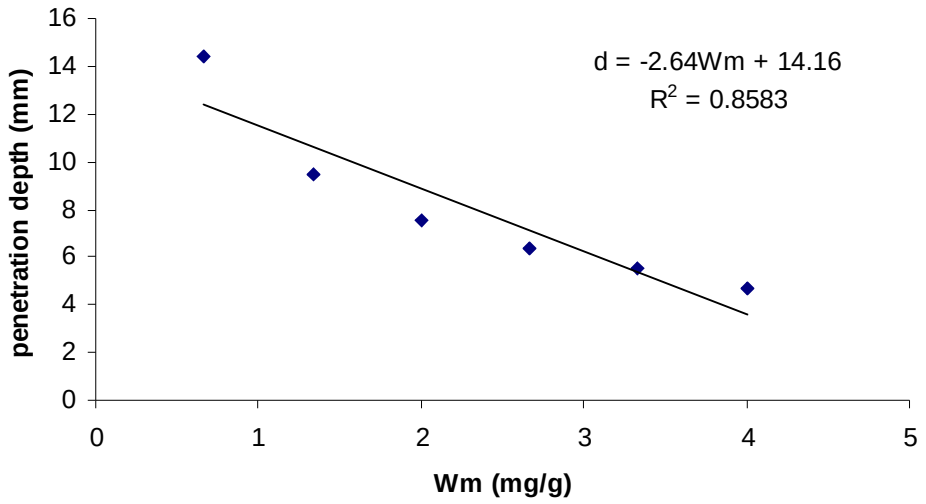

Figure 6-10 Sensitivity analysis: maximum capacity (W_m) (C_0 =1000 mg/L, H =120mm, K =0.15 L/mg, ρ_s =2600 g/L, ε =0.4)

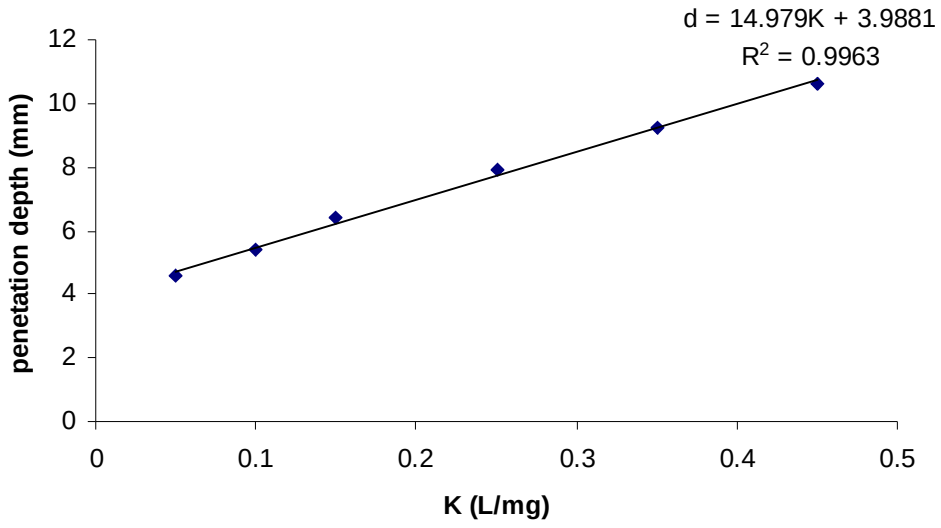

Figure 6-11 Sensitivity analysis: Langmuir parameter (K) (C_0 =1000 mg/L, H =120mm, W_m =2.67, ρ_s =2600 g/L, ε =0.4)

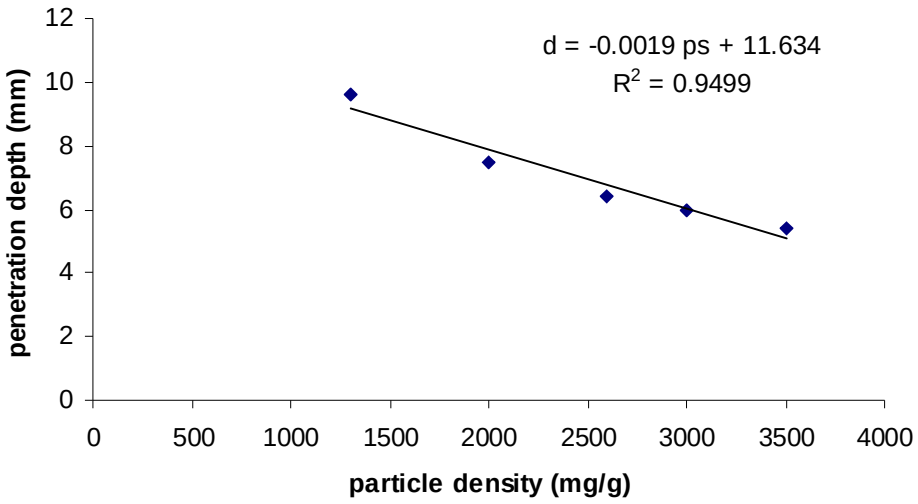

Figure 6-12 Sensitivity analysis: particle density (ρ_s) (C_0 =1000 mg/L, H =120mm, W_m =2.67, K =0.15 L/mg, ε =0.4)

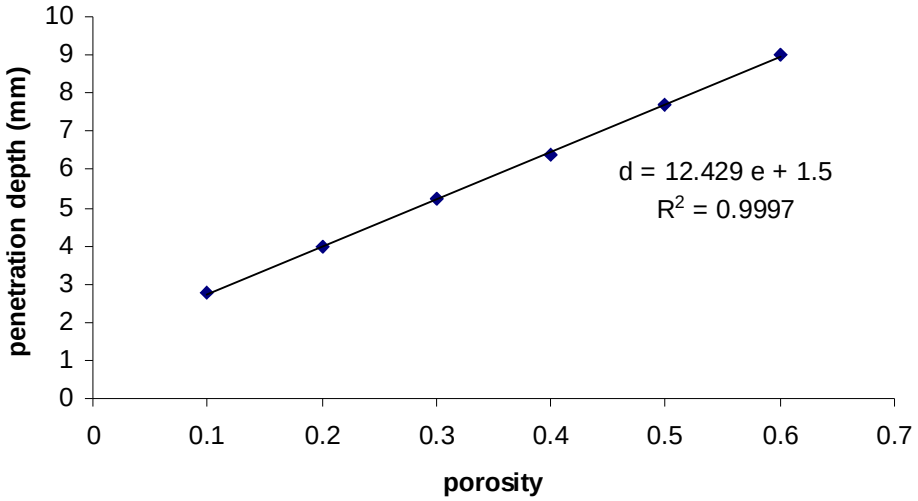

Figure 6-13 Sensitivity analysis: porosity (ε) (C_0 =1000 mg/L, H =120mm, W_m =2.67, K =0.15 L/mg, ρ_s =2600 g/L)

The above six figures indicate that the penetration depth of the diffusion profile are pretty well linearly related with C_0, W_m, K, ρ_s and ε. The penetration depth increases with C_0, K, ε and decreases with W_m and ρ_s. For H there is a turn point (in this case it is at 20 mm). Before the turning point the penetration depth increases with H and after the turning point it remains constant. For those linear relations the gradients of the line can be used to indicate how fast the penetration depth changes with those variations. However these gradients are based on the absolute numbers and don't reflect how fast the penetration depth will change with the relative change of variations. For example 0.1 is a very small change for ρ_s but a big change for K. To obtain the gradients based on relative changes we first normalize the variations by dividing each numbers by the minimum number in the data set and then do the linear regression again to get the gradient. Table 6-2 is a summary of the gradients based on relative change of five parameters.

Table 6-2 The gradients of linear relation between five parameters affecting penetration depth

Parameter	C_0	W_m	K	ρ_s	ε
gradient	0.134	-1.76	0.749	-2.44	1.24

From this table it appears that W_m, ρ_s and ε affect penetration depth more than the others. However particle density and porosity can be easily measured and it is not reasonable to make a significant change of them in the modeling. Thus W_m becomes the most sensitive parameters affecting the penetration depth in this diffusion modeling.

6.2.4 Modification of the Model and Its Evaluation

Figure 6-14 and Figure 6-15 are the pore water concentration and the total concentration profiles of Cu in Florida Phosphate predicted by numerical model and the experimental data set from XRF experiment. The shapes of the pore water concentration profiles are more similar to the profiles obtained from XRF experiment implying that the penetration of X-rays in XRF experiment may be limited so that most of the detection part is the pore water next to the migration column surface, or most of the metal is in water phase so migration in pore water is dominant.

From these two figures it also can be seen that the modeling underestimates the migration of Cu though model prediction of the distances among three profiles are much closer to those in the experiment data. This is a common situation in most of the profiles observed in migration experiments and suggests that in day 1 the migrations involve not only diffusion but also some processes other than diffusion. For example, two major processes could be considered are intermixing at the beginning of introducing the metal solution and the gravity effect due to the difference of the densities between metal solution and pure water.

Experiment data show that the density of the mixed metal solution (1000 ppm) used in the migration experiment is 1% larger than the density of distilled water (i.e. $\frac{\Delta\rho}{\rho} = 0.01$), approximately. In our migration experiment the metal solution pond over the solid layer. This density difference will produce gravity driving force inducing a downward advection. One way to estimate the advection velocity is using Darcy's Law:

$$q = -k_p \frac{\Delta h}{L} \tag{24}$$

k_p is the hydraulic conductivity, Δh is the hydraulic head across the medium, L is the length of the medium and q is the Darcy velocity. If the porosity is ε the actual average fluid velocity v in the interstitial space in the medium is given by q/ε. From the particle size distribution data in Chapter 3 we know the average particle size is 0.39 mm for sand and 0.31 mm for Florida Phosphate.

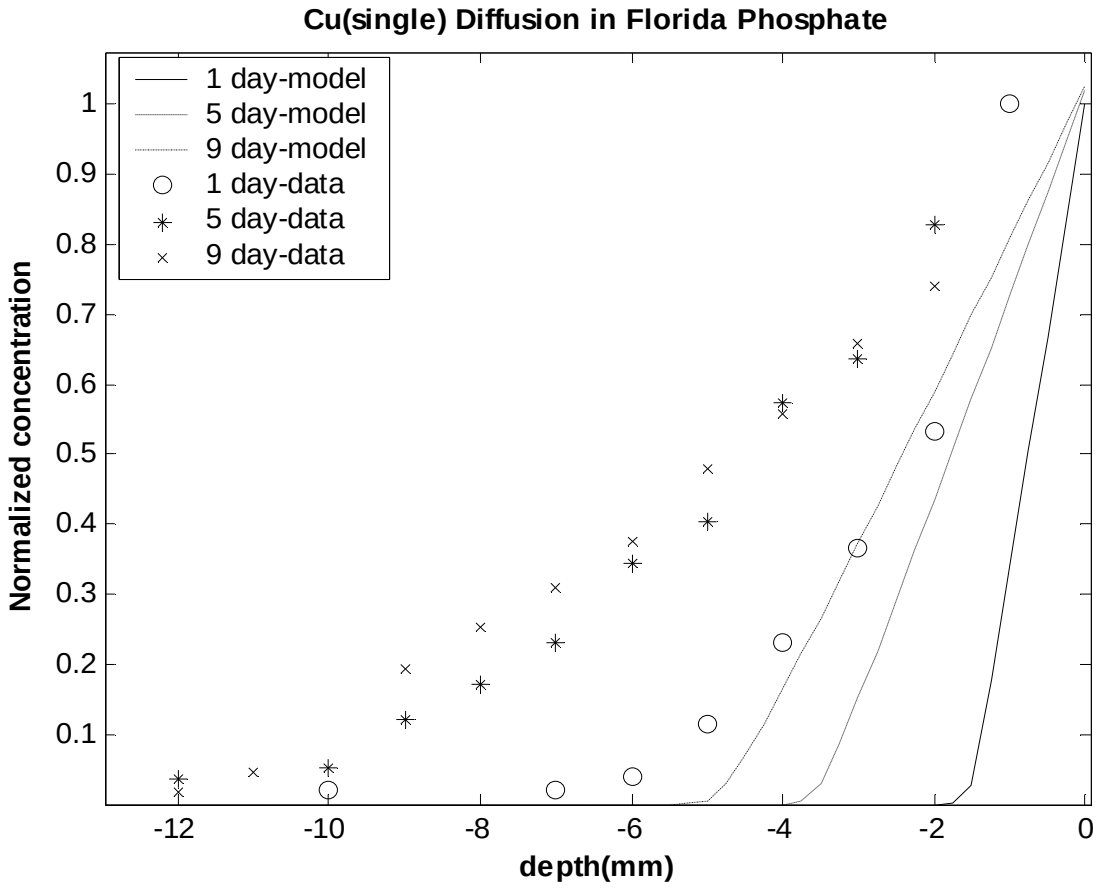

Figure 6-14 Comparison of modeling (pore water concentration) and XRF results: Cu diffusion in Florida Phosphate (Mono-element system)

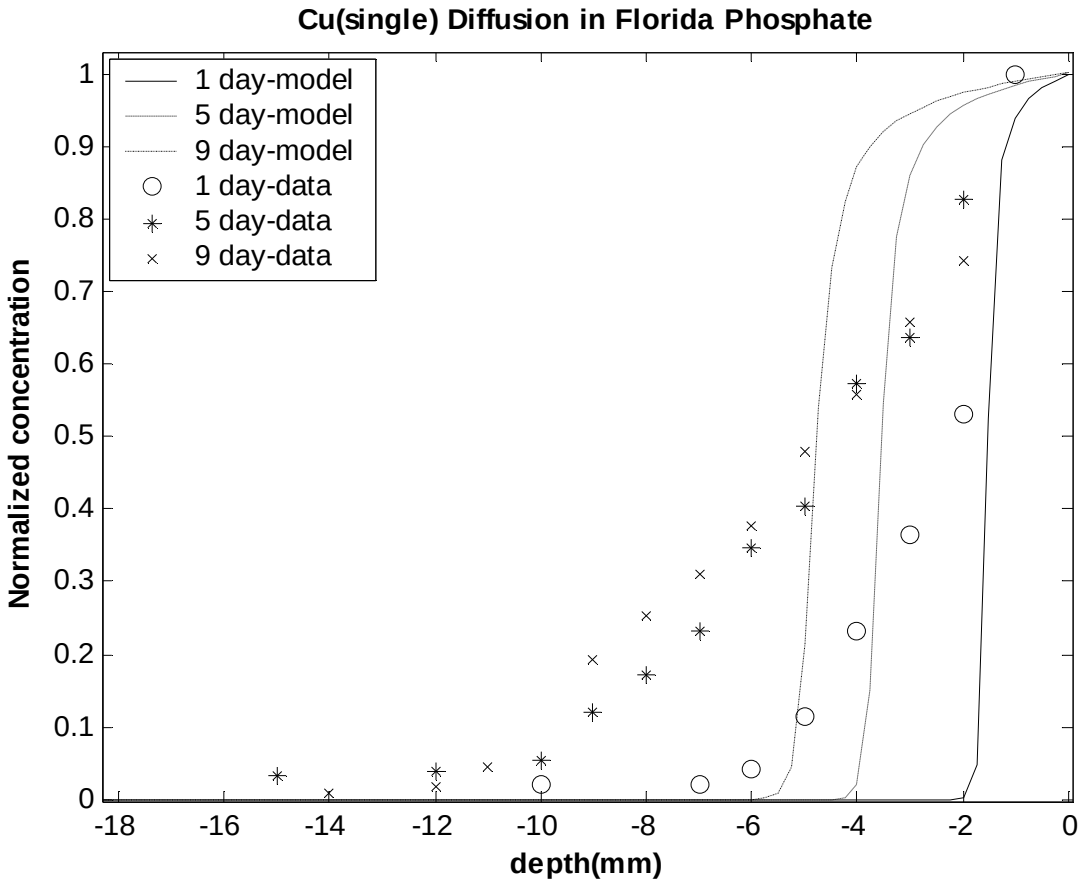

Figure 6-15 Comparison of modeling (total concentration) and XRF results: Cu diffusion in Florida Phosphate (Mono-element system)

Schroth et.al.(1996) related the particle size with hydraulic conductivity for highly uniform sand. For particle size of 0.39 mm the hydraulic conductivity is approximately 325 cm/h. If we approximate the driving force term $\frac{\Delta h}{L}$ as $\frac{\Delta \rho}{\rho} = 0.01$, then $v = q/\varepsilon = -325 \cdot 0.01/0.4 \approx 8$ cm/h. Similar calculation can be applied to Florida Phosphate when assuming similar particle shape and packing with sand and the calculated interstitial velocity $v \approx 5$ cm/h. This estimation of v should be an overestimate considering that when the migration starts the density difference will decrease with time and that there will be some counter-current flow. For the

future analysis, let's assume the pore water velocity is one order of magnitude smaller (i.e., 5 mm/h). The Genuchten and Aleves (1982)'s analytical solution (equation (25)) for advection–diffusion equation with constant boundary concentration condition can be used to estimate the migration of Cu in sand at 1, 3, 5 hours.

$$c(x,t) = c_i + (c_0 - c_i)\left[\frac{1}{2}erfc\left(\frac{R_f x - vt}{2\sqrt{DR_f t}}\right) + \frac{1}{2}\exp(\frac{vx}{D})\frac{1}{2}erfc\left(\frac{R_f x + vt}{2\sqrt{DR_f t}}\right)\right] \qquad (25)$$

c_0 and c_i are the initial concentration of water layer and solid layer respectively. D is diffusivity in water. R_f is retardation factor. For sand the adsorption is very weak and approximate R_f as 1. For Florida Phosphate from the isotherm of Cu (Mono-element system) in Florida Phosphate and average R_f can be taken as 40. Substitute these values to equation (25) and the calculated Cu migration profiles in sand at 1, 3, 5 hours are shown in Figure 6-16.

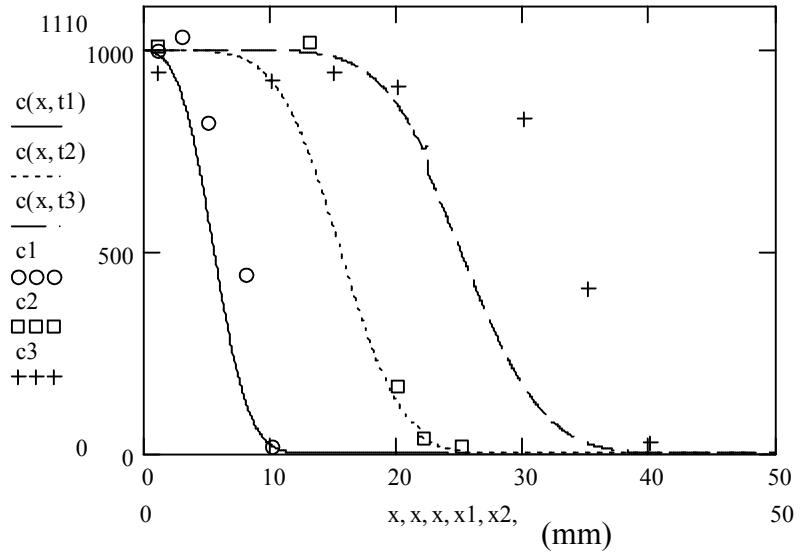

Figure 6-16 Calculated advection-diffusion profile of Cu in sand
(c(x,t1),c(x,t2),c(x,t3) are profiles at1 hour, 3 hour,5 hour respectively;
c1,c2,c3 are corresponding experiment data)

The one day migration profile of Cu in Florida Phosphate is calculated and shown in figure 6-17.

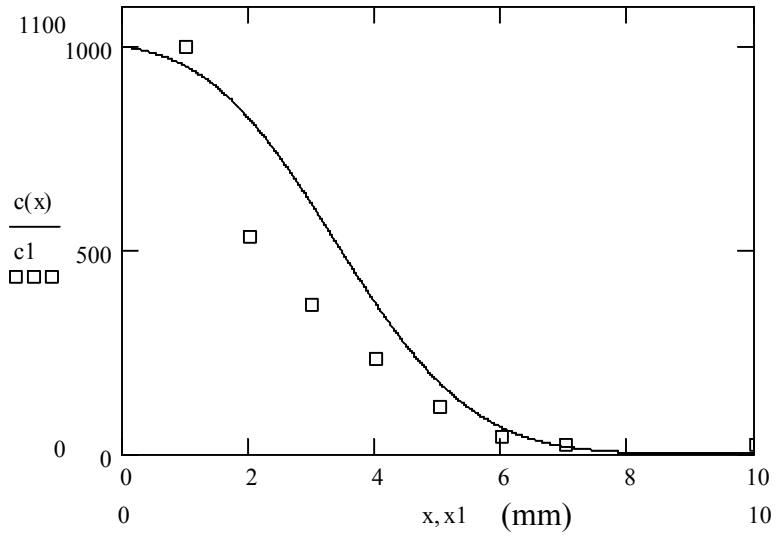

Figure 6-17 Calculated advection-diffusion profile (one day) of Cu in Florida Phosphate(Mono-element system) (c1 is experiment data)

All these estimations are very close to the profiles from experiment in Chapter 5. The discussions above indicate that in time span of one day the migration of metals is impacted by density differences and intermixing and subsequently is much faster than pure diffusion. From the experiment data we can see after one day the impact of density difference is much smaller and can be neglected. When using the day one profile as starting point the diffusive model can still be used to estimate the profiles afterward. Another modification to the diffusive model is based on the fact that during experiment the water layer is inevitably disturbed by many factors such as stirring when sampling at each time interval, shaking when moving the sample, temperature gradient, etc. These factors will make the actual average diffusivity in water layer much higher and so in the modified diffusive model the diffusivity in

water layer is increased by one order of magnitude. Figure 6-18 to Figure 6-20 are several representative examples of this modified diffusive modeling results comparing with experiment data. Table 6-3 is a summary of the penetration depths at C/C0=0.5 (the concentration decrease to half of the maximum concentration) for all modeling results of day 5 migration profile. We can see that after these two modifications the diffusive model basically agrees with the experiment data except for the cases of Zn.

Table 6-3. Comparison of modeling and experimental results of penetration depth

d_0.5(mm)		Cu (Single)	Cr(mix)	Cu(mix)	Zn(mix)
Florida Phosphate	data	4.6	7.7	10	40
	model	4.5	7.5	9	17
Sediment	data	6.5	6.5	6	5
	model	5	5	5	8

d_0.5(mm): migration depth at C/C0=0.5 (the penetration when the concentration decrease to half of the maximum concentration)

6.3 Kinetic of Metal Adsorption on Florida Phosphate

6.3.1 Adsorption Kinetics of Metals

The diffusive model in the previous sections assumes that the adsorption of metal ions on solid phase will reach equilibrium instantaneously. This may not be the case for the materials studied in this dissertation. The adsorption kinetics of metals in a mixed metal ion solution (Cr^{3+}, Cu^{2+}, Zn^{2+}, Pb^{2+}) onto Florida Phosphate was studied.

The following is a summary of the experiment procedure:

- Put 1000 mL Cr^{+3}, Zn^{+2}, Cu^{+2}, Pb^{+2} mixed water solution in a plastic bottle, extract a 30 μL water sample (volume small enough compared with 1000 mL) for ICP-MS analysis.

- Add 3.2 g Florida Phosphate(dry) to the 1000 ml solution
- Secure the plastic bottle and place in a reciprocal shaker
- At certain time intervals extract a 30 μL water sample from the bottle (note: for Florida Phosphate, the solid and water phase separate very fast when standing still)
- Analyze the samples by ICP-MS

The metal adsorbed in solid phase (Ws, mg/g) can easily calculated from the concentration remaining in water. Figure 6-21 to Figure 6-24 are the plots of partition coefficient (Kd) versus time for different metal species.

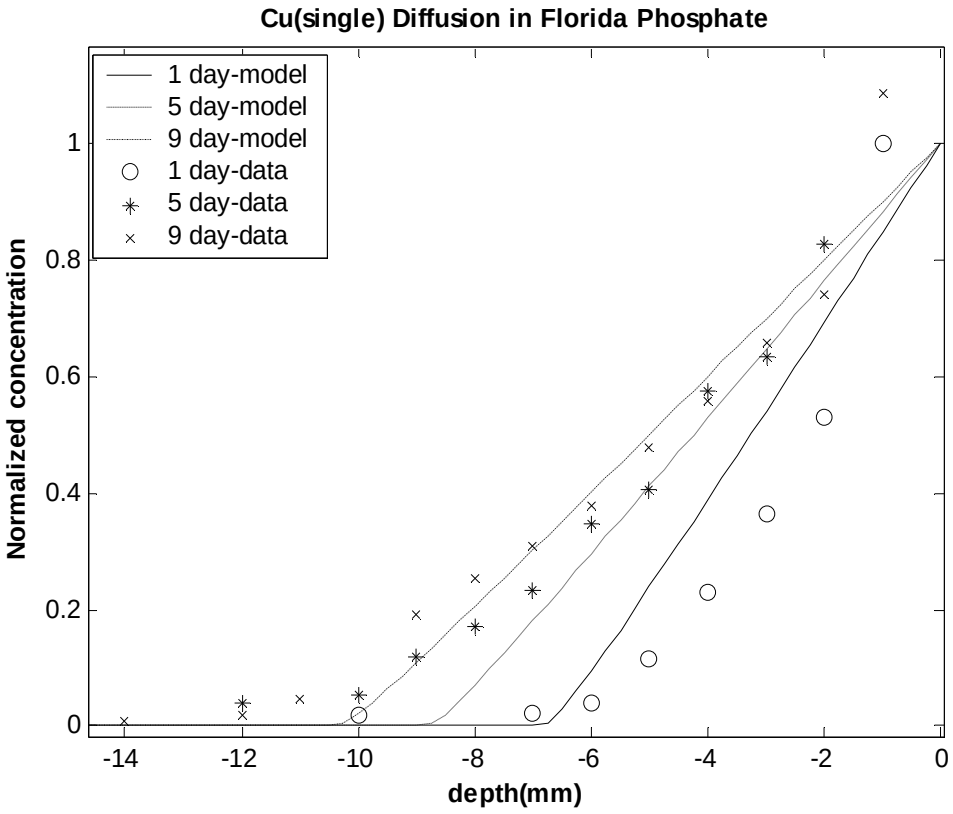

Figure 6-18 Comparison of modified modeling and XRF results: Cu migration in Florida Phosphate (Mono-element system)

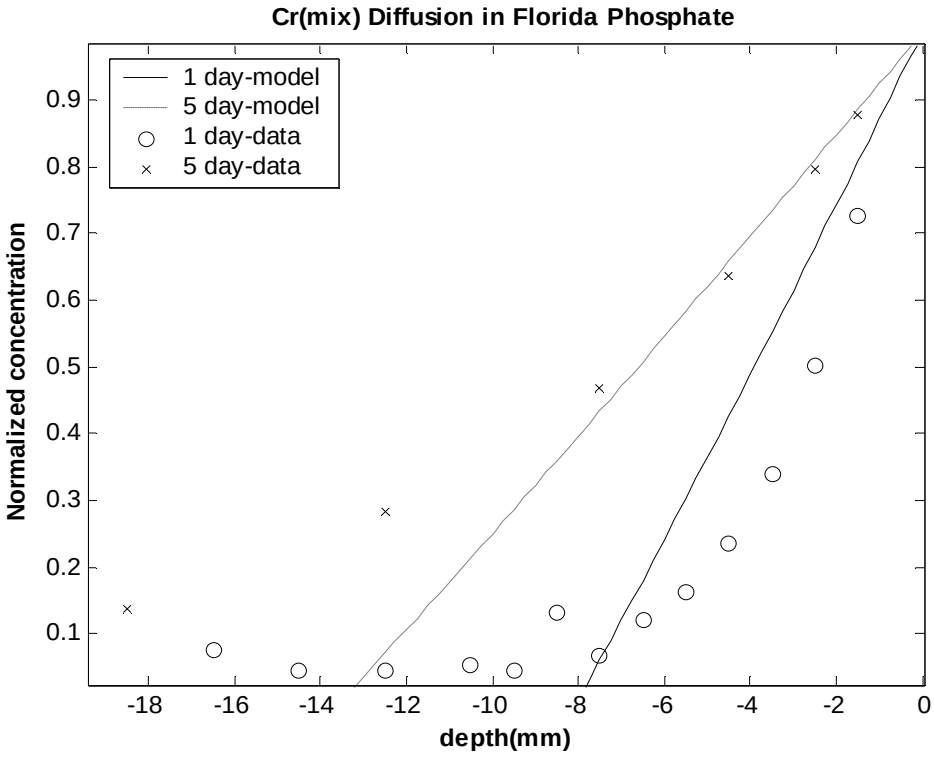

Figure 6-19 Comparison of modified modeling and XRF results: Cr(III) migration in Florida Phosphate (Tetra-element system)

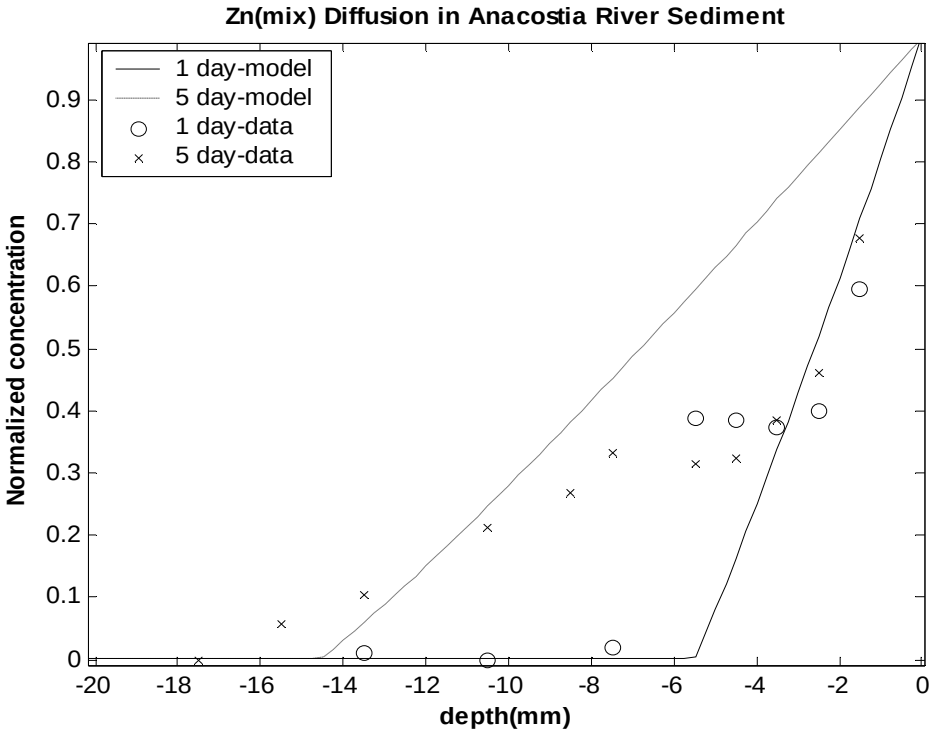

Figure 6-20 Comparison of modified modeling and XRF results: Zn migration in Anacostia River Sediment (Tetra-element system)

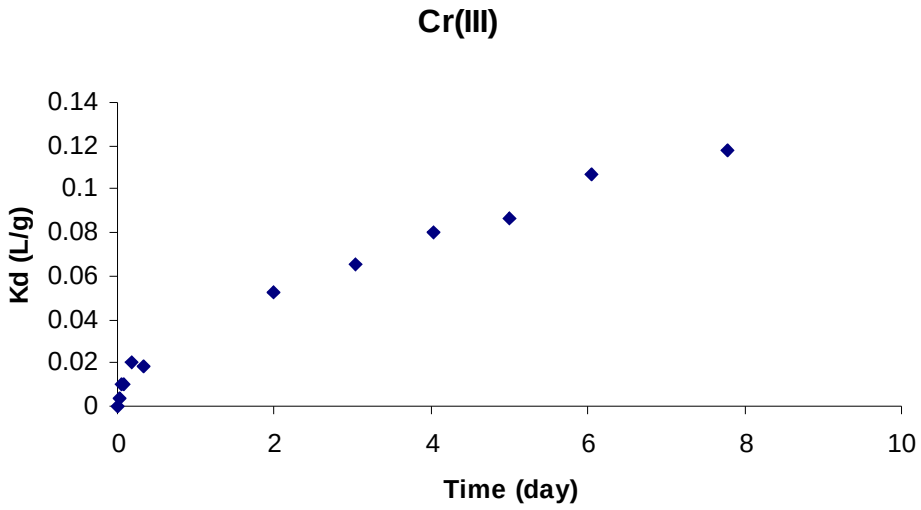

Figure 6-21 Cr(III) adsorption kinetic onto Florida Phosphate

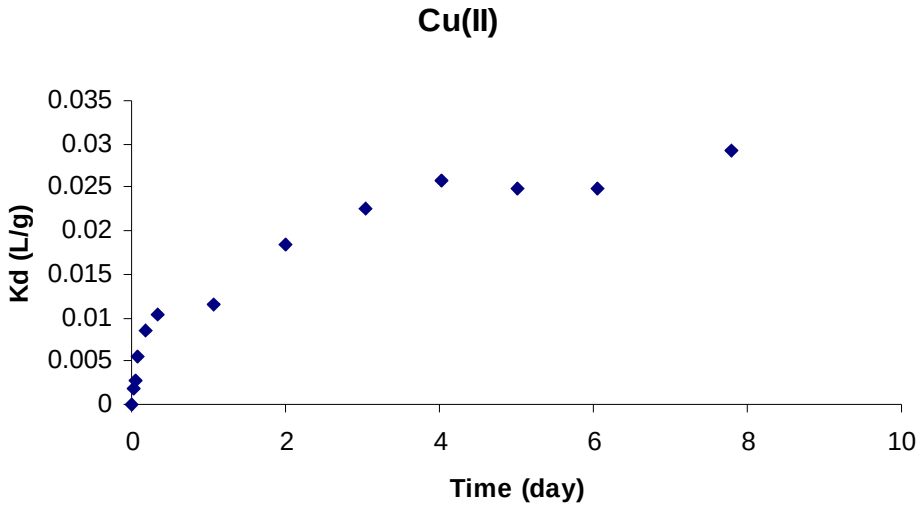

Figure 6-22 Cu(II) adsorption kinetic onto Florida Phosphate

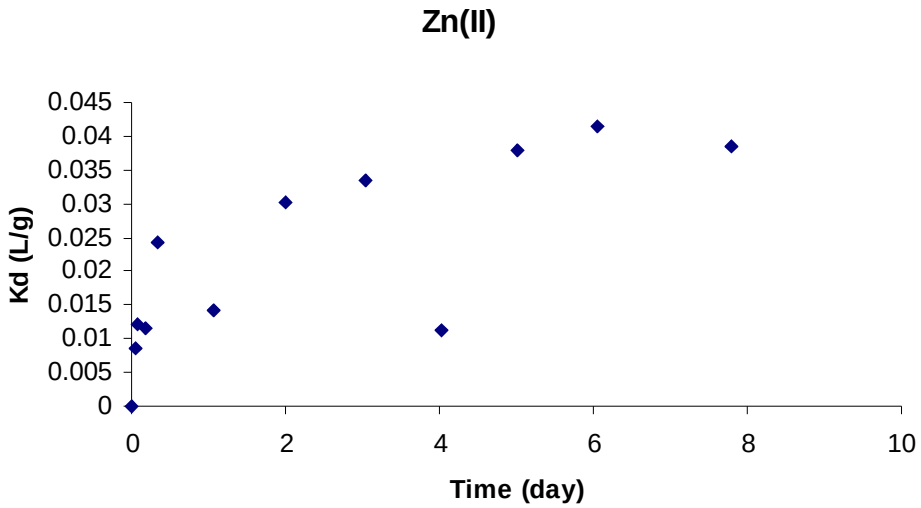

Figure 6-23 Zn(II) adsorption kinetic onto Florida Phosphate

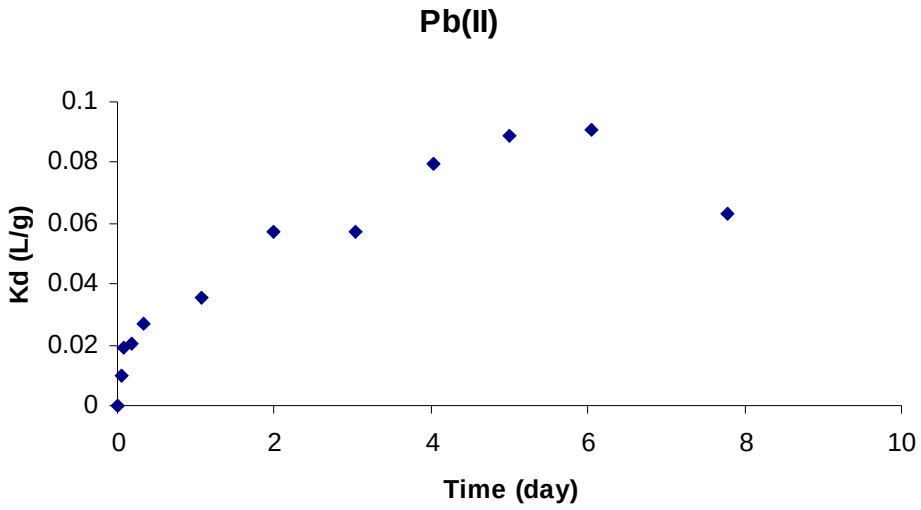

Figure 6-24 Pb(II) adsorption kinetic onto Florida Phosphate

6.3.2 Modeling of the Adsorption Kinetics

Define the concentration in solid when reaching equilibrium as We, k is the adsorption rate constant. It was found that Pseudo-First-Order equation (equation (26)) is the best to simulate the data among zero, first and second order kinetic equations.

$$\frac{dWs}{dt} = k(We - Ws) \tag{26}$$

Integrate equation (26) by applying initial condition (when $t = 0$, $Ws = 0$) gives:

$$\ln(We - Ws) = \ln We - kt \tag{27}$$

Equation (27) can be simplified to

$$Ws = We(1 - e^{-kt}) \tag{28}$$

The adsorption rate constant k can be obtained by doing linear regression on the kinetic data according to equation (27). Table 6-3 lists the rate constant for all four metal ions studied. R^2 is the fitness of the linear model.

Table 6-4 Adsorption rate constant of metals in Florida Phosphate

Metals	Cr^{3+}	Cu^{2+}	Zn^{2+}	Pb^{2+}
k (1/h)	0.0157	0.0153	0.0138	0.0216
R^2	0.90	0.91	0.72	0.92

Prasad et.al.(2004) studied the metal adsorption kinetic in a low cost sedimentary phosphate and found that for first order kinetic the half-life time (decided by k) remains constant independent of the initial adsorbate concentration (here is initial metal solution concentration). We can assume k is constant when assuming Florida Phosphate has characteristics similar to the sedimentary phosphate.

6.3.3 Diffusion Modeling Incorporating Adsorption Kinetics

Substitute equation (28) to equation (6) gives the governing diffusion equation incorporated adsorption kinetic:

$$\frac{\partial}{\partial t}(\varepsilon \cdot c + (1-\varepsilon)\cdot \rho_s \cdot We(1-e^{-kt})) = D_w \varepsilon^{4/3} \cdot \frac{\partial^2 c}{\partial x^2} \tag{29}$$

We is actually the isotherm which is a function of c. Then from equation (29) we can obtain:

$$\varepsilon \cdot \frac{\partial c}{\partial t} + (1-\varepsilon)\cdot \rho_s \cdot ((1-e^{-kt})\frac{\partial We(c)}{\partial c}\frac{\partial c}{\partial t} + kWe(c)e^{-kt}) = D_w \varepsilon^{4/3} \cdot \frac{\partial^2 c}{\partial x^2} \tag{30}$$

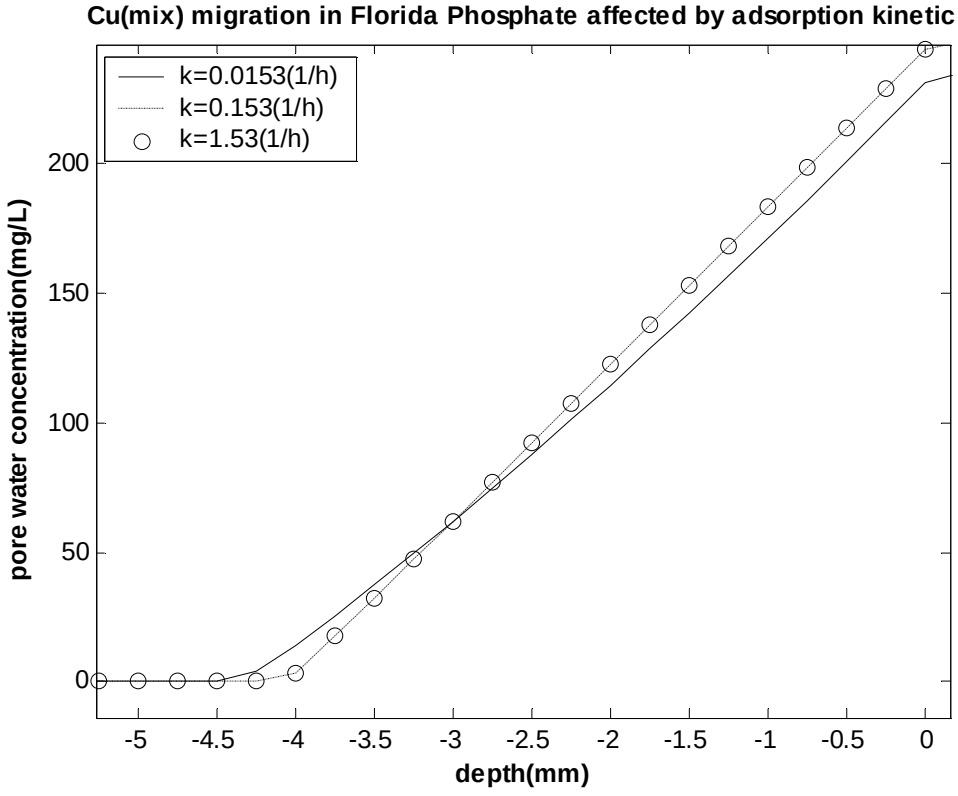

Figure 6-25 Cu migration in Florida Phosphate affected by adsorption kinetic (day 9 profiles in solid layer)

An explicit finite difference code was used to solve this PDE. The boundary and initial conditions and discretization method are same with those in section 6.2.2. Then equation (30) can be discretized to the following explicit form:

$$(\varepsilon + (1-\varepsilon)\cdot\rho_s(1-e^{-kj\Delta t})\frac{\partial We(c)}{\partial c}(i,j))\frac{c(i,j+1)-c(i,j)}{\Delta t} + (1-\varepsilon)\cdot\rho_s kWe(c(i,j)e^{-kj\Delta t}$$
$$= D_w\varepsilon^{4/3}\frac{c(i+1,j)-2c(i,j)+c(i-1,j)}{\Delta x^2} \quad (31)$$

Figure 6-25 is an example of how the rate constant k affects diffusion profile. Figure 6-25 shows that the diffusion becomes slower with the increase of rate constant k. When k increases from 0.153 $1/h$ to 1.53 $1/h$, the migration profiles basically has no change. In other word, when $k \to +\infty$, it will converge to the case assuming local equilibrium, in which the profile can be deemed as the profile when k=1.53 1/h. Also in the case shown in Figure 6-25 it can be seen that the adsorption kinetics has little effect to the migration profiles comparing with the other factors such as intermixing and the gravity effect induced by the density difference between metal solution and pure water.

6.4 Summary

A diffusion model that incorporates nonlinear sorption isotherm is developed to model the metal transport column experiments described in chapter 5. A finite difference method is used to solve this nonlinear problem (when isotherm is a function of pore water concentration). Sensitivity analysis reveals that maximum sorption capacity (one of the Langmuir parameters) is the most sensitive parameter affecting the diffusion.

The comparison of model result and data suggests that the experimental setup resulted in buoyancy effects which artificially enhanced metal migration, especially in day one's migration. In addition, the use of high metals concentration resulted in reducing the effectiveness of the capping material due to the limited sorption capacity exhibited by the Langmuir isotherm. When using initial measured migration profile as initial condition to estimate the subsequent profiles and simplifying the water layer as homogeneous layer the diffusive modeling results basically agree with the experiment data (see Table 6-3). The kinetics of metal adsorption in Florida Phosphate is investigated and the corresponding numerical modeling indicates that the diffusion speed decrease with the increase of adsorption rate constant. This effect is not enough to explain the discrepancies between the original model and data until the modified model considering buoyancy effects is introduced.

6.5 References

Carnahan, B., Luther, H. A., Wilkes, J.O., *Applied Numerical Methods*, John Wiley & Sons, Inc (1969).

Cheung, C.W., Ko, D.C.K., Porter, J.F., McKay, G., Binary Metal Sorption on Bone Char Mass Transport Model Using IAST, *Langmuir* 2003, *19,* 4144-4153

Choy, B. and D.D. Reible, *Diffusion Models of Environmental Transport*, CRC/Lewis Publishers (2000).

Crannell, B.S., Eighmy, T., Willson, C., Reible, D., Yin, M., "Pilot-Scale Reactive Barrier Technologies for Containment of Metal-Contaminated Sediments and Dredge Materials," A Final Report Submitted to the NOAA/UNH Cooperative Institute for Coastal and Estuarine Environmental Technology (CICEET), 2004.

Dawson, C.N., Simulation of nonlinear contaminant transport in groundwater by a higher order Godunov-mixed finite element method, Applications of Supercomputers in Engineering II, C.A. Brebbia, D. Howard, and A. Peters, eds., Computational Mechanics Publications, Southampton, UK, pp. 419-433, 1991

Fowler, K. R., Kelley, C. T., Pseudo-transient continuation for nonsmooth nonlinear equations. Technical Report CRSC-TR03-29, North Carolina State University, Center for Research in Scientific Computation, July, 2003.

Millington, R.J., Quirk, J.M. (1961) Gas Diffusion, *Trans. Faraday Society*, 57, 1200
Prasad, M., Saxena, X., Sorption Mechanism of Some Divalent Metal Ions Onto Low-Cost Mineral Adsorbent, *Ind. Eng. Chem. Res.* 2004, *43,* 1512-1522

Sauve, S., Hendershot, W. and Allen, H.E., Solid-Solution Partitioning of Metals in Contaminated Soils: Dependence on pH, Total Metal Burden, and Organic Matter, *Environ. Sci. Technol*. 2000, 34, 1125-1131

Schroth, M.H., Ahearn, S.J., Selker, J.S., Istok, J.D., Characterization of Miller-Similar Silica Sands for Laboratory Hydrologic Studies, *Soil Sci. Soc.* Am. J. 60: 1331-1339 (1996)

Serrano, S.E., Solute Transport under Non-Linear Sorption and Decay, *Wat. Res*. Vol. 35, No. 6, pp. 1525–1533, 2001

Van Genuchten, M.T., Alves, W.J.(1982) *Analytical Solutions of the One-Dimensional Convective-Dispersive Solute Transport Equation.* U.S. Department of Agriculture, Technical Bulletin No. 1661.

Wilke, C.R., Chang, P. (1955) Correlation of diffusion coefficients in dilute solutions, *AICHE J*., 1, 264.
Yin, M., C.S. Willson, and D.D. Reible, 2004, Investigation of Heavy Metal Migration from Contaminated Sediment to Capping material using XRF, presented at the 2004 AICHE Annual Meeting, November 7-12, 2004, Austin, TX.

Zhu, C., Anderson, G., *Environmental Application of Geochemical Modeling*, Cambridge University Press 2002.

Chapter 7

Conclusions and Recommendations

7.1 Conclusions

7.1.1 UNH Experiment

A series of pilot-scale migration tanks were established at the University of New Hampshire. These tanks contained various combinations of contaminated sediments (Newtown Creek and Anacostia River sediment) and capping materials (Ottawa sand, Florida phosphate, N.C. phosphate and GreatBay sediment). The metal (Fe, Cu, Zn, Pb) migration profiles were measured by synchrotron XRF in white light mode. Clear profiles with high spatial resolution were detected in these systems demonstrating that synchrotron XRF is a suitable analytical tool for these sediment and apatite materials. After 400 days' migration the lengths of transition zone (concentration changing from background concentration of contaminated sediment to background concentration of cap) are no more than 4 mm. Comparison with 30 day profiles suggests that these transition zone are essentially the intermixing zone indicating that there is no measurable metal migration in these capping system for 400 days. This suggests that under natural or field condition all these capping material are effective for the metals studied.

7.1.2 Sorption Isotherm

The sorption isotherms of four metal species (Cr(+3), Cu(+2), Zn(+2), Pb(+2)) under slightly acidic condition in three capping materials (Florida Phosphate, Phosphil and sand) and Anacostia River sediment are obtained. Most of the isotherm data can be fitted by the Langmuir isotherm quite well. The maximum sorption capacity of Cu in mono-element system is much greater then that in tetra-element system suggesting the

influence of competitive adsorption.

Among all the materials for all metals tested, sand has a significantly lower maximum sorption capacity (l or 2 orders of magnitude lower) for the tetra-element system than other materials. Examination of the maximum sorption capacity of the metals for the other three materials tested (Florida Phosphate, Phosphil and Anacostia river sediment) leads to the following observations:

- For Cr and Cu, the sequence is Sediment > Phosphil > Florida Phosphate
- For Zn, the sequence is Sediment > Florida Phosphate $\approx$ Phosphil
- For Pb, the sequence is Florida Phosphate > Phosphil > Sediment
- For Florida Phosphate, the sequence is Pb > Cu > Cr >Zn
- For Phosphil, the sequence is Pb > Cu > Cr >Zn
- For Anacostia Sediment, the sequence is Cr > Cu > Pb >Zn

7.1.3 Metal Migration

1) Migration column experiment investigated using ICP-MS

The migration profiles of four metal species (Cr, Cu, Zn and Pb, all in tetra-element system) in three materials (Florida Phosphate, Phosphil and Anacostia river sediment) are measured using ICP-MS. The maximum spatial resolution of this method is 1.32 mm. Advantages to this technique include a high detection limit (ppb level) and good element coverage. However, the slicing process is destructive and makes this method not suitable for samples with significant metal concentrations in pore water.

The trends in metal migration depths are:

- For Phosphil, the sequence of migration speeds is Zn > Cr $\geq$ Cu > Pb
- For Florida Phosphate, the sequence of migration speeds is Zn > Cu > Cr > Pb
- For Sediment, the sequence of migration speeds is Zn > Cu > Pb $\geq$ Cr

Except for Pb in the sediment, these sequences are consistent with the reverse order of maximum sorption capacity suggesting that the sorption capacity is the major factor affecting migration.

The migration depth in the solid phase is highly correlated with the metal depleted from pond solution (i.e. metal absorbed by solid layer). In addition, it was found that as the amount of metal absorbed by the solid layer increase, the migration depth decreased.

2) Migration column experiment investigated by XRF

Synchrotron XRF was used to measure the migration profiles of Cu in a mono-element system and Cr, Cu, Zn in tetra-element system in three materials (sand, Florida Phosphate and Anacostia river sediment). Results showed that Cu in a tetra-element system migrates much faster than in mono-element system in Florida Phosphate.

The high spatial and temporal resolution of this technique results in an improvement of the data quality of the migration profiles comparing to conventional slicing method. The nondestructive nature of XRF makes it suitable for measuring metals in porous media systems where there is a significant metal concentration in the aqueous phase (e.g. sand). The disadvantage of this technique is the low detection limit (ppm level, depending on matrix) compared to ICP-MS.

From the XRF experiments, the sequences of metal migration depths of the metals in a tetra-element system were found to be:

- For all these three metals, Sand > Florida Phosphate > Anacostia sediment
- For Florida Phosphate and Anacostia sediment, Zn > Cu > Cr

These sequences are exactly the reverse order of maximum sorption capacity.

From this set of experiments, it is clearly demonstrated that apatite materials are better capping materials than sand with respect to retardation for Cr^{3+}, Cu^{2+} and Zn^{2+}.

7.1.4 Diffusive Modeling

A diffusion model that incorporates nonlinear sorption isotherm is developed to simulate the metal transport in the column experiments described in chapter 5. Sensitivity analysis reveals that maximum sorption capacity (one of the Langmuir parameters) is the most sensitive parameter affecting the diffusion. The first day's migration in experiments involves processes other than diffusion (e.g. intermixing at the beginning, gravity driven movement caused by density difference between metal solution above and water below). When using the first day migration profiles as initial condition to predict the subsequent profiles, the model agrees with the experimental data for most cases.

7.2 Recommendations

- The diffusion model developed assuming local equilibrium conditions underestimates the migration speed of metals. This highlights the need to either verify the local equilibrium assumption or to collect kinetic sorption data. Local equilibrium assumes that the equilibrium of metal between water and solid is reached instantaneously. If this does not hold, the adsorption will be a kinetic process. That means in the process when the adsorption is reaching equilibrium, the metal concentration in the solid phase should be less than the equilibrium concentration and concentration in water phase will be larger than equilibrium concentration. In another words the average partition coefficient will be smaller and the retardation factor will decrease correspondingly. Thus, the estimated migration speed will increase. Therefore kinetic adsorption experiments at different initial concentrations are suggested.
- The diffusion model in chapter 6 also assumes that the adsorptions of metals are reversible. If some portions of the metal adsorption are nonreversible the amount of

metal in solid phase that will actually participate in the reversible partition process is less than the amount measured by adsorption isotherm. This leads to a smaller partition coefficient and faster migration. Combining desorption data with the kinetic adsorption data will reveal whether the adsorption process is reversible. Therefore desorption kinetic experiments are recommended.

- When considering the adsorption and desorption kinetics, the diffusion model will become much more complicated. Therefore, a new mathematical model incorporating these kinetic effects should be developed.
- XRF can only detect the total concentration of one metal including its all species and can not provide any information about the chemical bonding, oxidation state of the atom, etc, which are helpful for revealing the mechanism of metal interaction with capping materials and sediment. Synchrotron X-ray absorption spectroscopy (XAS) can provide information about vacant orbital, electronic configuration, site symmetry, bond angles and interatomic distances of the absorbing atom and these information can lead to many useful results (e.g. different species of a metal, such as Cr(III) and Cr (IV) can be differentiated by this technique). The use of XAS to investigate the interaction and migration of metal species in apatite and sediment will provide some insights into the fate and transport mechanisms in these materials.

Appendix A

Metal Migration Profiles in UNH Diffusion Tank Experiment

The following are the metal migration profiles of Batch 3 (after 400 days' migration) samples.

Tank 7 (Test)
Water
Great Bay Sediment
Newtwon Creek Contaminated Sediment

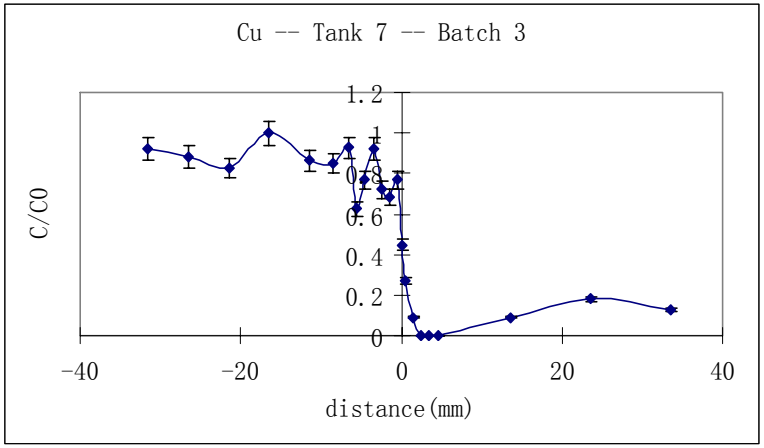

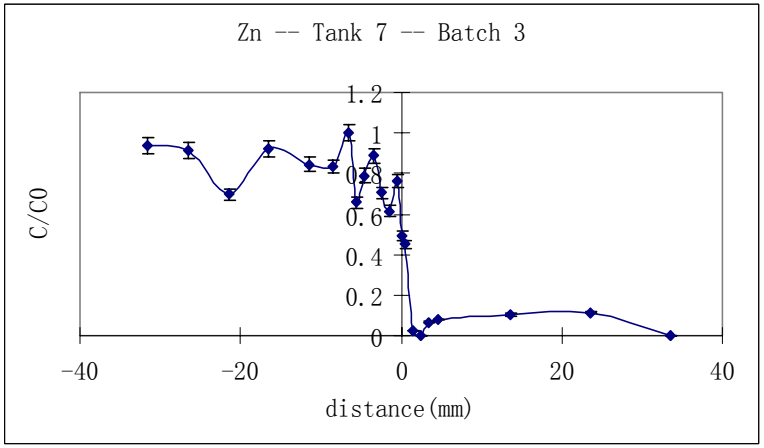

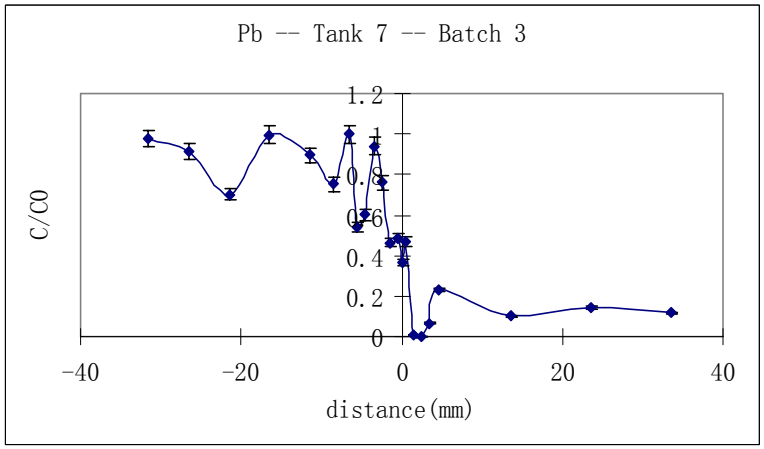

Tank 8 (Test)

Water

Ottowa Sand

Newtwon Creek Contaminated Sediment

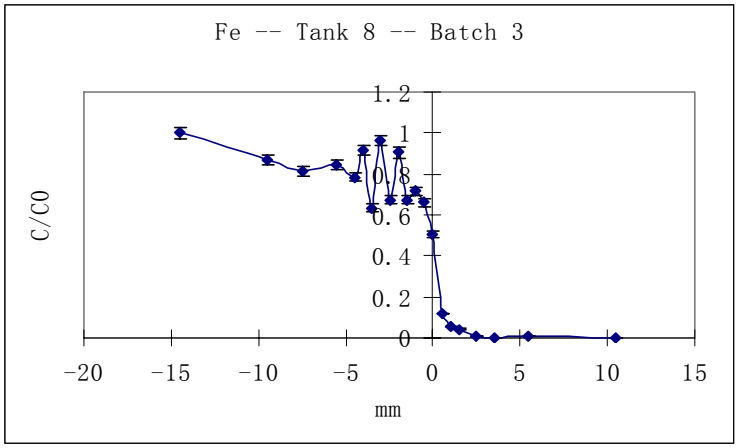

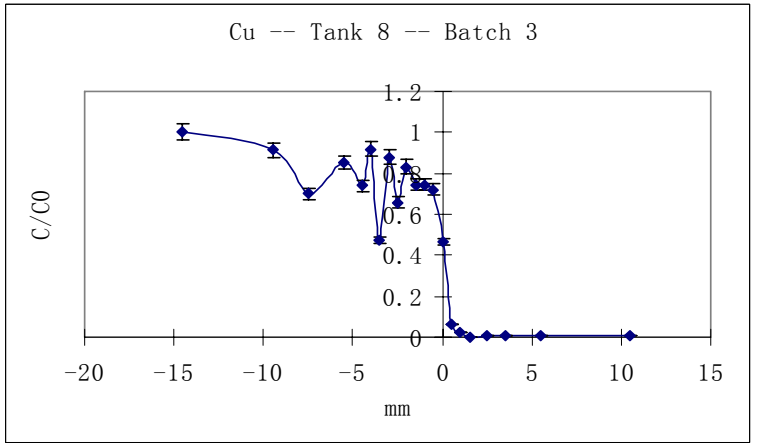

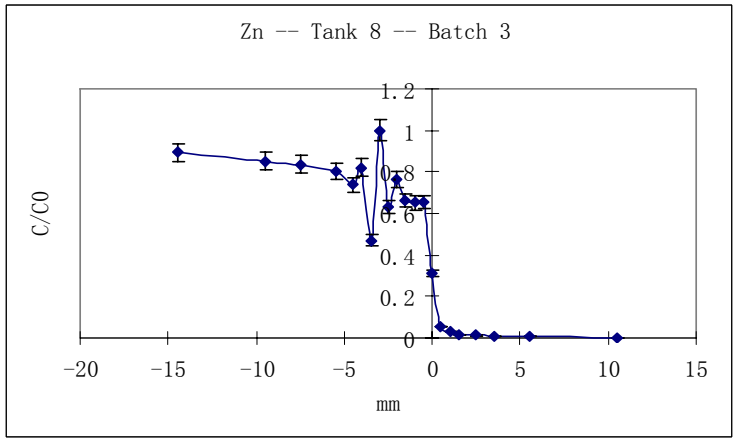

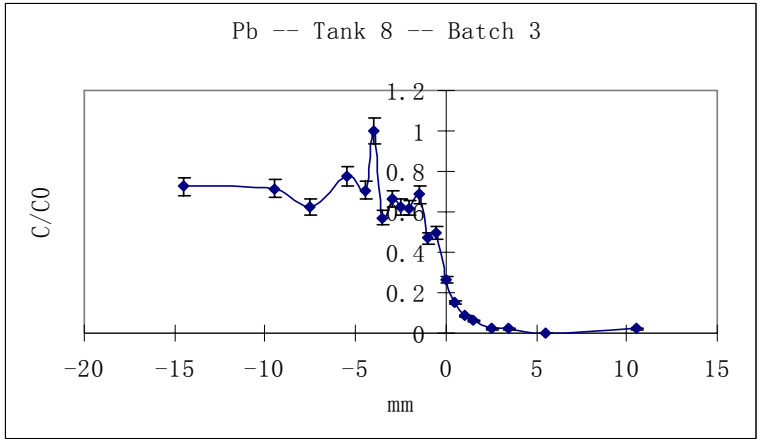

Tank 9 (Test)

Water

Great Bay Sediment

Anacostia River Contaminated Sediment

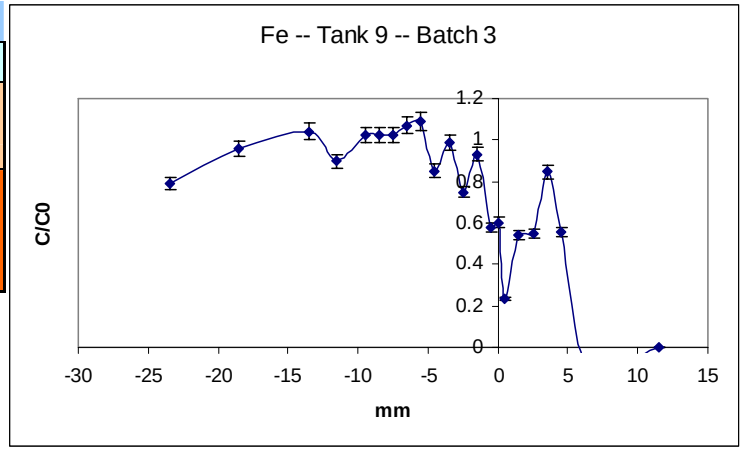

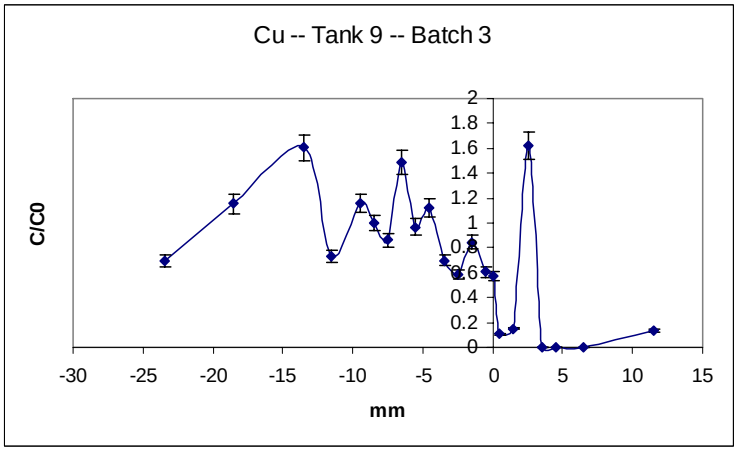

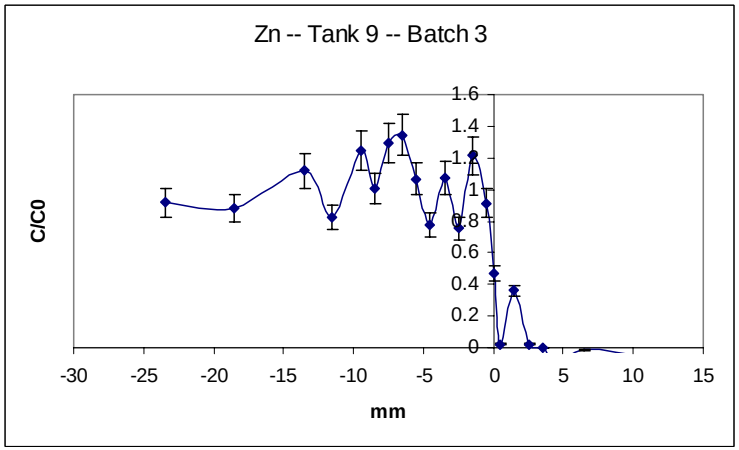

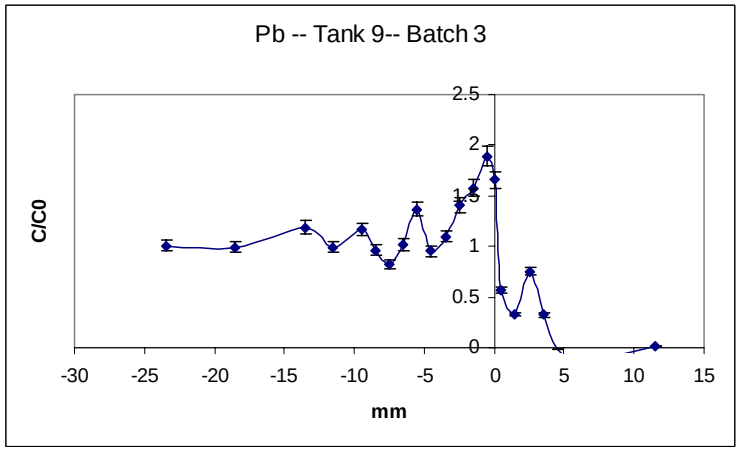

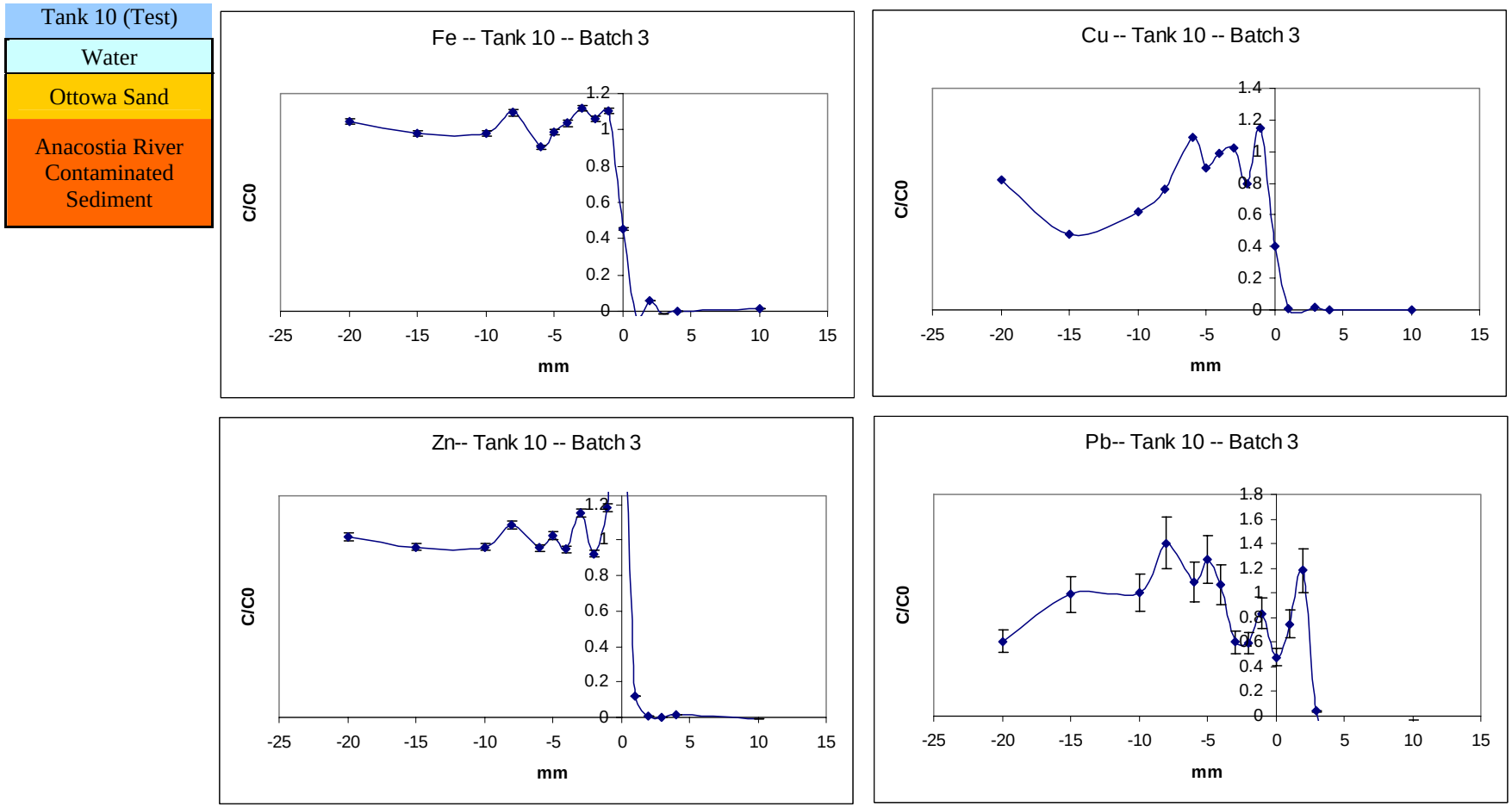
Tank 10 (Test)
Water
Ottowa Sand
Anacostia River Contaminated Sediment
Fe -- Tank 10 -- Batch 3
C/C0
mm
Cu -- Tank 10 -- Batch 3
C/C0
mm
Zn-- Tank 10 -- Batch 3
C/C0
mm
Pb-- Tank 10 -- Batch 3
C/C0
mm

Tank 11 (Test)

Water

Florida Phosphate (Rep 1)

Newtwon Creek Contaminated Sediment

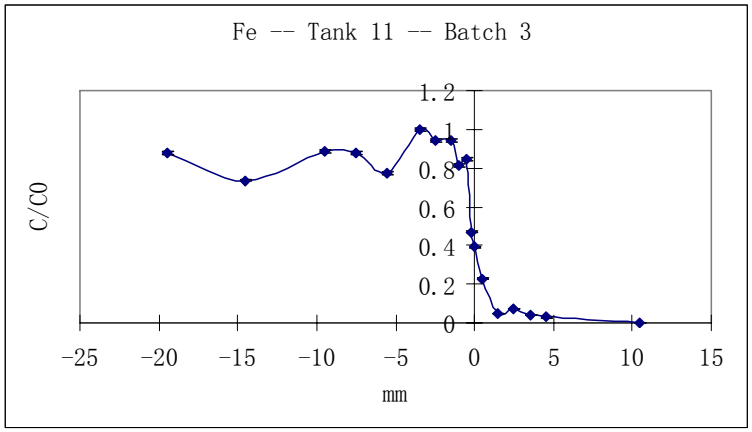

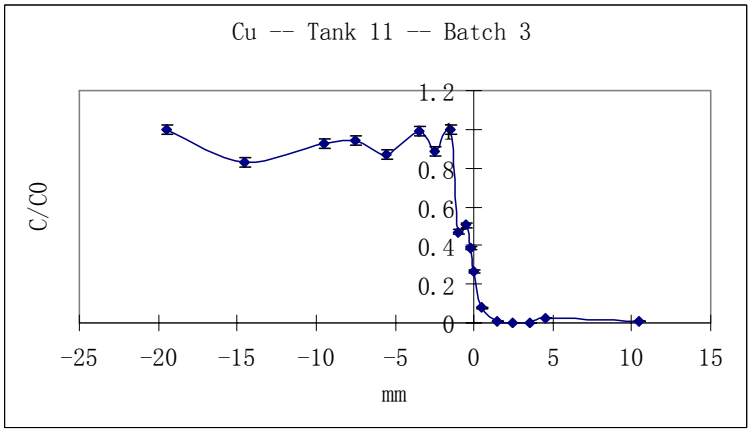

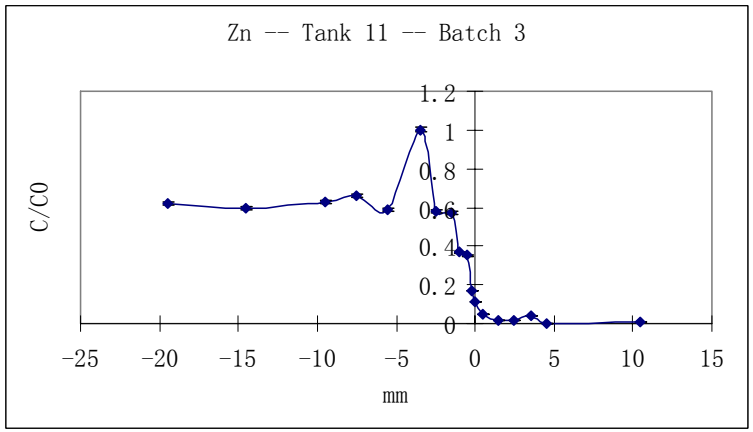

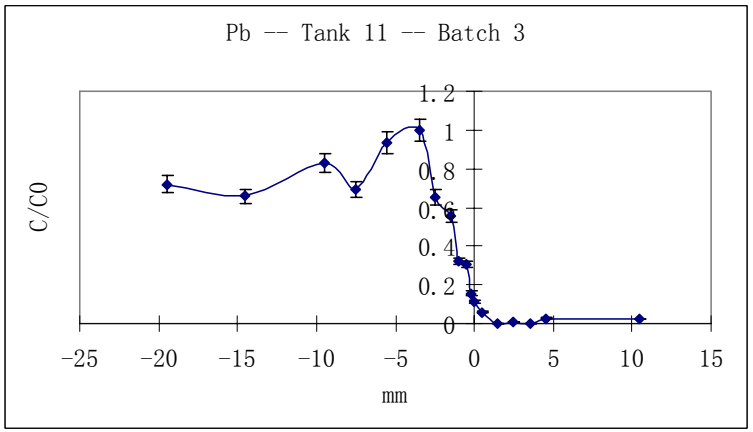

Tank 12 (Test)

Water

Florida Phosphate (Rep 2)

Newtwon Creek Contaminated Sediment

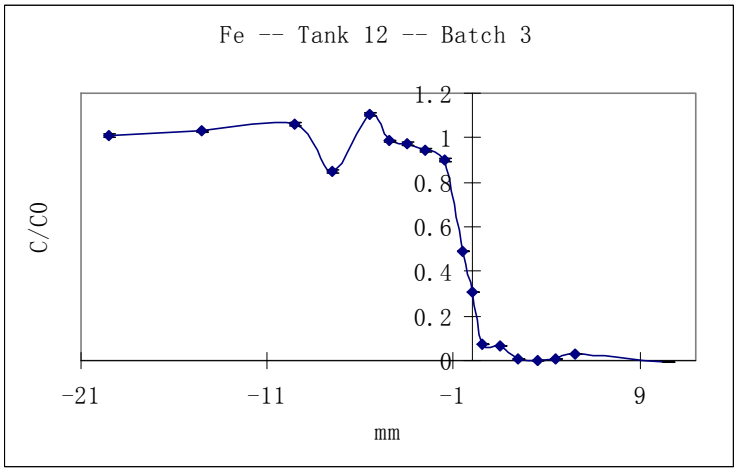

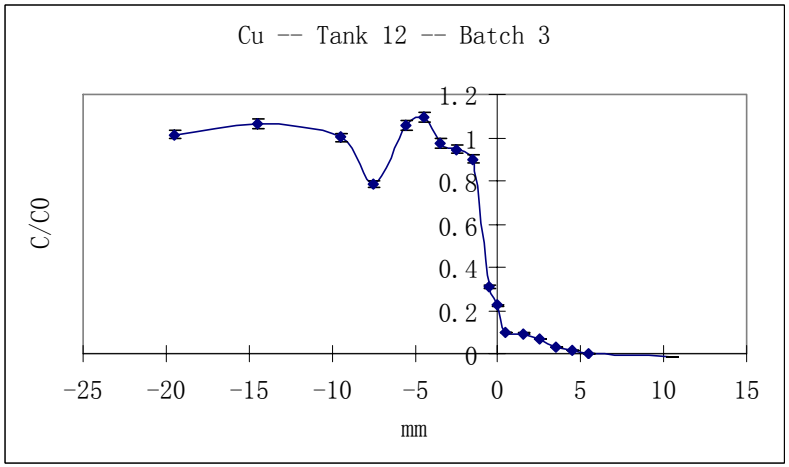

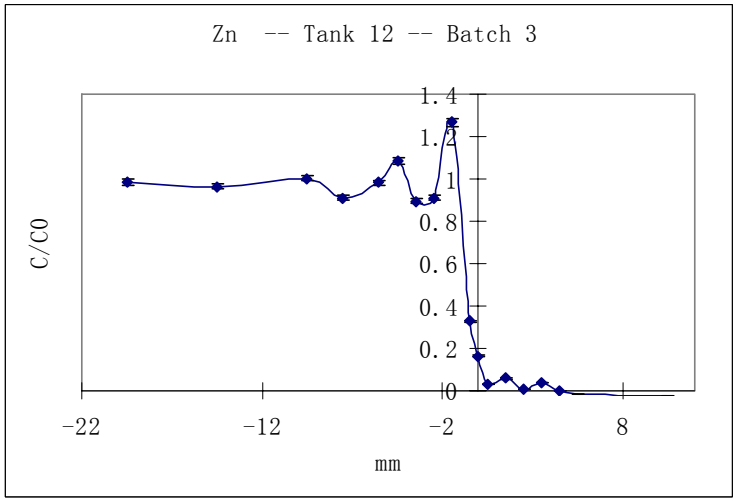

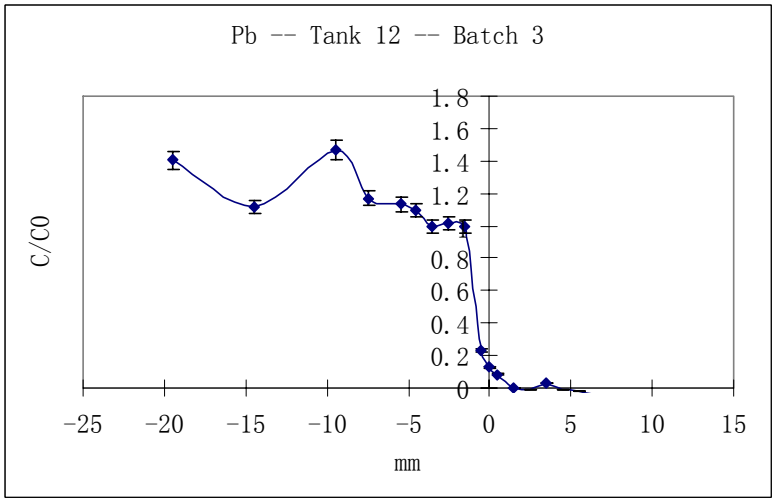

Tank 13 (Test)

Water

Florida Phosphate (Rep 1)

Anacostia River Contaminated Sediment

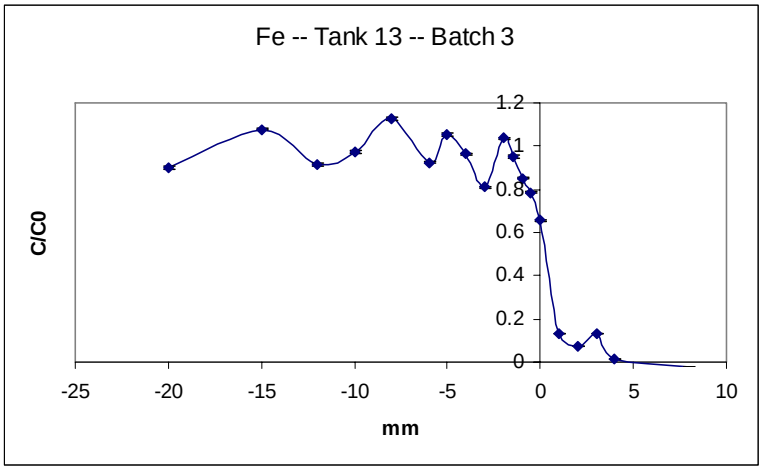

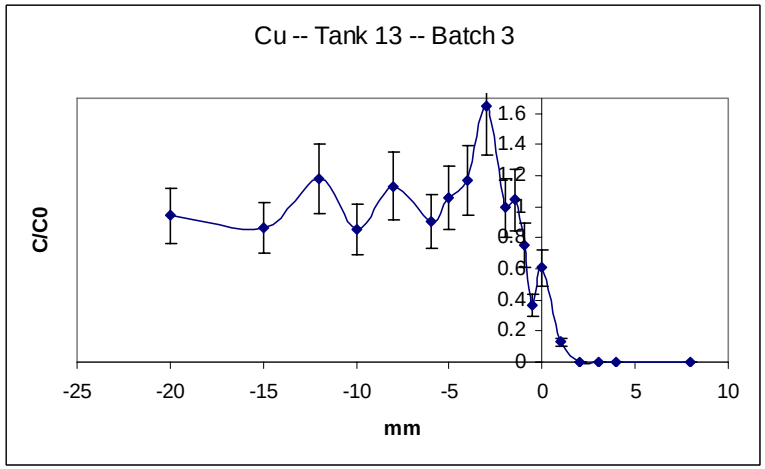

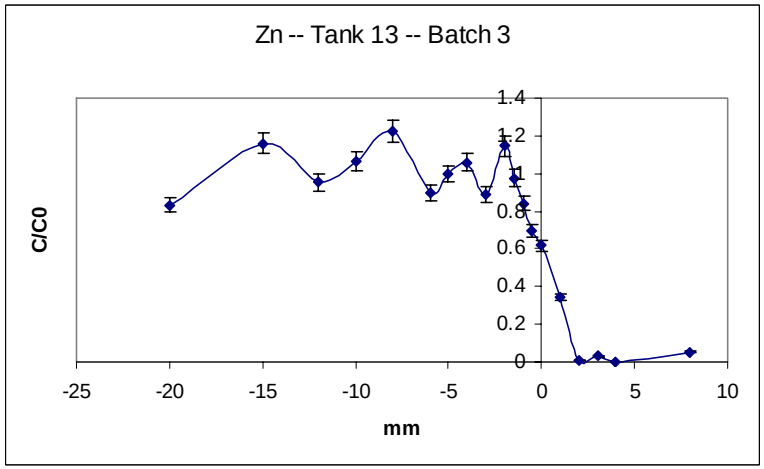

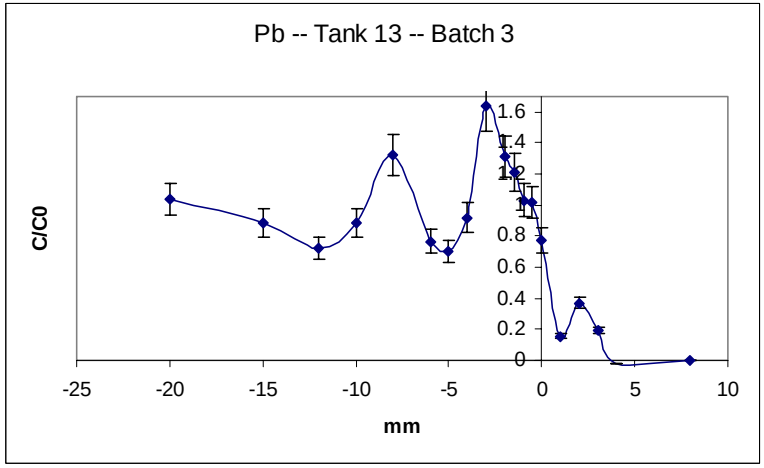

Tank 14 (Test)

Water

Florida Phosphate (Rep 2)

Anacostia River Contaminated Sediment

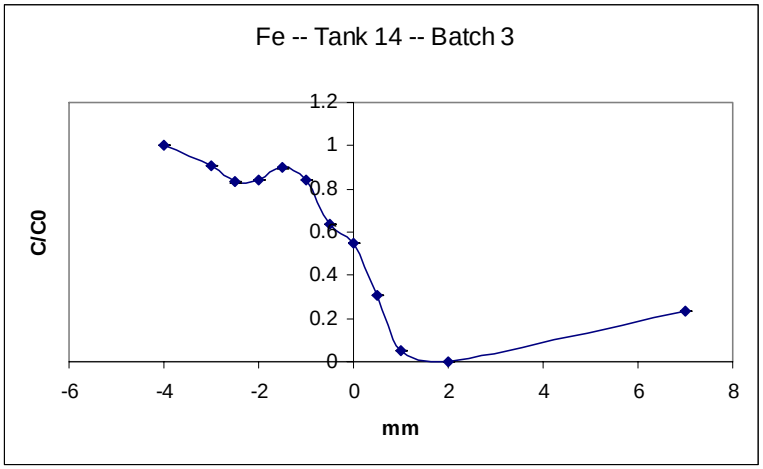

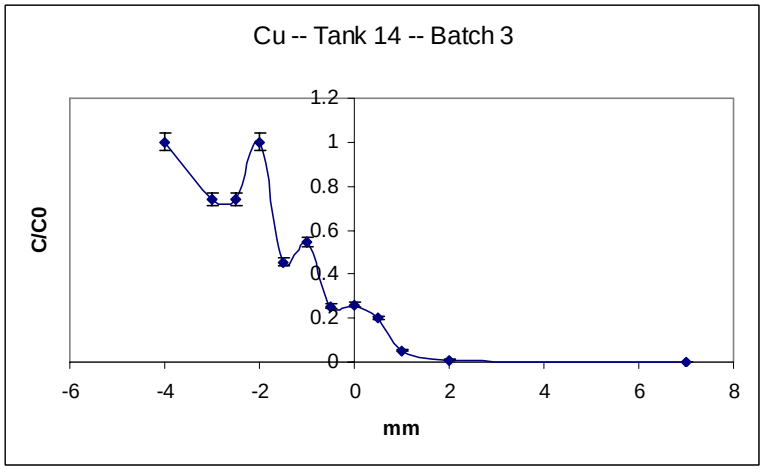

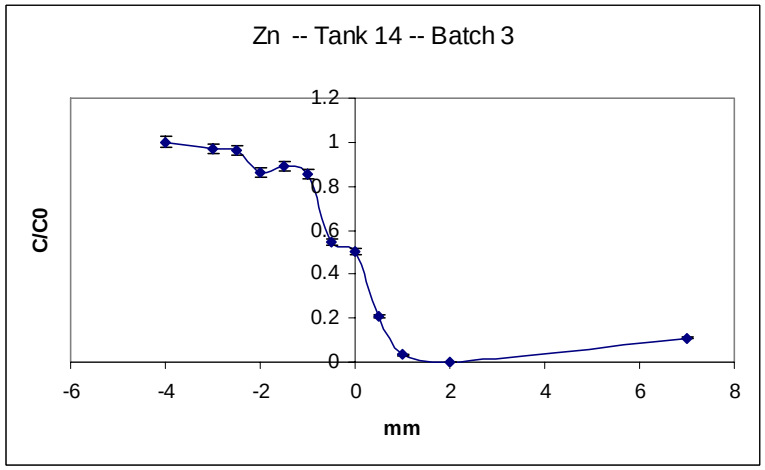

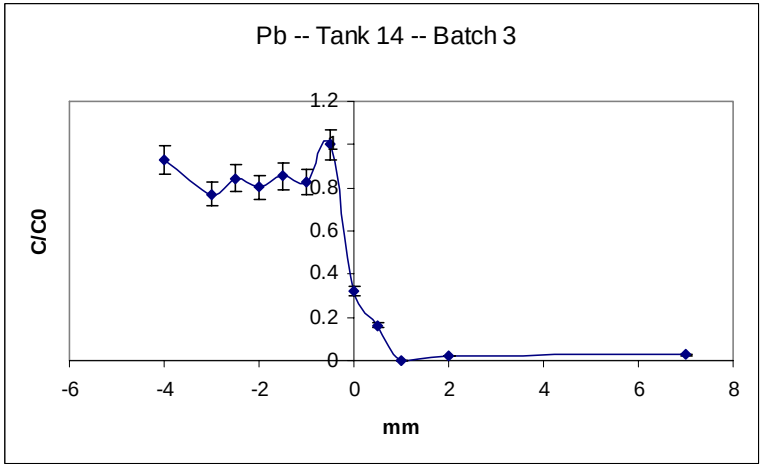

Tank 15 (Bio-exclusion)

Water

Great Bay Sediment

Newtwon Creek Contaminated Sediment

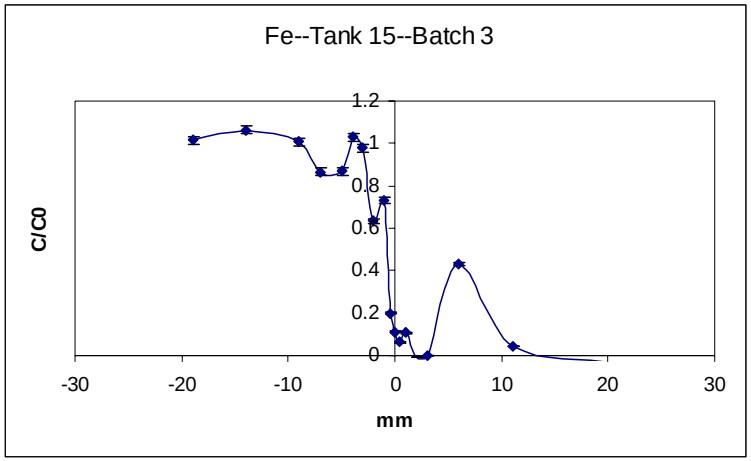

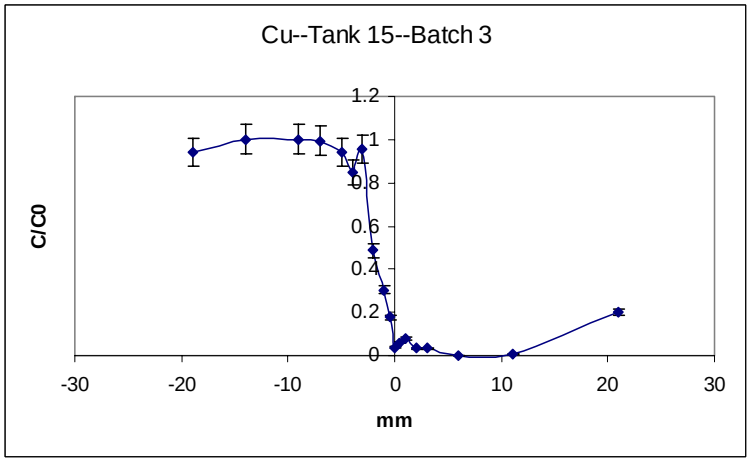

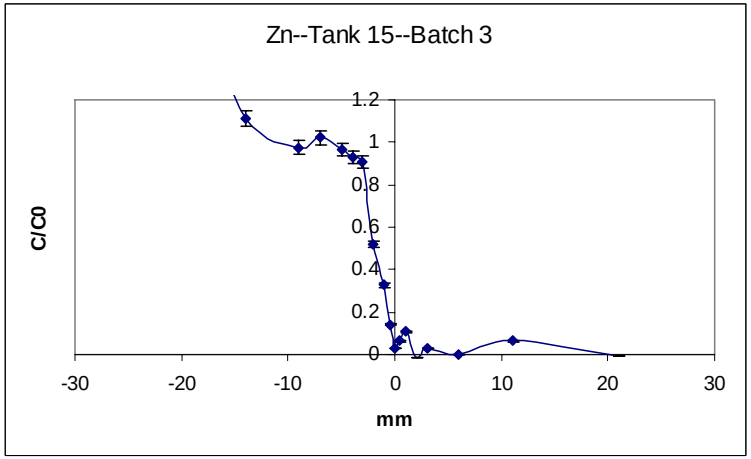

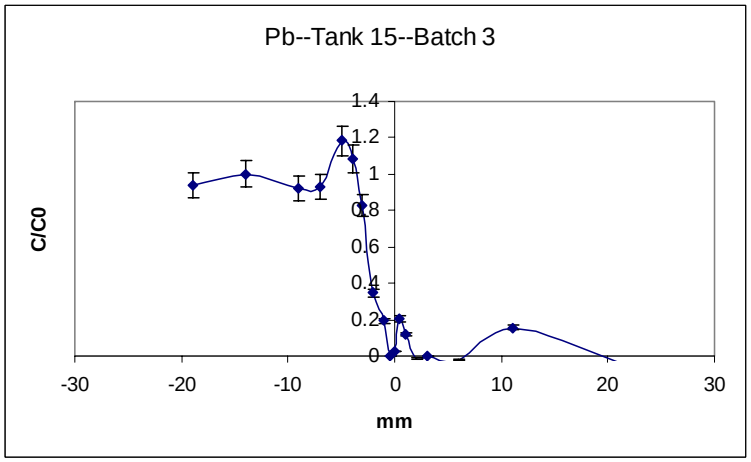

Tank 16 (Bio-exclusion)

Water

Florida Phosphate

Newtwon Creek Contaminated Sediment

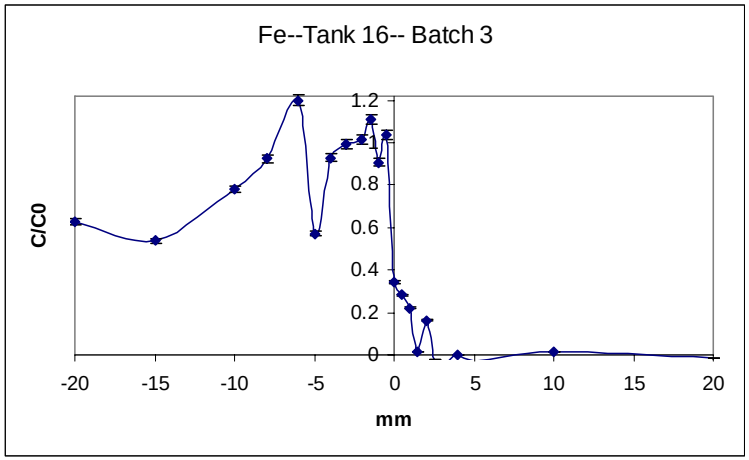

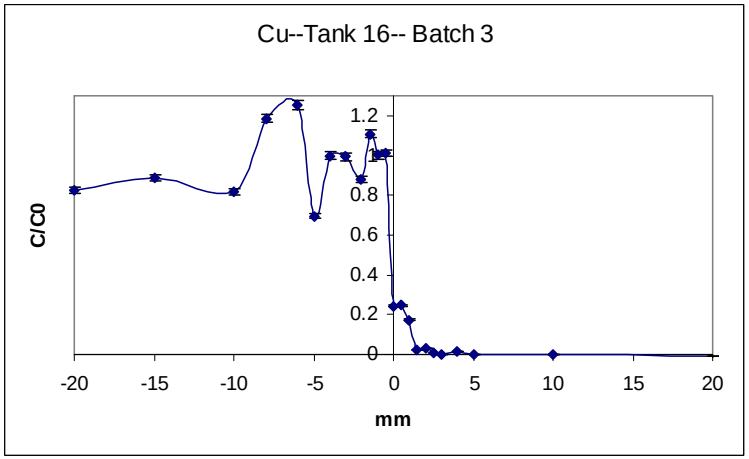

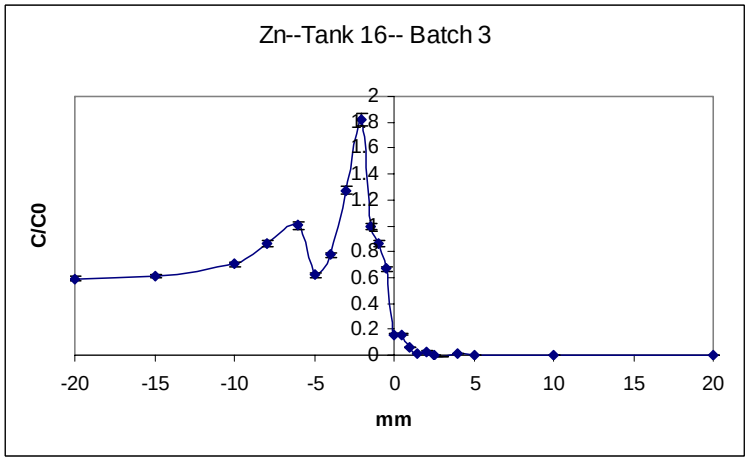

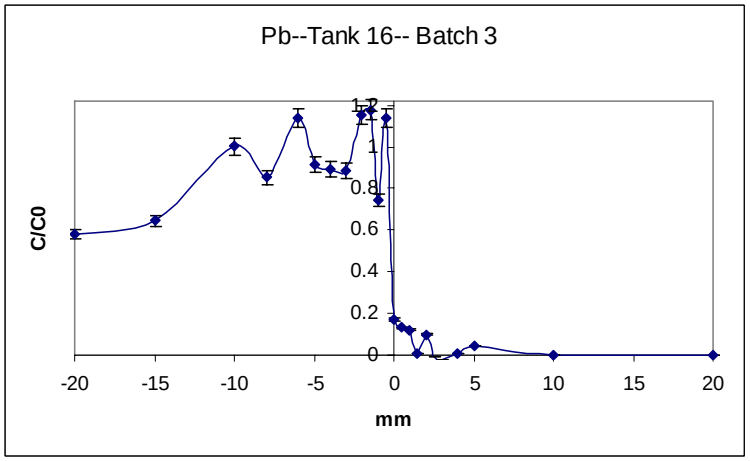

Tank 17 (Bio-exclusion)

Water

N.C. Phosphate

Newtwon Creek Contaminated Sediment

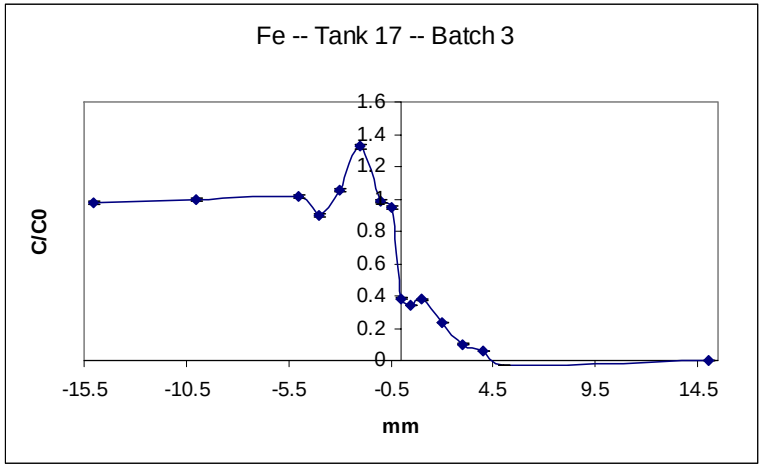

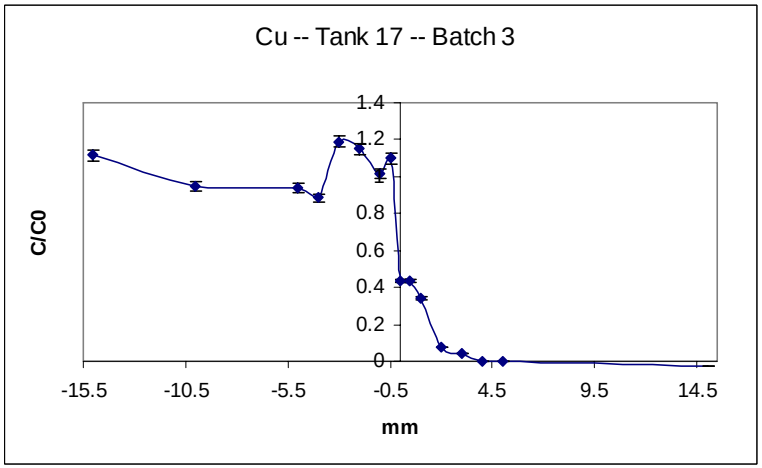

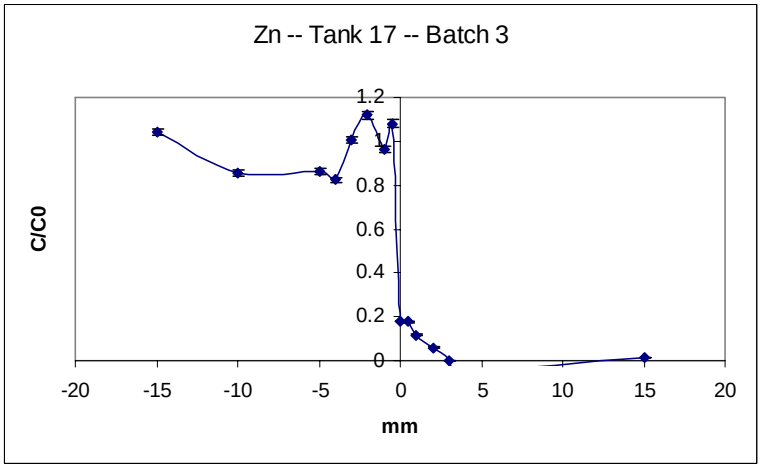

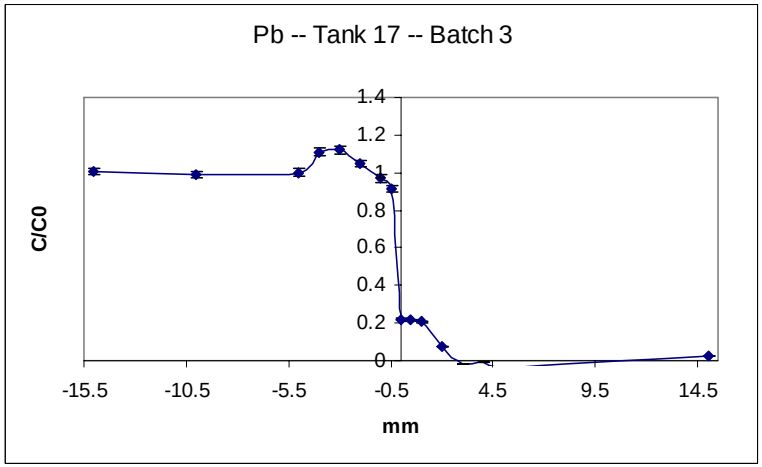

Tank 18 (Geofabric test)
Water
Great Bay Sediment
Florida Phosphate (Geofab)
Newtwon Creek Contaminated Sediment

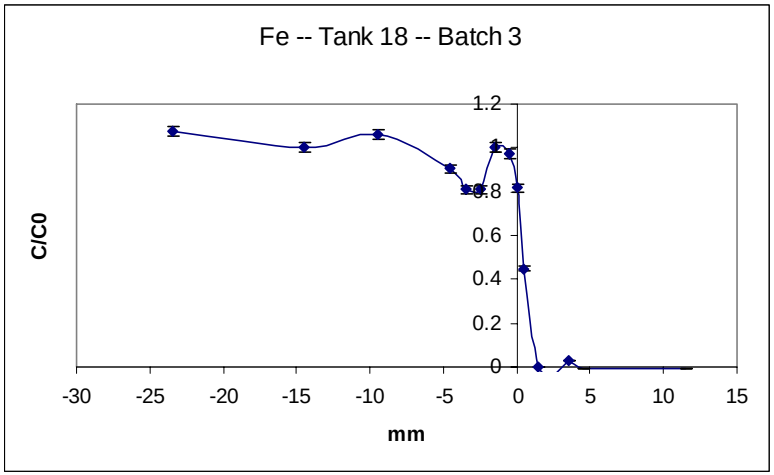

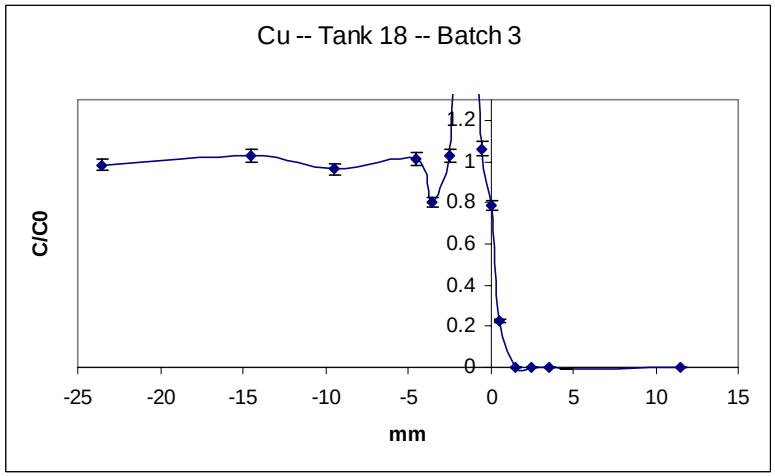

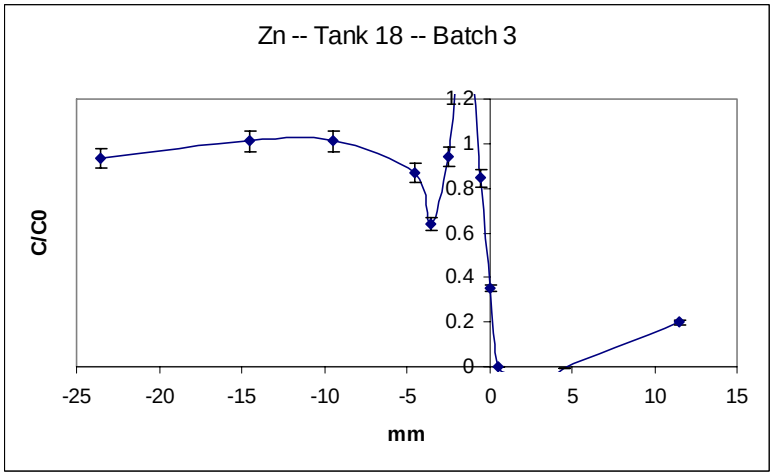

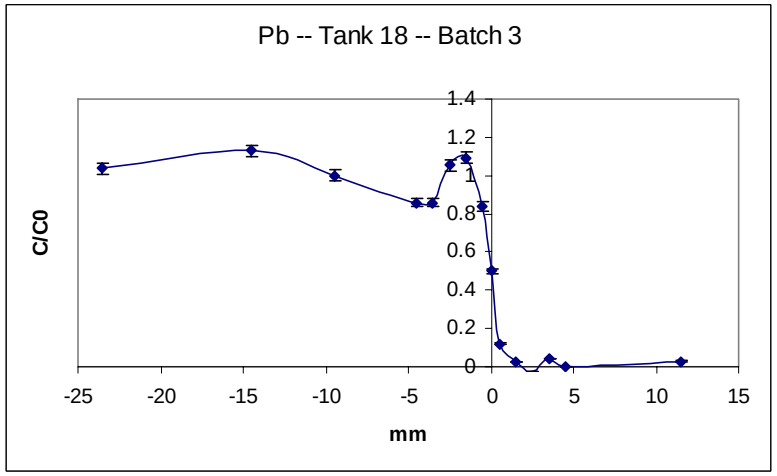

Tank 19 (Geofabric test)

Water

Great Bay Sediment

N.C. Phosphate

Newtwon Creek Contaminated Sediment

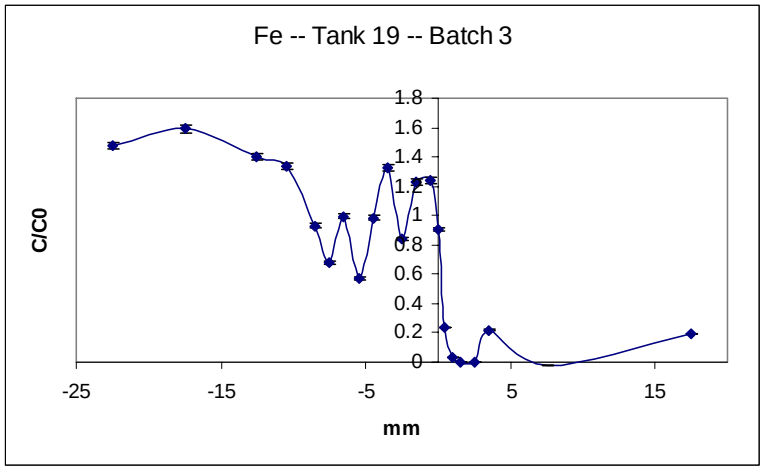

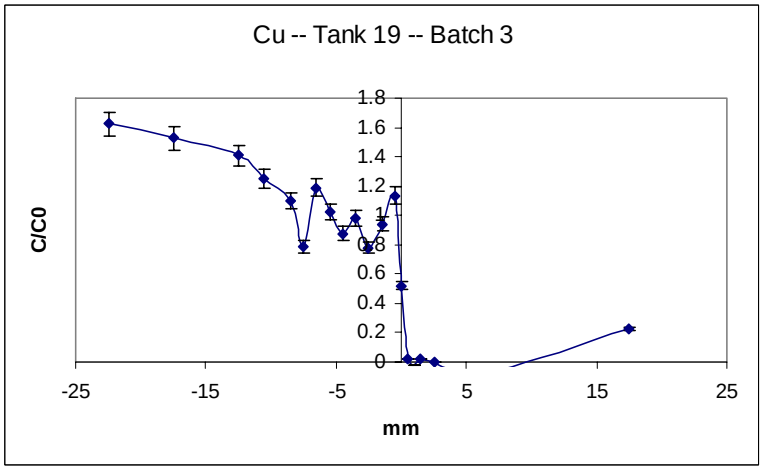

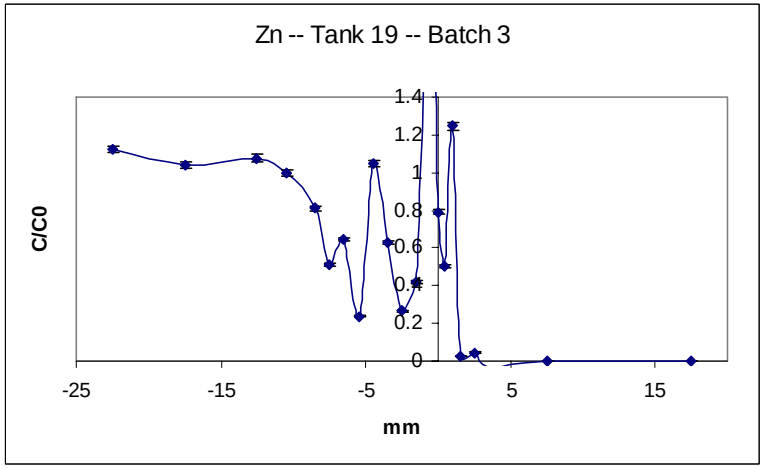

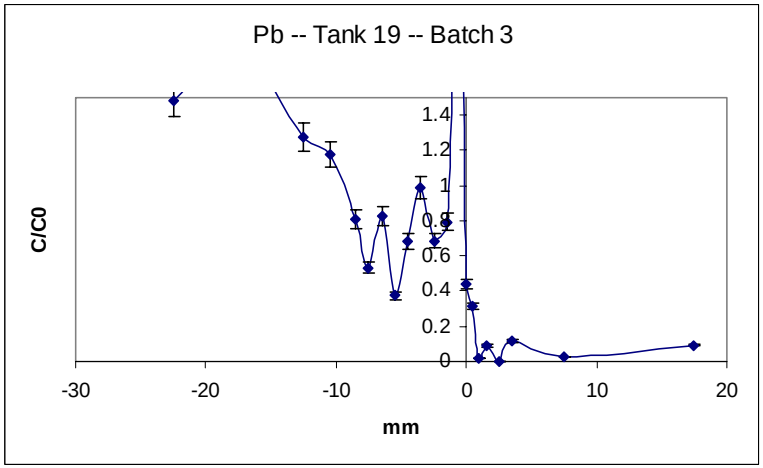

Appendix B

Selected MATLAB Code

The first code is diffusion model that incorporates Langmuir isotherm solving for Cu (in mono-element system) migration profiles (pore water concentration) in Florida Phosphate. The second code solves for its total concentration profiles. The third code is the diffusion model incorporated Langmuir isotherm and adsorption kinetic (see Chapter 6).

1. Code for pore water concentration profile:

```
clear;

TN=100;                          % one day is divided by TN (time discretion)
dt=86400/TN;

Ls=70;Lw=120;                    % lenght of two layers
Ns=280+1;Nw=120+1;               % spatial discretion
dx_1=Ls/(Ns-1);
dx_2=Lw/(Nw-1);

epsilon=0.4;rhos=2600;           % porosity,density
Dw=7.33e-4;                      % diffusivity
D0=7.33e-4;
De=D0*(epsilon)^(4/3);

Cs0=0.0003;                      %initial concentration
Cw0=1035;

f=zeros(Ns,1);
a=zeros(Ns+Nw-1,Ns+Nw-1);
b=zeros(Ns+Nw-1,10);

C=zeros(Ns+Nw-1,1);
C1=zeros(Ns+Nw-1,1);
C5=zeros(Ns+Nw-1,1);

C0=zeros(Ns+Nw-1,1);
for i=1:Ns
   C0(i)=Cs0;
end
```

```
for i=Ns+1:Ns+Nw-1
   C0(i)=Cw0;
end

for i=1:TN*9                        % 9 days

b(1)=0;a(1,1)=1;a(1,2)=-1;                  % boundary condition(Neumann) at the end point of solid layer

P1=0.4;P2=0.15;                     % Langmuir isotherm parameter

for m=2:Ns-1
   f(m)=(epsilon+(1-epsilon)*rhos*P1/(1+P2*C0(m))^2)/De;
end

for m=2:Ns-1
   b(m)=-dx_1^2/dt*f(m)*C0(m);
   a(m,m-1)=1;
   a(m,m)=-(2+dx_1^2/dt*f(m));
   a(m,m+1)=1;
end

b(Ns)=0;
a(Ns,Ns-1)=-De/dx_1;
a(Ns,Ns)=De/dx_1+Dw/dx_2;
a(Ns,Ns+1)=-Dw/dx_2;

for m=Ns+1:Ns+Nw-2
   b(m)=-dx_2^2/dt/Dw*C0(m);
   a(m,m-1)=1;
   a(m,m)=-(2+dx_2^2/dt/Dw);
   a(m,m+1)=1;
end

b(Ns+Nw-1)=0;a(Ns+Nw-1,Ns+Nw-2)=1;a(Ns+Nw-1,Ns+Nw-1)=-1;      % boundary condition(Neumann) at the end point of water layer

C=a\b;
C0=C;
if i==TN                        % 1 day
  C1=C;
end
if i==5*TN                       % 5 days
  C5=C;
end
end
```

```
Xs=-Ls:dx_1:0;
Xw=0+dx_2:dx_2:Lw;
X=[Xs,Xw];
C1=C1';C5=C5';C9=C';
plot(X,C1,X,C5,X,C9)

xlabel('depth(mm)','FontWeight','bold');
ylabel('pore water concentration(mg/L)','FontWeight','bold');
legend('1 day-model','5 day-model','9 day-model');
title('Cu(single) Diffusion in Florida Phosphate(pore water
concentration)','FontSize',10,'FontWeight','bold');
```

2. Code for total concentration profile:

```
clear;

TN=100;                          % one day is divided by TN (time discretion)
dt=86400/TN;

Ls=70;Lw=120;                    % lenght of two layers
Ns=280+1;Nw=120+1;               % spatial discretion
dx_1=Ls/(Ns-1);
dx_2=Lw/(Nw-1);

epsilon=0.4;rhos=2600;           % porosity,density
Dw=7.33e-4;                      % diffusivity
D0=7.33e-4;
De=D0*(epsilon)^(4/3);

Cs0=0.0003;                      %initial concentration
Cw0=1000;

f=zeros(Ns,1);
a=zeros(Ns+Nw-1,Ns+Nw-1);
b=zeros(Ns+Nw-1,10);

C=zeros(Ns+Nw-1,1);
C1=zeros(Ns+Nw-1,1);
C5=zeros(Ns+Nw-1,1);

C0=zeros(Ns+Nw-1,1);
for i=1:Ns
   C0(i)=Cs0;
end
```

```
for i=Ns+1:Ns+Nw-1
   C0(i)=Cw0;
end

for i=1:TN*9                          % 9 days

b(1)=0;a(1,1)=1;a(1,2)=-1;            % boundary condition(Neumann) at the end point of
solid layer

P1=0.4;P2=0.15;                       % Langmuir isotherm parameter

for m=2:Ns-1
   f(m)=(epsilon+(1-epsilon)*rhos*P1/(1+P2*C0(m))^2)/De;
end

for m=2:Ns-1
   b(m)=-dx_1^2/dt*f(m)*C0(m);
   a(m,m-1)=1;
   a(m,m)=-(2+dx_1^2/dt*f(m));
   a(m,m+1)=1;
end

b(Ns)=0;
a(Ns,Ns-1)=-De/dx_1;
a(Ns,Ns)=De/dx_1+Dw/dx_2;
a(Ns,Ns+1)=-Dw/dx_2;

for m=Ns+1:Ns+Nw-2
   b(m)=-dx_2^2/dt/Dw*C0(m);
   a(m,m-1)=1;
   a(m,m)=-(2+dx_2^2/dt/Dw);
   a(m,m+1)=1;
end

b(Ns+Nw-1)=0;a(Ns+Nw-1,Ns+Nw-2)=1;a(Ns+Nw-1,Ns+Nw-1)=-1;      % boundary
condition(Neumann) at the end point of water layer

C=a\b;

C0=C;

if i==TN                              % 1 day
  C1=C;
end

if i==5*TN                            % 5 days
```

```
   C5=C;
end

end

Xs=-Ls:dx_1:0;
Xw=0+dx_2:dx_2:Lw;
X=[Xs,Xw];

Ctotal=zeros(Ns,1);Ctotal1=zeros(Ns,1);Ctotal5=zeros(Ns,1);
for m=1:Ns
   Ctotal(m)=epsilon*C(m)+(1-epsilon)*rhos*P1*C(m)/(1+P2*C(m));
   Ctotal1(m)=epsilon*C1(m)+(1-epsilon)*rhos*P1*C1(m)/(1+P2*C1(m));
   Ctotal5(m)=epsilon*C5(m)+(1-epsilon)*rhos*P1*C5(m)/(1+P2*C5(m));
end

Ct=zeros(Ns,1);Ct1=zeros(Ns,1);Ct5=zeros(Ns,1);
for m=1:Ns
   Ct(m)=Ctotal(m)/Ctotal1(Ns);
   Ct1(m)=Ctotal1(m)/Ctotal1(Ns);
   Ct5(m)=Ctotal5(m)/Ctotal1(Ns);
end


plot(Xs,Ct1,'-k',Xs,Ct5,':k',Xs,Ct,'-.k')

xlabel('depth(mm)','FontWeight','bold');
ylabel('Normalized concentration','FontWeight','bold');
legend('1 day-model','5 day-model','9 day-model');
title('Cu(single) Diffusion in Florida Phosphate','FontSize',10,'FontWeight','bold');
```

3. Code for diffusion model considering adsorption kinetic

```
clear;

Ls=70;Lw=120;
N=280;M=120;
ds=Ls/N;dw=Lw/M;
epsilon=0.4;rhos=2600;
a=0.4;b=0.15;
Dw=7.33e-4;
```

```
D0=Dw;
De=Dw*(epsilon)^(4/3);
k=0.0153;

dt=120;
Nt=720;

Cs0=0.0003; Cw0=1000;
Cs=Cs0*ones(1,N+1);
Cw=Cw0*ones(1,M+1);
NCs=zeros(1,N+1); NCw=zeros(1,M+1);
Cs1=zeros(1,N+1); Cw1=zeros(1,M+1);
Cs5=zeros(1,N+1); Cw5=zeros(1,M+1);

H=zeros(1,N+1); K=zeros(1,N+1);

t1=3600*24;

for j=1:Nt*9

   for i=2:N
     H(i)=dt*(1-epsilon)*rhos*a*k*Cs(i)*exp(-k*j*dt)*(1+b*Cs(i))/((1+b*Cs(i))^2*(1-
exp(-k*t1))*epsilon+(1-epsilon)*rhos*a*(1-exp(-k*j*dt)));
   end

   for i=2:N
     K(i)=De*dt/ds^2/(epsilon+(1-epsilon)*rhos*a*(1-exp(-k*j*dt))/(1+b*Cs(i))^2/(1-
exp(-k*t1)));
   end

   for i=2:N
      NCs(i)=Cs(i)-H(i)+K(i)*(Cs(i+1)-2*Cs(i)+Cs(i-1));
   end
   NCs(1)=NCs(2);

   for i=2:M
      NCw(i)=Cw(i)+dt*D0/dw^2*(Cw(i+1)-2*Cw(i)+Cw(i-1));
   end
   NCw(M+1)=NCw(M);

   NCs(N+1)=(ds*D0*NCw(2)+dw*De*NCs(N))/(dw*De+ds*Dw);
   NCw(1)=NCs(N+1);

   Cs=NCs;Cw=NCw;

   if j==Nt
```

```
    Cs1=Cs;
    Cw1=Cw;
  end

  if j==5*Nt
    Cs5=Cs;
    Cw5=Cw;
  end

end

Xs=-Ls:ds:0;
Xw=0:dw:Lw;

X=[Xs,Xw];
C1=[Cs1,Cw1];
C5=[Cs5,Cw5];
C9=[Cs,Cw];

plot(X,C1,X,C5,X,C9)

xlabel('depth(mm)','FontWeight','bold');
ylabel('pore water concentration(mg/L)','FontWeight','bold');
legend('1 day','5 day','9 day');
title('Cu(single) Diffusion in Florida Phosphate(pore water
concentration)','FontSize',10,'FontWeight','bold');
```

Vita

Ming Yin was born in Maoming, Guangdong, China, in the Fall of 1970. He attended Olympic Mathematics competition when he was in high school. While at the Beijing University, Ming completed a bachelor of science degree in physics in 1992. Then he joined the Research Institute of China Petroleum&Chemical Corporation and worked as a research engineer. In 1997 he returned to campus and completed a master of science degree in chemical engineering in Xiamen University. In August 2000, he went to Louisiana State University and has been working toward a doctoral degree in chemical engineering, which will be conferred in May, 2007.